Studies on Poly (Lactic Acid) and Polysaccharide Gum based Bionanocomposites for Adhesive and Gas Barrier Film Applications

Thesis submitted in partial fulfillment of the requirements for the degree of

DOCTOR OF PHILOSOPHY

by

NEELIMA TRIPATHI

(Roll No.: 11610708)

Department of Chemical Engineering

Indian Institute of Technology Guwahati

Guwahati – 781 039, India

March, 2016

Dedicated to my beloved

Parents

& little Sister Shalini

Department of Chemical Engineering
Indian Institute of Technology Guwahati

CERTIFICATE

This is to certify that the research work in the thesis entitled "**Studies on Poly (Lactic Acid) and Polysaccharide Gum based Bionanocomposites for Adhesive and Gas Barrier Film Applications**", is carried out by me at the Chemical Engineering Department, Indian Institute of Technology Guwahati, under Dr. Vimal Katiyar. The results documented in this thesis are achieved by me and has not been submitted to any other University or Institute for the award of any degree or diploma.

(Neelima Tripathi)
Roll no.: 11610708
Department of Chemical Engineering
Indian Institute of Technology Guwahati
Guwahati - 781 039, India.

Department of Chemical Engineering
Indian Institute of Technology Guwahati

CERTIFICATE

This is to certify that the thesis entitled "**Studies on Poly (Lactic Acid) and Polysaccharide Gum based Bionanocomposites for Adhesive and Gas Barrier Film Applications**", being submitted by **Neelima Tripathi** for the award of Ph.D. degree has been carried out by her at the Chemical Engineering Department, Indian Institute of Technology Guwahati, under my guidance and supervision. The work documented in this thesis has not been submitted to any other University or Institute for the award of any degree or diploma.

(Dr. Vimal Katiyar)
Associate Professor
Department of Chemical Engineering
Indian Institute of Technology Guwahati
Guwahati - 781 039, India.

Acknowledgement

With great pleasure and profound sense of gratitude, I take this opportunity to express my heartfelt and sincere thanks to my learned guide Dr. Vimal Katiyar, for his valuable guidance and encouragement provided to me throughout the course of my PhD work. His great enthusiasm and extremely hard working attitude kept me inspired all through. I would like to acknowledge sincerely the support, encouragement and valuable criticism provided by my Doctoral Committee members Dr. Anil Verma, Dr. Vaibhav V. Goud, Dr. Amit Kumar and Dr. Mohammad Qureshi. I wish to place on record the use of facilities and sophisticated instruments available at Center of Excellence for Sustainable Polymers (CoE-SusPol) and Central Instruments Facility (CIF), IIT Guwahati for carrying out instrumental analysis part of my research work. I would also like to thank the head and all authorities of the department of chemical engineering for providing me all research and analytical facilities required for my work. I am thankful to the Science and Engineering Research Board (SERB) for awarding me the travel grant for international symposium in Canada. I am extremely thankful to the technical staff (teaching and non-teaching) of the chemical engineering department, particularly Ritumoni Kalita, Harsaraj Biswanath, Dipak Kumar Barman, Jayanta Kumar Mout, Dr. Lukumoni Borah, Debajit Borah, Pankaj Sekhar Baruah, Deep Jyoti Sinha, Sailen Das, Kalyan Boro and Bhagya Boro for providing me all help and assistance for the completion of my work. My heartfelt thanks are due to Akhilesh Kumar Pal for providing me timely help and support at all times along the way. My thanks are also due to all my labmates, especially Arvind Gupta, Prodyut Dhar, Surendra Singh Gaur, Gourhari Chakraborty, Medha Mili, Monika, Narendren S, Shasanka Sekhar Borkotoky, Melaku Tesfaye, Siddhartha Mohan

Bhasney, Sai Phani Kumar, Valapa Ravi Babu, Naba Kumar Kalita, Amit Pandey for all kinds of help and morale support made available to me in the lab. I wish to place on record, my thankfulness to my friends Surya Singh, Meneka Banik, Richa Sharma, Chitrita Kundu for boosting my morale at the difficult moments. Last but not least, from the core of my heart, I wish to acknowledge the encouragement, support and love from my parents and sister Shalini Tripathi. In the end, I wish to thank sincerely one in all who helped me directly or indirectly to complete my research work. *Blessings of Almighty are always solicited*.

Abstract

Nowadays, bio-based polymers such as poly (lactic acid) and polysaccharides have attracted much attention because of their environment friendliness and biodegradability. Poly lactic acid (PLA) has proved to be the most promising biodegradable polymer which has wide variety of applications. Due to its desirable properties such as transparency, bio-safety and compostability; it has promising applications in consumer goods, fibers, biomedicines and packaging. Literature survey revealed that the polysaccharide gums are not compatible with PLA due to its hydrophilic nature. Even though some of the polysaccharide gums have film forming ability but cannot be utilized in packaging and other applications due to some limitations. Hence, researchers have found many ways such as blending, mixing and grafting to avoid such limitations. As per the available literature, such techniques were used by using various initiators, catalysts, additives and solvents in order to improve the functionalization or productivity. It has been inferred that scanty efforts have been made to synthesize a bio-based adhesive with adhesive strength comparable to that of conventional adhesives for structural applications. It has also been observed that no work has been published as of now on: (a) preparation of modified hydrophobic gum based bionanocomposites using lactic acid, (b) use of gum based bionanocomposite for adhesive applications, and (c) use of gum based bionanocomposite for food packaging applications.

As a result of which, the present doctoral work was contemplated to focus on two applications such as (i) adhesive application, and (ii) packaging application. In adhesive application, the polysaccharide gums (gum arabic, guar gum, xanthan gum and gum rosin) were utilized by condensation polymerization with lactic acid to minimize their hydrophilicity. Further, the prepared modified gums were tested for adhesive application. In packaging application, the

modified polysaccharide gums (hydrophobic) have been utilized as a filler with PLA in order to improve its characteristic properties. The research work mainly focuses on developing novel polysaccharide gum based products from lactic acid which is a bio-derived monomer. These poly (lactic acid) based bio-nanocomposites would be studied as adhesive materials for binding different substrates and barrier material for reduction of oxygen and water vapour transmission. In one part of the thesis, the bio-based adhesive formulation, adhesion process for structural applications and properties have been discussed. According to the available literature, such polymers can be used as adhesives where low lamination strength is required and, to the best of our knowledge, no formulation using biodegradable, consisting of bio derived polyesters grafted with polysaccharide gums, is reported as adhesive for the high performance structural applications. However in this work, the formulated bio-based adhesive has the capability to bind construction materials such as glass and marble. Adhesive properties of conjugates/blends depend on their solubility behaviour, and is important for their application for bonding pieces of several materials; not limited to stones, glasses, granite, etc. This is noteworthy to mention that the above formulation is also used for enhancing the barrier properties of existing poly (lactic acid). This could be achieved by dispersion of grafted gum based micro and nano spheres in PLA matrix.

The thesis is organized in eight chapters as follows:

The chapter one briefly describes biopolymers, biodegradable polymers and polysaccharide gums. The benefits of the bio-based and renewable resources over petroleum based products have been discussed in detail. The chapter also provides general overview of the origin, chemical structure, properties, challenges and applications of bio-based polymers and polysaccharide gums. The chapter mainly focuses on discussing poly (lactic acid) and

polysaccharide gums such as gum arabic, guar gum, xanthan gum and gum rosin. The chapter also presents literature survey on bio-based materials such as poly (lactic acid) and polysaccharide gums. Some major outcomes reported so far on the synthesis of grafted polysaccharide gums have been highlighted. The thesis is focused on the two major applications such as adhesive application and bionanocomposite film fabrication by utilizing polysaccharide gums and poly (lactic acid).

The chapter two presents the materials used and protocols for various experiments performed in the research work. The procedures followed for the synthesis of modified gums have been included. The calculation methodology for converting raw experimental data into appropriate domain has been elaborated. The determination of characteristic properties for the samples for their analysis has also been discussed.

The chapter three focuses on selection of the polysaccharide gum among various polysaccharide gums such as gum arabic, guar gum, xanthan gum and gum rosin for the desired applications. The monomer lactic acid is used to graft with the polysaccharide gums by conventional heating and microwave heating method. The grafted composites are tested as an adhesive for structural applications and food packaging applications. The preliminary tests were conducted by the two synthesis methods and the grafting in the composites are studied. The synthesized composites are tested for the preliminary critical properties of both the applications.

The chapter four presents the investigation on gum arabic (GA) grafted poly l-lactic acid (PLA) bionanocomposite [GA-*g*-PLA] which is synthesized by using microwave heating in which the hydrophilic GA is grafted with in-situ grown lactic acid oligomer. The grafting at O-H and N-H groups in GA backbone with *oligo*-(L-lactic acid) (OLLA) chains is confirmed by FTIR

and NMR analyses. XRD, TGA, SEM and TEM analyses supports uniform dispersion of GA in OLLA due to effective grafting reaction. The prepared bionanocomposite is found to be amorphous in nature which was proved by XRD and DSC analyses due to unavailability of crystallization peak and broad peak of heat of fusion.

The chapter five elucidates the performance of microwave initiated gum arabic grafted poly l-lactic acid bionanocomposite for adhesive application. The single lap shear test is performed to check the binding ability of the synthesized bio-based adhesive. The various parameters of the adhesive are tested such as compression load, compression time and the effect of concentration of GA in the composite. The bio-based adhesive showed excellent adhesive strength for glass and granite substrates.

The chapter six presents the microwave synthesis of gum arabic-grafted-poly l-lactic acid (GA-*g*-PLA) by polycondensation reaction and its influence as an additive to improve the gas barrier properties of poly (lactic acid) (PLA) films, prepared by solution casting method. It is observed that during the synthesis of GA-*g*-PLA, hydrophilic gum is converted into hydrophobic due to grafting of in situ grown hydrophobic *oligo*-(lactic acid). Subsequently, PLA/GA-*g*-PLA bionanocomposite films are fabricated and characterized for structural, thermal, mechanical and gas barrier properties. Path breaking reduction in oxygen permeability (OP) of ~10 folds is achieved in case of PLA films containing GA-*g*-PLA as filler. However, water vapour transmission rate (WVTR) is reduced upto 27% after 5 wt% addition of filler. Reduction in OP of this order of magnitude enable the PLA to compete with PET in terms of enhancing shelf life and maintaining the food quality.

The chapter seven demonstrates the thermal degradation behaviour of poly lactic acid (PLA) and gum arabic-grafted-poly l-lactic acid (GA-*g*-PLA) based bionanocomposite films. The

GA-*g*-PLA is prepared by polycondensation of lactic acid in presence of gum arabic, and proved to be a unique bio-based filler. The thermal degradation of PLA is found to be a single-step process. Thermogravimetric Analysis hyphenated with Fourier Transform Infrared Spectroscopy (TGA-FTIR) is conducted to study the evolved gaseous products from PLA and PLA/GA-*g*-PLA samples, for interpreting the degradation pathways. Activation energies obtained by Flynn-Wall-Ozawa (F-W-O) and Kissinger-Akahira-Sunose (K-A-S) models are found to be in good agreement with Kissinger model as compared to Augis & Bennett model. The activation energies of neat PLA films are determined from Kissinger, Augis & Bennett, F-W-O and K-A-S models, and are found to be 254, 259, 257 and 260 kJ mol^{-1}, respectively. For the composite films, it is observed that the activation energy of degradation is dependent on its conversion.

The chapter eight highlights the major inferences drawn from the doctoral work and presents an outlook for future studies.

Contents

List of Figures

List of Tables

Nomenclature

Abbreviations

ASTM	American society for testing and materials
DSC	Differential scanning calorimetry
FDA	Food and drug administration
FESEM	Field emission scanning electron microscopy
FTIR	Fourier transform infrared spectroscopy
F-W-O	Flynn-Wall-Ozawa
GA	Gum arabic
GG	Guar gum
GR	Gum rosin
ICTAC	International confederation of thermal analysis and calorimetry
K-A-S	Kissinger-Akahira-Sunose
LA	Lactic acid
GA-*g*-PLA	Gum arabic-grafted-poly lactic acid
OLLA	Oligomer of l-lactic acid
OP	Oxygen permeability
OTR	Oxygen transmission rate
PBAT	Poly(butylene adipate-co-terephthalate)
PBSA	Polybutylene succinate
PC	Polycarbonates
PCL	Polycaprolactones
PE	Polyethylene

PEA	Polyesteramides
PEG	Poly (ethylene glycol)
PET	Poly(ethylene terephthalate)
PHA	Polyhydroxyalkanoates
PLA	Poly (lactic acid)
PP	Polypropylene
PTT	Poly(trimethylene terephthalate)
ROP	Ring opening polymerization
SEM	Scanning electron microscopy
SSP	Solid state polymerization
TEM	Transmission electron microscopy
TGA	Thermogravimetric analysis
TGA-FTIR	Thermogravimetric analysis hyphenated with fourier transform infrared spectroscopy
XG	Xanthan gum
XRD	X-ray diffraction
WVTR	Water vapour transmission rate

Notations

A	Pre-exponential factor
E_a	Activation energy
$\overline{E}_a$	Average activation energy
K	Avrami kinetic constant
R	Universal gas constant
T_o	Onset degradation temperature

T_c	Crystallization temperature
T_m	Melting temperature

Greek letters

β	Heating rate
θ	Diffraction angle
α	Degree of conversion

Chapter 1

Introduction

The chapter briefly describes biopolymers, biodegradable polymers and polysaccharide gums. The benefits of the bio-based and renewable resources over petroleum based products have been discussed in detail. The chapter also provides general overview of the origin, chemical structure, properties, challenges and applications of bio-based polymers and polysaccharide gums. The chapter mainly focuses on discussing poly (lactic acid) and polysaccharide gums such as gum arabic, guar gum, xanthan gum and gum rosin. The chapter also presents literature survey on bio-based materials such as poly (lactic acid) and polysaccharide gums. Some major outcomes reported so far on the synthesis of grafted polysaccharide gums have been highlighted. The thesis focuses on the two major applications such as adhesive application and bionanocomposite film fabrication by utilizing polysaccharide gums and poly (lactic acid).

1.1. Introduction

Non-renewable resources like fossil fuels, radioactive materials and some aquifers are depleting at a very fast pace. These resources are very limited on earth and their continuous consumption is causing irreparable damage to the environment. The change in climate due to environmental pollution results in global warming. This leads to a great demand of developing bio-based materials having similar or better characteristic properties than that of petroleum

based products because of their environment friendliness and biodegradability. Hence, society is getting more inclined towards developing biopolymers and growing interest in innovative process technologies. The demand of bio-based polymeric materials is exponentially growing compared to conventional materials due to their remarkable properties such as low density, chemical resistance, low toxicity and low cost.

The biopolymers are considered to be environment friendly because the carbon atoms in these materials are originated from atmospheric carbon-dioxide which is fixed through photosynthesis of plants. During incineration, these materials do not produce additional carbon-dioxide in the environment which helps in suppressing the carbon-dioxide levels in the atmosphere **(Kimura, 2013)**. However, the bio-based polymers also have certain limitations, such as inferior thermal properties, poor gas barrier and low mechanical properties **(Gonzalez et al., 2013).**

It is noteworthy to mention that the term 'biopolymer' refers to polymers that are bio-based, biodegradable or both **(Imre et al., 2013)**. Bio-based polymers are macromolecules which are produced from renewable feedstock such as cellulose, silk, starch, lignin and polysaccharide gums. Another class of bio-based polymers are natural-based synthetic polymers in which the monomers are derived from renewable resources such as poly lactic acid (PLA). **Kimura, 2013** classified bio-based polymers into two main categories as (i) naturally obtained polymers, (ii) polymers synthesized from biomass-originated monomers, also named as synthetic polymers. The natural polymers are further classified into two categories:

(a) biomass polymers or the naturally occurring polymers which can be directly used including chemically modified polymers such as modified starch, regenerated cellulose, chitin and cellulose acetate.

(b) Bio-engineered polymers or polymers bio-synthesized using microorganisms and plants such as bacterial cellulose, poly (glutamic acid) and poly(3-hydroxyalkanoate)

Furthermore, synthetic polymers can also be categorized into two categories:

(a) New metabolite polymers from biomass feedstock. They are synthesized by polymerization of metabolic products which are obtained from naturally occurring substances by break down of the biomass. Polylactides (PLA), aliphatic bio-polycarbonates (PC), polyamides (nylon), poly(trimethylene terephthalate) (PTT), poly(butylene succinate) (PBS) are a few examples of metabolite polymers. Here, PLA is synthesized from bio-derived L-lactic acid, PC is prepared from isosorbide, polyamide such as Nylon 11 is prepared from amino-carboxylic acid obtained from castor oil, PTT consists of bio-derived 1,3-propanediol and PBS consists of bio-synthesized succinic acid.

(b) Conventional petrochemical polymers which are produced from bio-derived monomers such as bio-polyethylene (PE) and bio-polypropylene (PP).

The biodegradable polymers can be defined as the polymers that degrade by the action of bacteria, fungi, algae and various other microorganisms **(Platt, 2006)**. These polymers break down and lose their original identity, and the degraded products are compatible with nature i.e. does not produce toxic effects which can pollute the environment. Biodegradable polymers based on their origin are classified in figure 1.1.

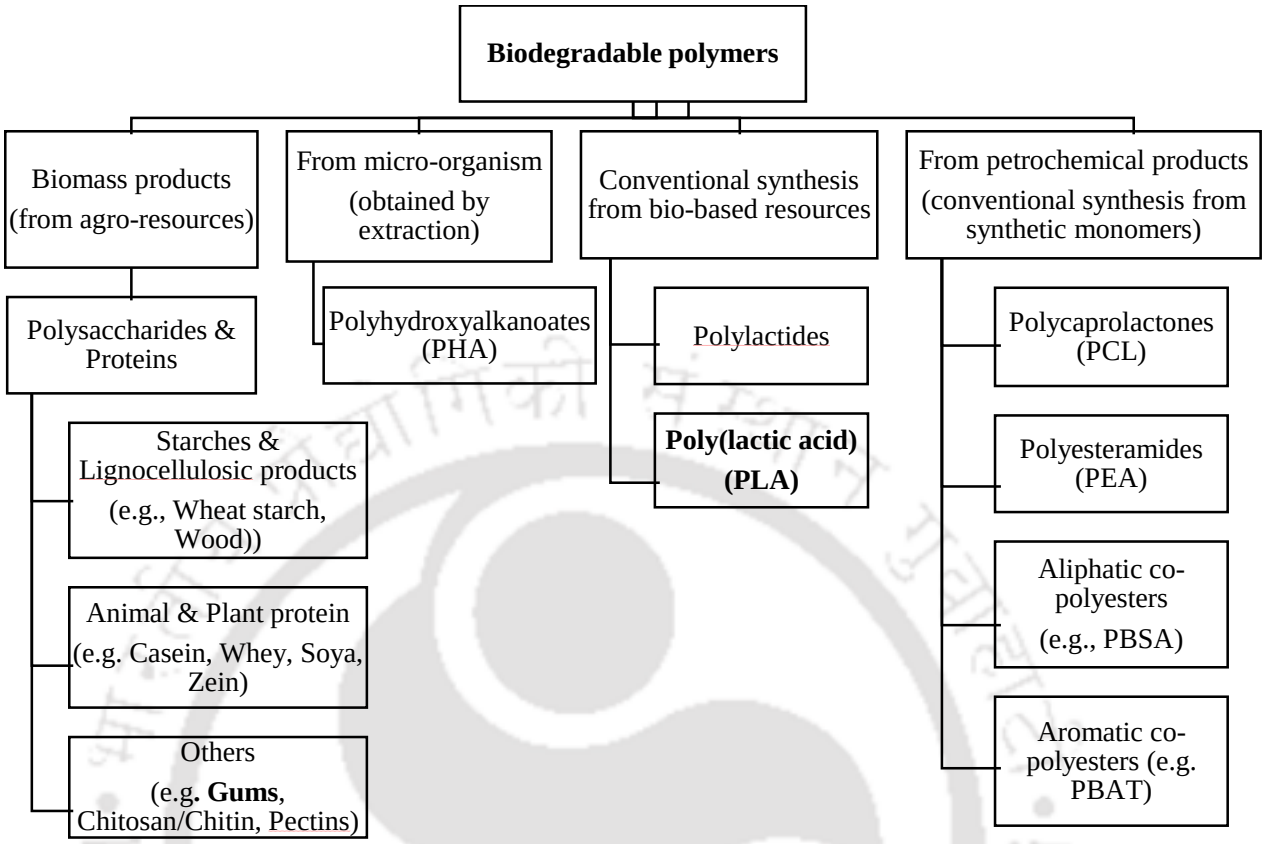

Figure 1.1. Classification of biodegradable polymers.

Biodegradation of polymers is usually carried out in two steps. First is depolymerization or chain cleavage; other is mineralization. In depolymerization, long polymer chains are broken into small parts; and in mineralization, biomass, minerals, salts, water, carbon dioxide, and methane are formed from small oligomeric fragments **(Bastioli, 2005)**.

The use of the bio-based polymers for packaging applications is increasing day by day due to depletion of petroleum-based resources and increasing concerns due to environmental pollution **(Carrasco et al., 2014; Raquez et al., 2013)**. Different bio-based polymers used in packaging applications are poly (ε-caprolactone) (PCL), poly (hydroxyl alkanoates) (PHAs) and poly (ethylene glycol) (PEG). Amongst these poly (lactic acid) (PLA) is a promising

bio-based, renewable and biodegradable thermoplastic polyester derived from lactic acid (2-hydroxy propionic acid) which can be used for the preparation of eco-friendly packaging materials **(Rhim et al., 2013; Ramos et al., 2014; Auras et al., 2004)**.

1.1.1. Poly (lactic acid)

PLA is the first renewable bio-based synthetic polymer that has been exploited for commercialization at a large scale **(Goncalves et al., 2013; Rudnik et al., 2011)**. PLA has great potential to replace conventional non-renewable petroleum-based polymers **(Zhang et al., 2014)**. It is derived from renewable resources such as corn, sweet potato, cane molasses and beet sugar. It is an environment friendly thermoplastic polymer which is a bio-based, biocompatible and biodegradable material **(Zhang et al., 2014; Maharana et al., 2009; Reddy et al., 2013).** PLA has proved to be the most promising biodegradable polymer which has wide variety of applications. Due to its desirable properties such as transparency, bio-safety and compostability; it has promising applications in consumer goods, fibers, biomedicines and packaging which may result in exorbitant use of it in near future. Hence, systematic and rigorous study of degradation for PLA is of great concern towards its recyclability and nontoxic incineration process.

Poly lactic acid (PLA) lies in the class of degradable polymers which are primarily synthesized in the laboratory using monomers which are generally derived from bio feedstock. PLA is an example of the class where stereospecific lactic acid is prepared by the fermentation of starch based agro feedstock such as sugarcane, corn, sugar beet pulp, etc. The basic building block for PLA is lactic acid (LA), which exists in two optically active configurations L(+) lactic acid and D(-) lactic acid (figure 1.2). LA (2-hydroxy propanoic acid) is an organic acid having bifunctionality as it has $-COOH$ and $-OH$ groups. LA is produced by fermentation of different

carbohydrates (namely glucose, sucrose, lactose and maltose) obtained from renewable resources such as sugar cane, sweet potato and corn **(Maharana et al., 2009)**. The fermentation can be performed by maintaining few important parameters such as atmospheric conditions, temperature, pH-value and agitation. LA can be obtained by conducting fermentation in batch or in continuous process by using bacteria, fungi or yeast **(Sodergard et al., 2002)**. LA can also be synthesized directly from sugars such as glucose, sucrose and fructose using solid Sn-Beta zeolite catalyst **(Kimura, 2013)**. Another intermediate monomer for PLA synthesis is lactide and obtained by depolymerization of low molecular weight PLA under reduced pressure to give a mixture of L-lactide, D-lactide, or meso-lactide (figure 1.2.). Lactide is also formed by the dimerization of polycondensated lactic acid **(Sodergard et al., 2002)**.

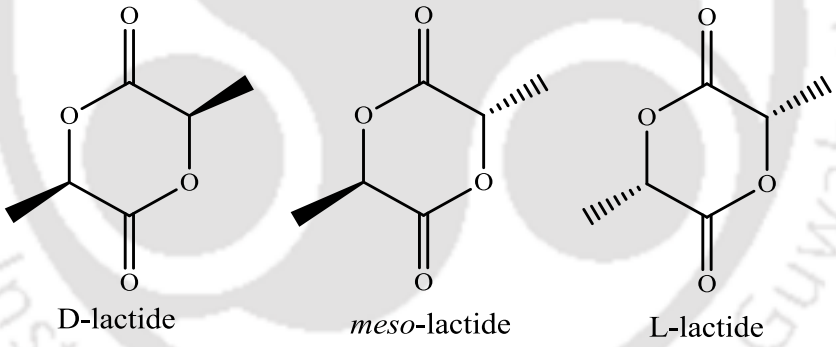

Figure 1.2. Structure of isomeric lactides.

Synthetic environment friendly polymers with precursors from natural resources such as PLA, have shown enormous potential to substitute a wide variety of conventional fossil based packaging plastics and have been demonstrated to be commercially viable. In view of this, a detailed description about various aspects of PLA such as synthesis, properties and processing have been discussed below. PLA belongs to the family of aliphatic polyesters. It is a

biodegradable polymer with a reasonable shelf life for a wide variety of consumer products, such as paper coatings, films, moulded articles, and fiber applications **(Datta et al., 1995)**.

PLA can be synthesized by various synthesis routes such as direct polycondensation, azeotropic dehydrative condensation, ring opening polymerization (ROP), melt polycondensation (MP) and solid state polymerization (SSP) of low molecular weight PLA **(Lunt et al., 1998)**. LA is polymerized by direct polycondensation to yield a viscous to brittle glassy material with molecular weight up to 10,000 Da depending on the polymerization conditions. The statistical presence (low concentration) of reactive end groups causes various unwanted side reactions such as transesterification, ester exchange and backbiting equilibrium reactions, which favours the formation of lactide as byproduct **(Garlotta, 2002)**. Subsequently, in order to avoid this unwanted equilibrium, PLA synthesis from LA is performed in the presence of a catalyst and organic solvents via azeotropic dehydrative condensation process. In this process, water is removed from the reaction system via azeotropic distillation with the organic solvent **(Ajioka et al., 1995)**. The average molecular weight of the PLA depends on the presence of moisture content, organic solvent and the type of solvent. When the solvent has high moisture content, ~ 400-500 ppm, the average molecular weight of PLA obtained is 15,000-50,000 Da. Although the polymerization time is also high (~50 h), under optimum conditions, this process yields PLA with molecular weight greater than 10^5 Da, **(Enomoto et al., 1994)**. In order to achieve high molecular weight PLA, polycondensation synthesis of moderate molecular weight PLA is first carried out through the melt polycondensation (MP) of LA in the presence of an appropriate catalyst **(Moon et al., 2001)**. Subsequently, the molecular weight is enhanced by lowering the temperature below the melting point of PLA, and carrying out SSP of the moderate molecular weight PLA prepolymer. In solid state

polymerization, reaction can be favored over depolymerization and other side reactions, because of restricted mobility of PLA chains and their end groups, and due to high activation energy required for unwanted side reactions. Particularly, in the process of crystallization of the resultant pre-polymer, both reactive end groups and catalyst, are concentrated in the amorphous region leading to the preferential condensation between the reactive end groups of pre-polymer, yielding PLA of high molecular weight upto 600,000 Da **(Moon et al., 2001)**. Scheme 1.1. illustrates the process of polymerization of lactic acid. As one of the simplest polymerization, addition polymerization of lactide, the dimer of lactic acid is capable of yielding high molecular weight PLA in short polymerization times (minutes to a few hours) via ROP.

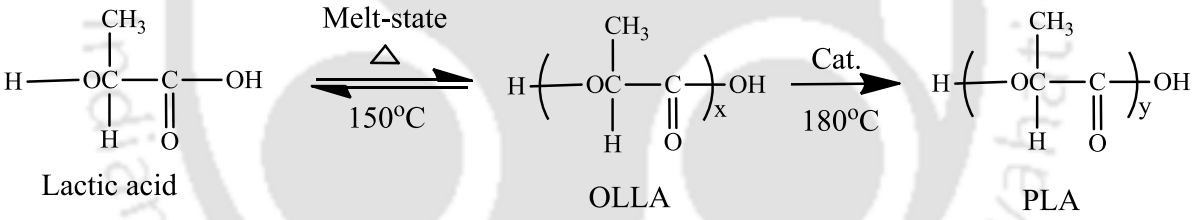

Scheme 1.1. Lactic acid polymerization.

High molecular weight PLA is a glossy, colorless, stiff, thermoplastic polymer with properties similar to polystyrene. In this section, thermophysical, mechanical, electrical, rheological, solubility and degradation characteristic properties of poly (L-lactic acid) are presented. PLA is a semicrystalline polymer with higher glass transition and equilibrium crystalline, melting temperatures, which decrease with increase in content of D-isomer. Polymer prepared from meso- or rac-lactide, is generally amorphous. The melt enthalpy estimated for a pure PLA of 100% crystallinity reported by various authors lies in the range between 93 J g^{-1} and 148 J g^{-1}

(Lunt et al., 1998; Miyata et al., 1998). The melting temperature and degree of crystallinity, are dependent on the molar mass, purity and thermal history of the polymer. However, PLA is a slowly crystallizing material, similar to poly (ethylene tetraphthalate). The fastest rates of crystallization for pure PLA occur in the temperature range of 110-130 °C, yielding spherulitic crystalline morphology. Spherulitic growth rate for PLA has been determined at 125 °C, to be 4 μm min^{-1}.

The mechanical properties of PLA are significantly influenced by its molecular weight and degree of crystallinity. By controlling these two parameters, the mechanical properties of PLA can be varied, ranging from soft and elastic plastics to stiff and high strength materials. The tensile strength and modulus of PLA increase by a factor of two, when its M_w is raised from 50,000 to 100,000 Da **(Hartmann, 1998)**. The impact strength and softening temperature increase with crystallinity and molecular weight. However, after annealing of the same PLA, the impact resistance increases due to the crosslinking effects in the crystalline region, while the tensile strength increases presumably due to the stereoregularity of the chain. However, electrical properties such as volume resistivity, dielectric constant and dielectric loss tangent of PLA at room temperature are similar to those of cross linked polyethylene (XLPE), currently used as the insulating material for cables and electric wires. The mean value of the impulse break down strength of PLA is about 1.3 times that of PE. Thus, there is a possibility for the insulation thickness reduction of electric wire and cable. Further, solubility of PLA depends on its molecular weight and degree of crystallinity. Amorphous PLA is soluble in most organic solvents such as chlorinated solvents, tetrahydrofuran, benzene, acetonitrile, and dioxane. Crystalline PLA is soluble only in chlorinated solvents and benzene at elevated temperatures. The most superior solvent till date is 1,1,1,3,3,3-hexafluoro-2-propanol (HFIP). Typical

non-solvents for lactic acid based polymers are water, alcohols (e.g., methanol, ethanol, propylene glycol), and unsubstituted hydrocarbons (e.g., hexane and heptane). PLA melt is viscoelastic in nature, exhibiting a flow behavior that is a combination of irreversible viscous flow due to the polymer chain slippage as well as reversible elastic deformation due to molecular entanglement.

Advances in the manufacturing processes of PLA together with improvements in the material properties have realized its applications in various fields including paper coating, fibers, films and packaging. The growing waste disposal problems throughout the world requires ban on some of the petroleum based polymer products such as plastic bags. In this respect, biodegradable PLA can prove to be a viable alternative to petrochemical-based plastics for several applications **(Lunt et al., 1998)**. PLA can also be used in fibers for woven & non-woven fabrics starting from cord & rope to mattresses carpeting and clothing **(Oksman et al., 2006)**. PLA blended with cotton, wool, and silk can be used to make exercise clothing, suits and even a 100 % corn fiber wedding dress. Other applications in this field include PLA carpet tiles and action wear **(Gupta et al., 2007)**.

In recent years, the demand for biodegradable polymers with excellent material properties has been growing at an enormous rate. However, PLA is considered not suitable for high strength, high performance and high temperature applications, due to its weak mechanical properties and low heat deflection temperature. In order to improve its mechanical properties such as storage modulus, flexural modulus, ultimate tensile strength and distortion at break, PLA is used with layered silicates. In literature, poly lactic acid clay nanocomposite (PLACN) with montmorillonite (MMT), synthetic mica and smectite clays, have been reported **(Chang et al., 2003)**. Virgin polymers may not meet the requirements of several food packaging applications

due to medium gas barrier properties and also require enhancement in resistance to fire and ignition or sometimes to simply reduce the cost. PLA is mixed with particles of other materials, so as to yield composite materials for enhanced properties.

Across the wide range of applications, it offers a sustainable alternative to polymeric materials used for food packaging, because of its advantages such as high transparency, processability and rigidity with relatively low crystallization rate **(Burgos et al., 2013)**. On the other hand, some of the characteristic properties of PLA, that are considered inadequate for its application as a food packaging material are poor heat stability, inferior mechanical properties and low gas barrier properties as compared to current petroleum-based polymers such as polyethylene terephthalate **(Ramos et al., 2014)**. However, PLA could be employed to make better packaging materials by modifying it with other natural polymeric materials, such as cellulose, chitosan, clay, polysaccharide gums and many more **(Arrieta et al., 2015; Bonilla et al., 2013; Raquez et al., 2013; Reddy et al., 2013)**. Hence, interest is growing on the effect of fillers on PLA to improve its characteristic properties.

1.1.2. Polysaccharide gums

The natural polysaccharides have many advantages over synthetic polymers such as low cost, easy availability, nontoxicity and biodegradability. Among the different polysaccharides, gums have tremendous applications in many fields due to its emulsifying and stabilizing properties, and are used in beverages, paints, cosmetics and pharmaceuticals. The term ‘gum’ describes the polysaccharides which have the ability to form a viscous solution, gel or stabilize the emulsion systems. The water soluble gums are also known as ‘hydrocolloids’ **(Mirhosseini et al., 2012)**. Polysaccharide gums are natural biopolymer which are abundantly available in nature. These gums find tremendous industrial applications in various fields due to their

renewability, non-toxicity and biodegradability. This thesis work is focused on four different polysaccharide gums such as gum arabic, guar gum, xanthan gum and gum rosin which are selected based on their different origin and characteristic properties.

1.1.2.1. Gum arabic

Among the various polysaccharides, Gum Arabic (GA) is a natural, biocompatible and biodegradable complex polysaccharide derived from an exudate of Acacia trees namely *Acacia senegal* and *Acacia seyal* **(Nayak et al., 2012; Ali et al., 2010)**. Gum arabic is a neutral or slightly acidic salt of complex polysaccharide containing Ca, K and Mg cations. The GA molecule has been mainly divided into three main fractions namely arabinogalactan (AG), arabinogalactan-protein (AGP) and glycoprotein (GP) components, which differ mainly in molecular mass and protein content. GA has around 90% AG fraction of ~300 kDa molecular mass with very little (~1%) associated protein, 10% AGP fraction of ~1500 kDa molecular mass, and 1% GP fraction. The AG fraction contains very little associated protein content. On the contrary, AGP and GP fractions contain around ~10% and ~20-50% of proteinaceous part respectively **(Wang et al., 2014)**.

The main chain is a highly branched macromolecule consisting of galactose units linked with β-1,3-glycoside (36-42%) (Figure 1.3). The side chains present in different fractions, which differs from product to product, are formed by L-arabinose (24-29%), L-rhamnose (12-14%), D-galactose and D-glucuronic acid (16-17%). In the principal chain, they branch off from carbon 6 of galactose units. Molecular weight observed for gum arabic was in the range $M_n > 250,000$ and $M_w \sim 880,000$ Da. (**Parija et al., 2001)**.

GA has been used in a wide range of applications such as lithography, ceramics, textiles, cosmetics, pharmaceuticals and in food, etc. It is used as a thickener, emulsifier and as a

stabilizing agent in food industries **(Islam et al., 1997; Verbeken et al., 2003)**. GA has been given a GRAS (Generally Recognized as Safe) status by United States Food and Drug Administration (USFDA) **(Nayak et al., 2012)**. Hence, it can be adopted as an additive in polymer food packaging.

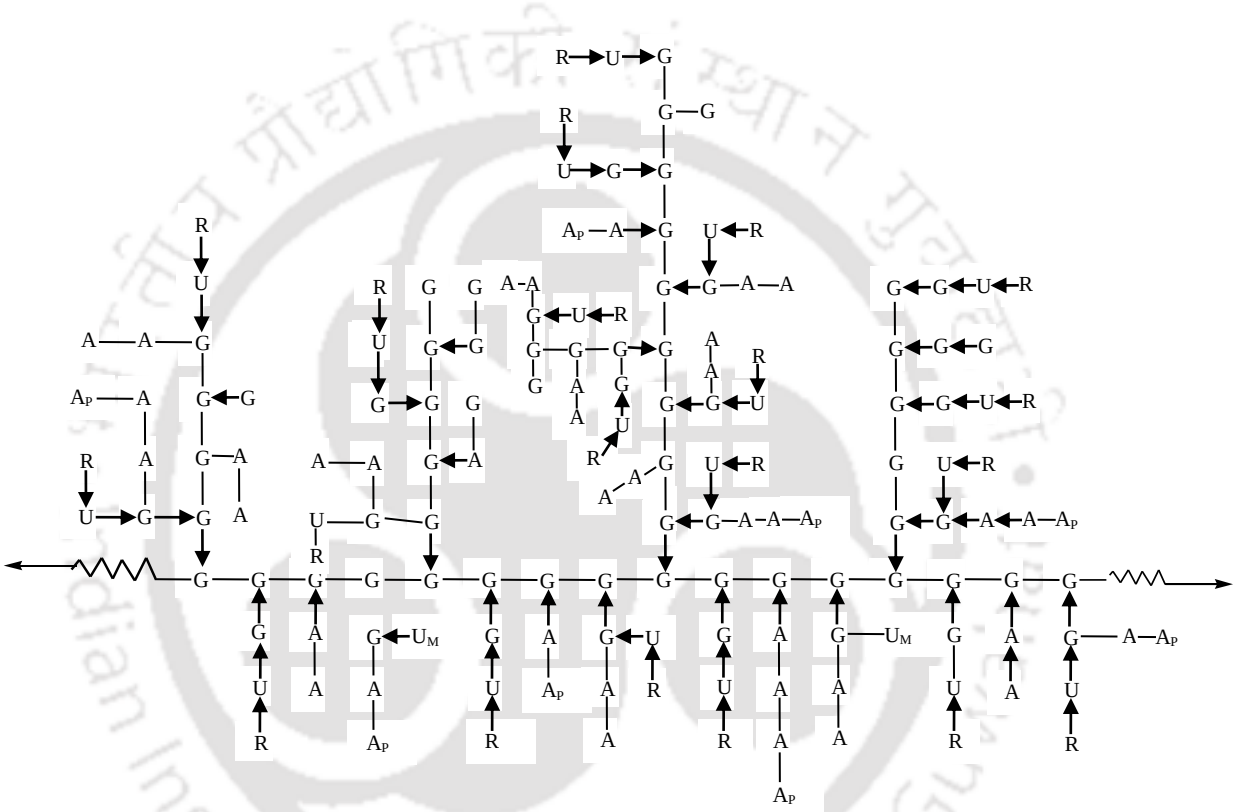

Figure 1.3. Illustration of a possible structural fragment of *A.senegal* gum having various components: R, rhamnose; Um, 4-O-methyglucuronic acid; U, glucuronic acid; Ap, arabinopyranose; A, arabinose; and G, galactose **(adapted from Islam et al., 1997)**.

1.1.2.2. Guar gum

The term guar is derived from the word "guaran" which is a naturally occurring polysaccharide **(Shahid et al., 2013; Abdel-Halim et al., 2011)**. Guar gum (GG) is a polygalactomannan obtained from the seeds of a leguminacea plant or the Indian cluster bean, *Cyamopsis tetragonolobus.* **(Manna et al., 2015; Saurabh et al., 2013; Rao et al., 2010)**. GG is mainly the ground endosperm of guar beans **(Abdel-Halim et al., 2011).** India produces 80 percent of GG of world production **(Saurabh et al., 2013)**.

Chemically, GG is a heteropolysaccharide composed of the sugars; galactose and mannose (**Saurabh et al., 2013)**. The backbone is a linear chain of (1-4)-linked β-D-mannopyranose and short side-branches are composed of ((1-6)-linked α-D-galactopyranose which are connected at every alternate mannose units (figure 1.4.) **(Manna et al., 2015; Gupta et al., 2011; Saurabh et al., 2013; Abdel-Halim et al., 2011)**. Because of the hydroxyl groups present in the molecule they are capable of absorbing water, which increases the hydrophilic properties **(Oprea, 2013)**. These nine OH groups in a single unit help in forming hydrogen bond to mineral surfaces **(Wang et al., 2005)**.

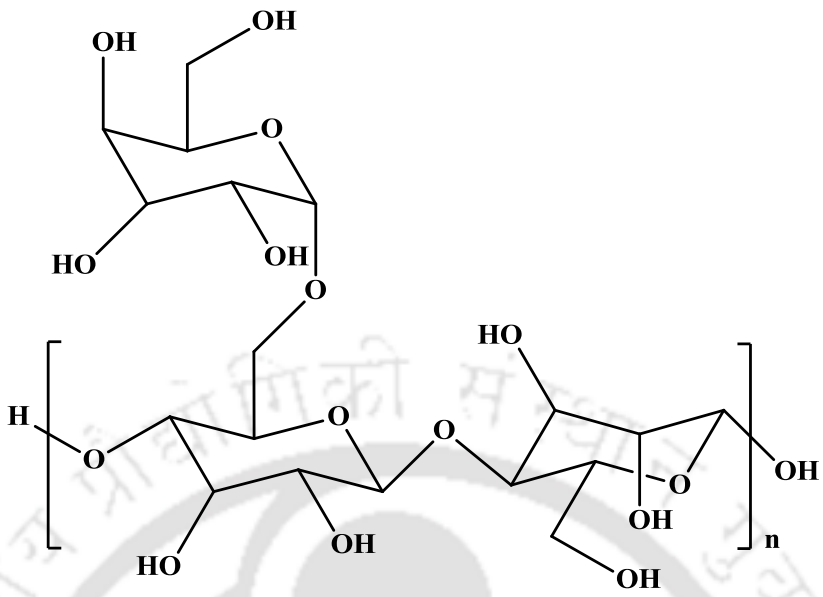

Figure 1.4. Molecular structure of guar gum.

GG is a promising component for bio-based biodegradable plastics due to its low cost, non-toxicity, easy availability and biodegradability **(Oprea, 2013; Soppirnath et al., 2002).** It is non-ionic and hydrophilic in nature which can entrap large amount of water in the range of subzero to 78 °C **(Pandey et al., 2006; Das et al., 2011)**. It has good solubility in cold water and its aqueous solution is highly viscous. It can be used in food, cosmetic and paper industry due to its capability to bear high shearing rate **(Wan et al., 2007)**. GG and its derivatives can also be used in textile industries. Some of its limitations are batch to batch variation, tendency of viscosity reduction upon storage, uncontrolled rates of hydration and microbial contagion **(Shahid et al., 2013)**.

1.1.2.3. Xanthan gum

Xanthan gum is an exopolysaccharide produced by the bacterium *Xanthomonas campestris*. Xanthan gum is an anionic hetero-polysaccharide with a primary structure consisting of repeated pentasaccharide units. These pentasaccharides are formed by two glucose units, two

mannose units and one glucuronic acid unit in the molar ratio 2.8:2.0:2.0 (Figure 1.5.) **(Garcia-Ochoa et al., 2000)**.

The primary structure of xanthan gum contains a cellulosic backbone (β-D-glucose residues) and a trisaccharide side chain of β-D-mannose-β-D-glucuronic acid-α-D-mannose attached with alternate glucose residues of the main chain. The non-terminal D-mannose unit in the side chain contains an acetyl function. The anionic character of this polysaccharide is due to the presence of both glucuronic acid and pyruvic acid groups in the side chain **(Talukdar et al., 1995).**

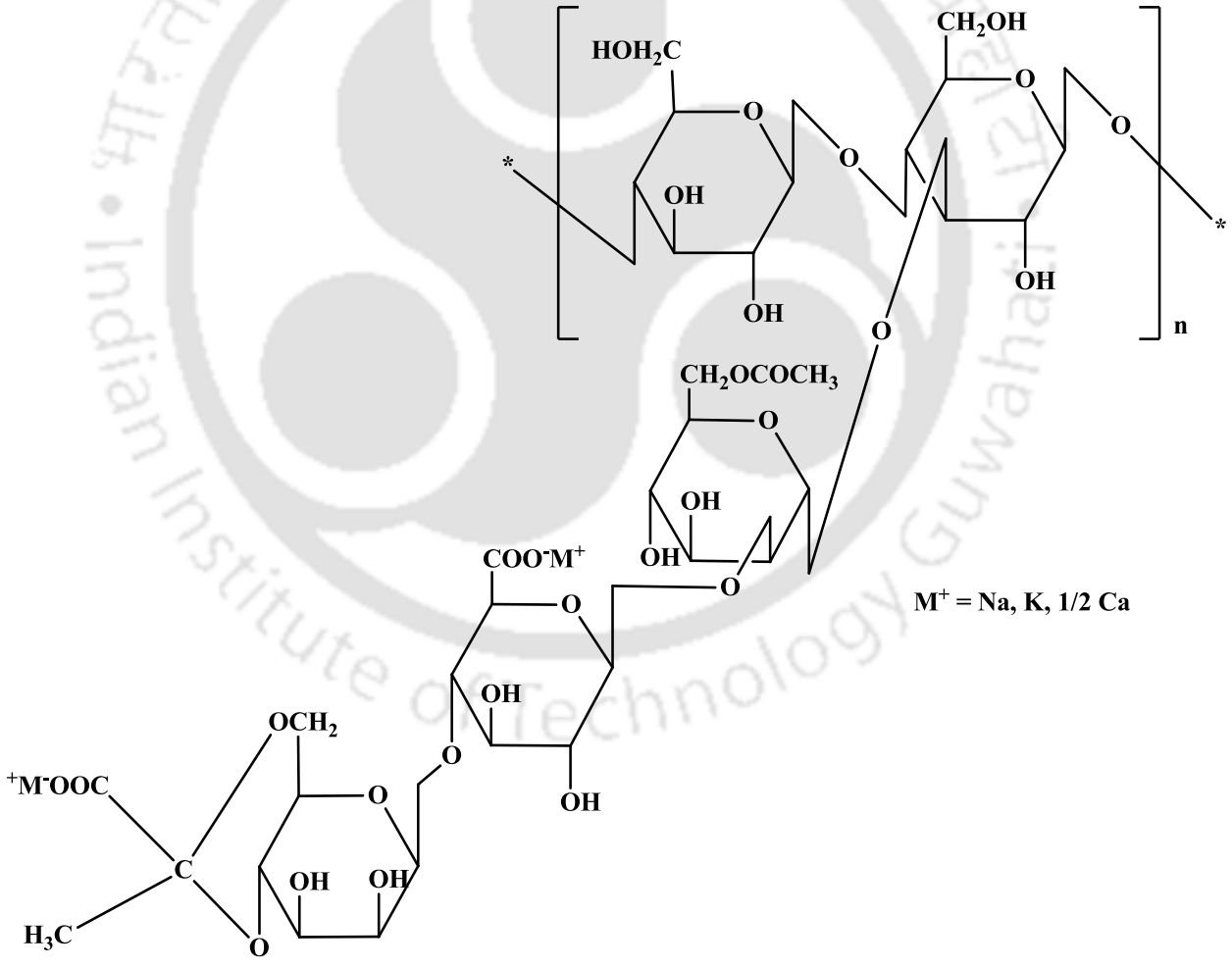

Figure 1.5. Molecular structure of xanthan gum.

The average molecular weight of xanthan gum is between 2,000,000-7,500,000 Da and 15,000,000-50,000,000 Da **(Lo et al., 1996; Bilanovic et al., 2011)**. The xanthan gum is produced by different *Xanthomonas* bacteria such as *X. vasculorum*, *X. gummisudans*, *X. juglandis*, *X. phaseoli*, *X. campestris* and *X. fragaria*. They are grown and inoculated in a bioreactor to form xanthan gum.

1.1.2.4. Gum rosin

Rosin is a thermoplastic acidic product obtained from exudates of pine trees and stump wood of various species of pine. Based on various sources, rosin is classified into three main types (a) gum rosin (b) wood rosin and (c) tall rosin. Gum rosin is recovered as residue from the distillation of turpentine which is obtained from crude turpentine pitch. Rosin is a complex mixture of naturally occurring high molecular weight organic acids also called rosin acids and related neutral materials. The rosin acids are monocarboxylic acids of alkylated hydrophenanthrene nuclei. The neutral minor or non-acidic constituents of rosin are mixture of high molecular weight alcohols, esters, aldehydes and hydrocarbons. The rosin acids and non-acidic components are generally in the ratio of 9:1 but may vary according to the source of the rosin and the extent to which it is purified. The overall chemical reactivity of rosin is mainly due to monocarboxylic acid. The predominant rosin acid in pale refined unmodified rosin is abietic acid. Other constituents are isomers of abietic acid having double bonds at different positions in the hydrophenanthrene ring or having a methyl and vinyl group instead of the isopropyl substituent. The molecular structures of the rosin acids are shown in figure 1.6. Rosin and its derivatives are extensively used in various applications in the chemical industry. They are used as industrial chemicals to modify the properties of existing formulations or to bring forth new performance characteristics of the desired products. They

are widely used in paints, varnish and coatings, ink formulations, adhesives, etc. **(Maiti et al., 1989)**

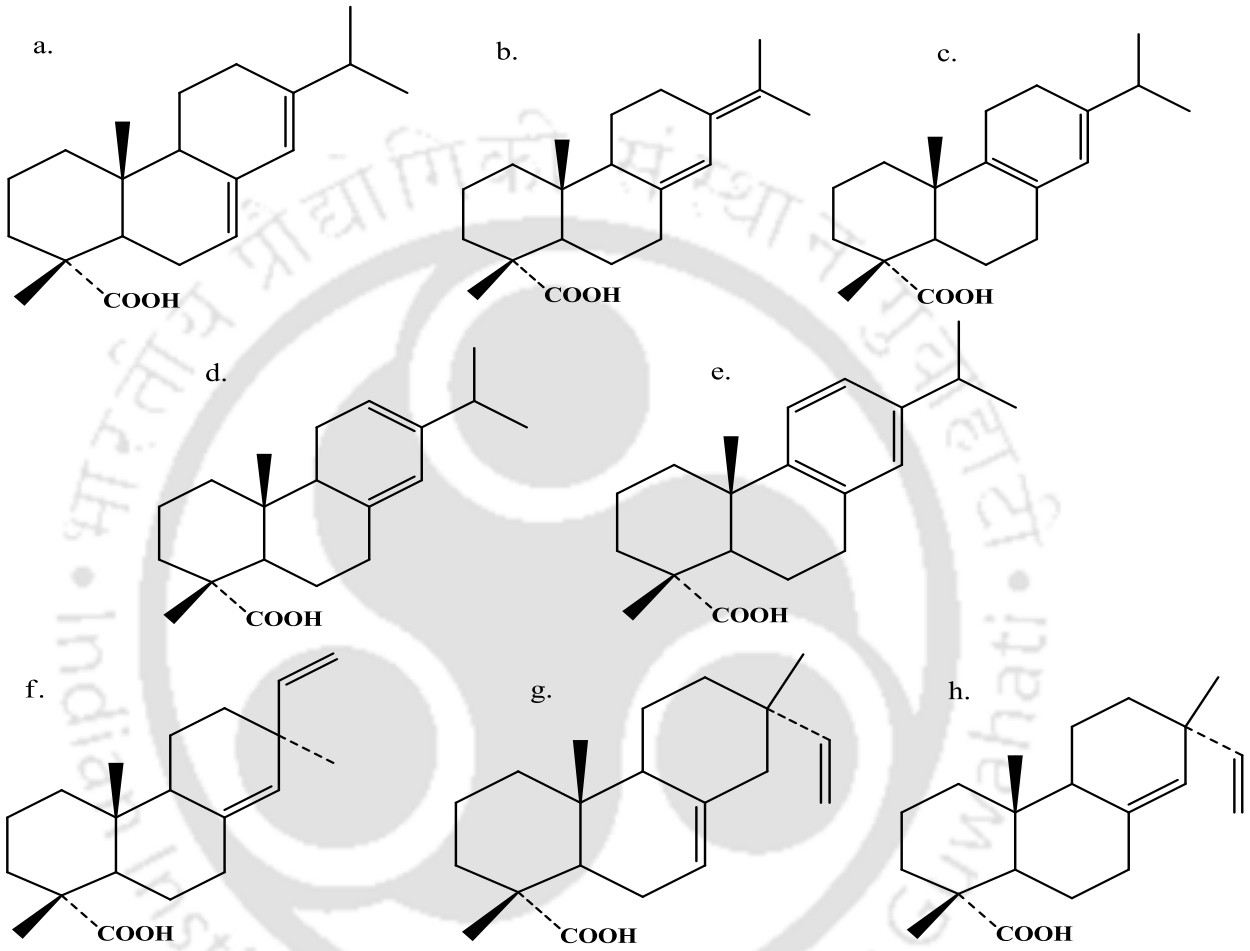

Figure 1.6. Molecular structures present in rosin: **(**a) abietic, (b) neoabietic, (c) palustric, (d) levopimaric, (e) dehydroabietic, (f) pimaric, (g) isopimaric, (h) sandaracopimaric **(Illing et al., 2009)**.

The subsequent section will be further highlighting the prior arts published in various journals and patents in line with research work carried out on poly (lactic acid) and polysaccharide gum based bionanocomposites for adhesive and gas barrier film applications.

1.2. Literature Review

1.2.1. Grafting of polysaccharide gums

Tiwari et al. (2008), synthesized electrical conducting gum acacia-graft-polyaniline using microwave irradiation. In the process, gum acacia and aniline were reacted in the presence of ammonium peroxydisulfate as oxidant/initiator and hydrochloric acid via microwave-accelerated oxidative radical polymerization. The reaction was conducted for 40 s exposed to 500 W microwave power. It was observed that electrical conductivity of GA improved for about 104 times after grafting of polyaniline (PANI). Initiator has been used in this prior art to improve grafting but no catalyst has been used in the current proposed art.

Kaith et al., 2010 was studied the grafting of gum arabic and methacrylic acid. The copolymer was synthesized in the presence of potassium persulfate as initiator by free radical polymerization. The three-dimensional cross-linked structure of the copolymer was achieved by using hexamethylene tetramine which acts as a crosslinker. The reaction has was carried out in vacuum between 250-550 mm Hg for 120-360 min. It was observed that the produced copolymer was temperature and pH sensitive and exhibited salt-resistant swelling. It has wide applications in drug delivery devices and water treatment industries.

Abdel-Razik et al., 2013, studied graft copolymerization of acacia gum and acrylonitrile in aqueous media using potassium permanganate in the presence of nitric acid as a catalyst. The copolymerization was carried out in closed Pyrex cells. The reaction was carried out between 0.5 to 3 h by keeping the cells between 40 W fluorescent lambs. The polymerization was

stopped by pouring the obtained product in methanol and the product was precipitated out. The successful grafting of acrylonitrile onto acacia gum was observed using redox system in air which was induced by visible-light irradiation. The percentage grafting obtained for the system was 268%.

Tiwari 2007, studied the grafting of gum arabic and polyaniline by radical polymerization by using peroxydisulfate as initiator and oxidant. Grafted gum arabic and polyaniline (GA-*g*-PANI) was synthesized by dissolving GA in water and then adding aniline and HCl. The reaction mixture was heated at 40 °C while stirring. Peroxydisulfide was added after 30 min to initiate grafting. The grafting was conducted for 2 h which was neutralized by NaOH. The maximum electrical conductivity of the product at pH 1 was 5.18×10^{-2} S cm^{-1} which can be used for preparing environmentally friendly semiconductor devices and can be used for sensor applications.

Mishra et al., 2015 synthesized a graft copolymer of partially carboxymethylated guar gum (CMGOH) and N-vinylformamide (NVF) by free radical polymerization. The reaction was conducted using 2,2-Azobis [2-(2-imadazolin-2-yl) propane] dihydrochloride (AIPH) as initiator. The grafting of CMGOH, NVF and sulphuric acid was conducted at different temperature (35 to 55 °C) and reaction time (60 to 180 min). AIPH was added as initiator. The reaction was conducted for 30 min in an inert atmosphere. The grafted copolymer was precipitated in water-methanol (1:4) mixture which was filtered afterwards. Based on the metal ion uptake, swelling behaviour and flocculating properties, it was concluded that the synthesized product can be used in applications which requires flocculation and superabsorbtion.

Likhitha et al. 2014, studied the guar gum grafted sodium acrylate/cloisite synthesized via conventional and microwave assisted technique for the preparation of superabsorbent nanocomposites. The synthesis was conducted in an inert atmosphere by dissolving 1 g GG in 250 ml distilled water. Thereafter, 2 g sodium acrylate was added to the dispersion. APS (100 mg) and MBA (95 mg) were added to the solution which act as initiator and crosslinker respectively. In the conventional heating method, reaction was conducted at 70 °C for 1 h. After completion of the polymerization, the solution was washed with acetone in which the desired copolymer was precipitated. In microwave heating method, the reaction was conducted at 70 °C at 800 W. In the conventional heating method, the reaction was conducted from 10 to 60 min whereas, in microwave heating, the reaction was carried out from 2 min to 15 min. The maximum percentage grafting in conventional method was around 8.8 % after 60 min, however 11.12 % grafting was obtained in microwave heating method after 10 min. Hence, the enhanced reaction rates were observed in the microwave technique with respect to the conventional heating technique. Enhanced swelling properties were also observed on addition of cloisite on to the grafted material. The increased water holding capacity was due to the exfoliation caused by dispersed cloisite into the polymer matrix. The nanocomposites proved to be a superabsorbent within a wide pH range.

Pandey et al. 2014, studied the grafting of guar gum onto N,N´-*dimethylacrylamide*. The grafting was carried out in an inert atmosphere and was initiated by using potassium peroxymonosulphate/glycolic acid redox pair. The reaction was carried out by mixing N,N´-*dimethylacrylamide*, sulphuric acid and glycolic acid with guar gum solution. The reaction was terminated by passing air into the reaction vessel. Thereafter, the graft copolymer was obtained by precipitating the copolymer into the water-methanol mixture. The results

detected that grafting occurred at hydroxyl groups present in guar gum. The enhancement in physicochemical properties such as metal ion sorption, flocculation and swelling was observed.

Pandey et al. 2012, studied the microwave induced emulsion copolymerization of xanthan gum and ethylacrylate. Potassium peroxydisulphate (KPS) was used as initiator in the synthesis. The effect of monomer concentration, initiator concentration, microwave power and exposure time was also investigated. The grafting was conducted by dissolving 0.1 g of xanthan gum in distilled water. KPS and EA were added to the solution and reaction was conducted in domestic microwave with 2450 MHz microwave frequency. The power output was maintained from 0 to 900 W with exposure time in the range of 5 to 20 s. After the reaction, xanthan-*graft*-polyethylene was precipitated in acetone to remove the unreacted homopolymer. It was concluded that the chemical modification increased the adsorption capacity of Pb^{2+} to four times than that of xanthan gum.

1.2.2. Adhesive application of bio-based materials

Polysaccharide gum based adhesive

Norstrom et al., 2014 prepared an environment friendly wood adhesives by dispersing guar gum, xanthan gum, locust bean gum and tamarind gum. The dispersion of gums were prepared by mixing the gums in de-ionized water and heating at 60 °C for 6 h in an oil bath. The film formation of the adhesives were tested by applying the materials on glass surfaces. It was found that the locust bean gum and guar gum form inhomogeneous and rough surface when applied. Transparent and smooth film was formed by the xanthan gum dispersions, although the air bubbles were present in it. Tensile shear strength of all the gums applied on wood substrates were less than 16 MPa. Hence, it was concluded that the gums were evaluated as wood adhesives.

Lactic acid based adhesive

Edgington et al. (1997), developed biodegradable/compostable hot melt adhesive consisting polyester of 2-hydroxypropanoic acid (lactic acid). Different formulations were prepared using poly (lactic acid), tackifier, plasticizer, stabilizer etc. The hot melt adhesive were demonstrated for Kraft paper adhesion.

Viljanmaa et al. (2002), formulated lactic acid based hot melt adhesives using co-monomers based on poly (ε-caprolactone) (PCL) and poly (L-lactide) (PLLA) (molar ratio 81:19) was developed. The polymerization of PLLA and PCL was done in the presence of tin-octoate catalyst. The prepared adhesive can be used in biodegradable packaging materials i.e. for different variety of cardboards whereas maximum lap shear strength was reported around 1.2 MPa, and 1.5 MPa for KLB (Kraft linerboard).

Viljanmaa et al. (2003), modified PCL/PLLA (molar ratio 81:19) hot melt adhesive. Acetic anhydride was used to chemically stabilize the formulation and was limited by unwanted thermal degradation caused during processing. The formulated adhesive was used for laminating commercial polylactide based film and cardboard. It was concluded that the adhesive can be applied with normal processing equipment.

1.2.3. Packaging applications of bio-based materials

Polysaccharide gum based films

Wyasu et al., 2012 improved the film forming ability of gum arabic by using some additives such as cross-linking agents and plasticizers. The 25 g of the crushed gum arabic grains were dissolved in 100 ml water and 10 ml of various additives were added. The additives used in the work were pure glycerol, diethyl glycol and ethylene glycol. The films were cast on thin layer chromatographic plate. High extent of blistering was observed for neat gum arabic film

which was reduced with the addition of the additives. High level of smoothness, softness and flexibility was observed for the films prepared using additives. From the scratch adhesion test, it was also observed that the plasticized films heve better quality than that of non-plasticized gum arabic film.

Li et al., 2015 prepared the films using peanut protein isolate (PPI) which were glycated with gum arabic. It was compared that the neat PPI, PPI-gum arabic mixtures and glycated PPI-Gum arabic conjugate films. The PPI and gum arabic conjugates were prepared initially by mixing in water in 1:1 weight ratio and the pH was adjusted to 7.0. Then the solution was lyophilized at -70 °C. The mixture was then incubated at 60 C and 79% relative humidity for 3, 6, and 9 days. The three types of films namely neat PPI, PPI-gum arabic mixtures and glycated PPI-Gum arabic conjugate were prepared by mixing the components with 10 % (w/w) deionized water. The plasticization effect was imparted by 25% glycerol in each solution. The solutions were dispersed by magnetically stirring. The degassing was done under vacuum. Films were poured onto polystyrene Petri dishes. Finally, the films were dried in oven at 50 °C. The cross-linking of PPI with gum arabic resulted in 2 to 2.5 fold reduction in water vapor permeability with respect to neat PPI films. After 3 days of glycation, increase in tensile strength was observed but decrease in water vapor permeability. However, reduction in elongation was observed. It was concluded that different degree of glycation has significant effect on properties of the film.

Sakloetsakun et al., 2015 prepared chitosan-gum arabic polyelectrolyte complex films to study the physicochemical, mechanical and mucoadhesive properties. For the preparation of films, initially the dispersed solution of chitosan and gum arabic were prepared. The dispersed chitosan solution was prepared by dispersing low molecular weight chitosan in 1% (v/v) acetic

acid solution and the pH was adjusted by using acetate buffer. The GA dispersions (5%, w/v) were prepared in acetate buffer at different pH. Thereafter, under vigorous agitation CS-GA dispersions were prepared in weight ratios of 1:0, 1:0.25, 1:0.5, 1:0.75 and 1:1. The solutions were then cast onto films and the films were prepared by solvent evaporation method. It was observed that chitosan and gum arabic form a continuous films of different concentration. High mechanical strength was observed for CS-GA films as compared to CS films. However, it was also observed that the addition of GA reduces the extensibility of the films which leads to more brittle films. Furthermore, no significant change in water vapor permeability was observed for the films. It was concluded that CS-GA (1:0.5) films exhibited relatively low erosion, puncture strength and water uptake with respect to neat chitosan film. It was suggested that they molecularly interact via intermolecular hydrogen bonding and electrostatic forces due to which relatively lower water vapour permeability, low water uptake, erosion and puncture strength were observed as compared to neat chitosan film. It was also suggested that using chitosan-gum arabic films can be advantageous for the formulation of drug delivery systems and coatings.

Ali et al., 2010 prepared coating of gum arabic for tomato fruit to enhance the shelf life and postharvest quality. The coating solutions were prepared by dissolving gum arabic in purified water at 5, 10, 15 1nd 20 % (w/v). The solutions were stirred magnetically at 40 °C for 60 min. After cooling, glycerol monostearate (1.0%) was added as plasticizer to impart flexibility and strength. The fruits were then dipped into the solutions for 2-3 min. Thereafter, the fruits were air-dried, packed and stored in 20 °C and 80-90 % RH. From the results it was observed that 10% gum arabic which was used as an edible coating delayed the ripening process as well as the storage life of tomatoes was extended up to 20 days without any off-flavor or spoilage.

Das et al., 2011 developed a water resistant biomaterial biocide film by using guar gum. The benzoylation of guar gum was carried out in water medium by reacting guar gum with benzoyl chloride and propyl amine spacer to achieve high degree of hydrophobicity. The guar gum benzamide (GGBA) was synthesized from the obtained guar gum alkyl amine (GGAA). Initially, GGAA was dispersed in aqueous sodium hydroxide solution and benzoyl chloride was further added in reaction mixture. The filtered resultant GGBA was washed with n-hexane, ethanol:water (50:50, v/v) and water. The GGBA film was produced by dissolving it into DMSO into propylene dish which was dried in air oven. The synthesized guar gum benzamide was resistant to water and soluble in dimethyl sulfoxide (a non-aqueous solvent). The breaking point tensile strength of the film having thickness 0.162 mm was observed at 21.95 MPa. The water contact angle and water vapor permeability of the film were 90.35° and 0.28 g mm kPa^{-1} h^{-1} m^{-2} respectively. It was also observed that the synthesized cast film strongly inhibit gram positive and gram negative organisms such as *Bacillus subtilis*, *Escherichia coli*, *Salmonella enterica* and *Staphylococcus aureus*. The strong absorption of UV region was observed by guar gum benzamide.

Gupta et al., 2012 prepared guar gum-polyvinyl alcohol (GG-PVA) blend films by mixing glutaraldehyde as crosslinker and citric acid as additive. The blend films were prepared by dissolving GG and PVA separately in water. After that, GG-PVA (0.6-0.4 weight fraction) was mixed well with citric acid and glutaraldehyde in different fractions. The obtained homogenous gel like solutions were cast on polypropylene disc and kept for drying. The increase in tensile strength was observed with increase in glutaraldehyde content. However, decrease in % elongation, degree of swelling and porosity was observed on addition of glutaraldehyde as

compared to noncrosslinked films. It was concluded that glutaraldehyde was an effective crosslinker for guar gum-polyvinylalcohol films in the presence of citric acid.

Saurabh et al., 2013 studied the effect of gamma radiation dose in physicochemical, mechanical and barrier properties of guar gum based films. A ^{60}Co gamma irradiator was used having dose rate of 4.1 kGy hr^{-1} and exposed to GG and control unirradiated GG films at various dose. The GG films were prepared by mixing GG (1.5 g) into 150 ml water with glycerol (acts as a plasticizer). The solution was poured in glass plate and kept for drying at 80 °C. The irradiated films also showed 15% improvement in water vapor barrier properties. Significant increase in tensile strength was observed for GG films irradiated up to 500 Gy as compared to non-irradiated control films. However, tensile strength decreases with increase in exposure to irradiation dose when kept more than 500 Gy.

Manna et al., 2015 studied the synthesis of carboxylmethyl guar gum (CMGG) from the native guar gum (GG). Thereafter, CMGG was grafted with gelatin and mixed with curcumin to prepare a biomaterial. Initially, CMGG-g-gelatin was prepared by using N-hydroxy succinamide and 1-ethyl-3(3-dimethyl aminopropyl) carbodiimide (EDC) due to which covalent bond was formed between CMGG and gelatin. Consequently, curcumin loaded CMGG-*g*-gelatin film was prepared by non-covalent interaction method. Firstly, 1 mg ml^{-1} of curcumin in acetone was mixed with CMGG-*g*-gelatin solution. The precipitated product was removed which was formed during the mixing of the components. Thereafter, the obtained solution was poured into polypropylene plate and kept for drying. The enhancement in thermal stability and mechanical property was observed in CMGG-*g*-gelatin film with respect to neat CMGG and gelatin film. As curcumin has antibacterial activity, incorporation of curcumin in CMGG-*g*-gelatin film can efficiently be used as wound healing material. It was also observed

the improvement in functional properties of gelatin as well as guar gum on incorporation of curcumin into CMGG-g-gelatin.

Veiga-Santos et al., 2005 studied the effect of pH modification, additives (propylene glycol, sodium phosphate, sucrose and soybean oil) and deacetylated xanthan gum on hydrophilicity, water activity and mechanical properties of cassava starch-xanthan gum films. The films were prepared according to the casting technique, by blending of cassava starch (3-5% w/w) with water and acetylated or deacetylated xanthan gum (0–1% w/w), propylene glycol (0–1% w/w), sodium phosphate (0–0.2% w/w), sucrose (0–2% w/w) and soybean oil (0-0.06% w/w). Medium pH was adjusted and heated to 75 °C with constant stirring. The films were cast on Petri plastic dishes. The control film was prepared by adding 5% cassava starch in water and neither additives were added nor pH was adjusted. On comparison of acetylated and deacetylated xanthan gum, it was observed that the deacetylated xanthan gum has higher effect on elongation at break. It was observed that, on removing the acetylated group from the molecular chains of the gum associate resulted in increase in viscoelasticity. This on interaction with starch network resulted in higher elongation at break. The deacetylated gum also resulted in increase in water absorption which was due to the positive effect of deacetylated xanthan gum on water absorption kinetic of the film. It was also observed that the addition of sucrose and deacetylated xanthan gum resulted in slight increase in hydrophilicity.

Ge et al., 2015 studied the effect of amino-functionalized montmorillonite (NH_2-MMT) content with gelatin and dialdehyde xanthan gum (DXG) as the crosslinking agent to prepare composite edible films. The DXG was used as it was the ideal cross-linking agent of gelatin as it improves properties of gelatin as well as restricts the phase separation between gelatin and DXG. The DXG was prepared by dissolving xanthan gum in water and then adding sodium

periodate solution. The pH was adjusted to 5.0 and stirred for 4 h at 40 °C. Thereafter, the oxidized product namely DXG was precipitated and, washed with distilled water and anhydrous ethanol. The NH_2 was grafted on the attapulgite surface to prepare NH_2-MMT. The gelatin based composite films were prepared by blending gelatin powder (1 g) with 15 ml distilled water for 30 min at 40 °C. Then, NH_2-MMT (0.02 g) was added and the obtained mixture was frozen for 24 h at -20 °C. Consequently, DXG solution was added as crosslinking agent and glycerol was added as plasticizer at room temperature. After stirring at 40 °C, the mixture was poured onto PTFE dishes. The control film was prepared by crosslinking DXG with gelatin. It was observed that the amino-functionalization of MMT provides active sites to crosslink and produce compact networks among gelatin, dialdehyde xanthan gum and amino-functionalization of MMT. It was concluded that several properties such as water resistance, UV light barrier property, thermal stability and mechanical property increased with NH_2-MMT content in the composite films. It was observed that the compact network structure among NH_2-MMT, gelatin and DXG was imparted because of the active sites provided by NH_2-MMT for crosslinking DXG.

Bueno et al., 2014 studied the molecular confirmation of xanthan chains in xanthan hydrogel films prepared in presence of citric acid (XCA) and in absence (XNT). From the study it was observed that ordered conformation (helixes) of xanthan chains were present in XNT hydrogel films and disordered conformation (coils) in XCA films. The xanthan-based hydrogel films were prepared homogenization and then centrifugation for 3 to 5 min at 18,000 and 3600 rpm. Then, the films were prepared by casting xanthan aqueous solution (6 g l^{-1}) with and without citric acid (0.3 g l^{-1}) at 45 °C overnight. It was also observed that the ability to load and release

proteins was controlled by hydrogels and proteins net charges in XNT and XCA hydrogel films.

Guo, et al., 2014 studied the preparation of oxidized xanthan gum with different aldehyde content which was used as crosslinking agent for gelatin edible films. The gelatin-xanthan gum and gelatin-oxidized edible films were prepared by the casting method using glycerol as a plasticizer. Oxidized xanthan gum was prepared by dissolving 1.0 g xanthan gum in 25 ml distilled water. Sodium periodate solution was added to the xanthan gum solution at different concentration. The pH of the solution was maintained at 5.0 which was stirred in the dark for 4 h at 40 °C. Thereafter, the oxidized xanthan was precipitated, recovered and cross-washed with distilled water and ethanol. The gelatin-xanthan gum and gelatin-oxidized xanthan gum were prepared by dissolving gelatin (10%, w/v) in distilled water at 60 °C and adding glycerol (20 wt% on gelatin dry weight). Xanthan or oxidized xanthan gum solution (1%, w/v) was added at concentration of 5 wt% (based on dry gelatin weight) into gelatin solution which was stirred and then was cast onto teflonated petri dishes. It was observed that xanthan gum drastically reduced the moisture content, water vapor permeability and total soluble matter. Great improvement in thermal stability and mechanical properties were observed in gelatin film. Similarly in gelatin oxidized xanthan gum films, increase in thermal stability, mechanical properties and water barrier properties were observed with increase in the oxidization level of xanthan gum due to the covalent bonds formed between gum and gelatin. However, reduction in thermal stability and mechanical properties were observed on excessive degradation of xanthan gum.

Jina et al., 2015 studied the influence deacetylation degree (DD) of konjac glucomannan on tensile strength, elongation at break, transparency and FTIR. The phase separation of konjac

glucomannan/xanthan gum blended films were also investigated through film forming properties. The blend films were prepared by dissolving xanthan gum into distilled water and stirred for 2 h. Deacetylated konjac glucomannan (DKGM) was prepared by dissolving KGM powder into Na_2CO_3 solution at 80 °C. Thereafter, obtained DKGM was mixed with xanthan solution and glycerol. The mixture was stirred for 30 min at 80 °C. The resultant solution was cast into films. Higher elongation at break and moisture absorption was observed for DKGM/XG blend films than that of pure DKGM films. It was concluded that safety, easy production, cost saving and controlled degradability makes the blend films potential candidate which can be applied for studying phase separation between two macromolecules.

Gutierrez et al., 2014 designed a novel functional nanostructured polymeric blend using gum rosin. The thin films were prepared by dissolving S4VP and GR in a one-step pathway using spin-coating at 2000 rpm for 120 s. Gum rosin was used to fabricate novel polymeric blends with long range order nanopatterns using poly(styrene)-*block*-poly(4-vinylpiridine) S4VP block copolymer as nanostructuration agent.

Poly lactic acid based films

Onyari et al., 2008 prepared hydrophobic PLA and hydrophilic GA blend films. The films were prepared from 2% solution of PLA in chloroform. Then, 0-90% of GA was added in the solution to obtain PLA/Gum arabic blends which were mixed and sonicated for about 20-30 min. Thereafter, the films were prepared by conventional solvent casting method from chloroform solution. The casting was done on glass petridishes to obtain the films. The biodegradation study was conducted using thermophilic bacteria. It was observed that the thermophiles isolate 1 was active at 45 °C and the activity reduces with decrease in temperature

that is at 37 °C. It was also observed that thermophiles isolate 4 was active at 37 °C as well as at 25 °C. It was concluded that thermophiles isolate enhances the degradation of blend films.

Burgos et al., 2013 studied the plasticization effect of oligomeric lactic acid (OLA) in poly(lactic acid) (PLA) films. The films were prepared by melt-blending PLA and OLA at different concentrations between 15 to 25 wt%. The aging of the films were also studied by storing the films for 3 months under ambient controlled conditions. The PLA-OLA films were prepared by drying the PLA pellets overnight at 60 °C. Thereafter, the pellets were milled to fine particle size to increase the contact area as well as accurate mixing of plasticizer or OLA into polymer matrix. The pre-mixing of PLA with OLA was done manually at different concentrations. The components were then melt-blended in high-shear roller rotors with 50 rpm speed at 170 °C. The pressure between the press plates was increased to 5 MPa which was maintained for 5 min. From the results it was observed that, the incorporation of OLA into PLA film resulted in decrease in elastic modulus and oxygen barrier property but increase in elongation at break. The decrease in elastic modulus suggested the decrease in rigidity of PLA films due to plasticization effect imparted by OLA. The enhancement in ductility was confirmed by the increase in elongation at break which was correlated with decrease in glass transition temperature. As the elongation at break was higher for the OLA plasticized films compared to glycerol, PEG or DOA suggested that PLA-OLA blend films can be used for the applications which require higher ductility. Increase in oxygen transmission rate was explained by the increase in free volume in the matrix caused by plasticizer. The OTR × e values of 25 wt% OLA film showed two times enhancement with respect to neat PLA film. As PLA-OLA films showed lower OTR × e values than that of LDPE films, suggested that PLA-OLA films could be acceptable for food packaging applications. OLA proved to be an

efficient plasticizer for PLA which significantly decreased glass transition temperature and considerably improved ductile properties. Among the different concentration films, PLA-20 wt% OLA proved to be the only one which maintained amorphous state with adequate properties required for manufacturing flexible films. High compatibility of OLA with PLA was also observed as no phase separation was detected till 25 wt%.

1.3. Gaps in the Prior Art

Extensive literature survey revealed that very less efforts were made to improve the characteristic properties of polysaccharide gums for adhesive and food packaging applications. It was observed that the polysaccharide gums were not compatible with PLA due to its hydrophilic nature. Even though it has been demonstrated that some of the polysaccharide gums have film forming ability, they cannot be utilized in packaging and other applications due to some limitations. Hence, researchers have found many ways such as blending, mixing and grafting to avoid such limitations. As per the available literature such techniques were conducted by using various initiators, catalysts, additives and solvents in order to improve the functionalization or productivity. In such a way, a lot of reduction in polymer waste was noticed but the extensive use of additives is not making the polymeric products fully bio-based and biodegradable, which is also an area of concern. It was also inferred from the literature survey that very less efforts are made to synthesize a bio-based adhesive with comparable adhesive strength as in conventional adhesives for structural applications due to its hydrophilicity.

Based on the literature survey, it was observed that no work has been published on: (a) the preparation of modified hydrophobic gum based bionanocomposites using lactic acid, (b) use

of gum based bionanocomposite for adhesive applications and (c) use of gum based bionanocomposite for food packaging applications.

As a result of which, the present doctoral work focused on the two applications such as (i) adhesive application and, (ii) packaging application. In adhesive application, the polysaccharide gums (GA, GG, XG and GR) are utilized to minimize their hydrophilicity by condensation polymerization with lactic acid. Further, the prepared modified gums are tested for adhesive application. In packaging application, the hydrophobic modified polysaccharide gums are utilized as a filler with PLA in order to improve its characteristic properties.

1.4. Objectives of the Present Work

To achieve the overall objective, preliminary research have to be examine towards

- the screening and selection of lactic acid grafted polysaccharide gums for adhesive and food packaging applications,
- the detailed characterization of the optimized bionanocomposite obtained for the applications,
- the detailed study of bio-based adhesive showing the highest adhesive strength,
- the detailed study of the masterbatch which gave the best properties after preparation of bionanocomposite with PLA for food packaging applications,
- and the thermal degradation kinetic study of the film to predict material behavior under high-temperature applications or working conditions such as processing, storage of materials and service life time.

Chapter 2

Materials and Methods

This chapter presents the materials used and protocols for various experiments performed in the research work. The synthesis procedures followed for the synthesis of modified gums have been included. The calculation methodology for converting raw experimental data into appropriate domain have been elaborated. The determination of characteristic properties of the samples for their analysis have been discussed.

2.1. Materials

L-lactic acid (LA; PH 90) was procured from Purac®, India. Poly (Lactic Acid) (PLA) (granular form; 2003D; density: 1.24 g cm^{-3}) was procured from NatureWorks®, USA. Gum arabic (GA) from acacia tree (branched polysaccharide), guar gum (GG), xanthan gum (XG) and gum rosin (GR) were purchased from Sigma-Aldrich (India). Chloroform (extra pure, Merck, India) was used as a solvent for film fabrication, and chloroform (HPLC grade, Merck, India) was used for analysis. Deuterated water (D_2O) and deuterated chloroform ($CDCl_3$) were procured by Sigma-Aldrich (India). Millipore water (Metrohm, ELIX 3) was used for cleaning purpose. All the chemicals were used without further purification. Glasses and granite pieces were purchased from the local market of Guwahati, India, which were utilized in shear test.

2.2. Methods

2.2.1. Conventional heating method for the synthesis of gums grafted poly l-lactic acid

Initially, 100 g of lactic acid (LA) was taken in a round bottom flask (RBF) and 10 % (wt/wt) of GA was added into it for modification using polycondensation reaction in absence of catalyst. The solution was stirred using magnetic bead at ~ 400 rpm. In argon (Ar) atmosphere, it is heated for 150 min at 150 °C. Thereafter, vacuum was applied for 390 min. During initial 240 min, the vacuum inside the reactor raised from 1000 to 0.5 mbar and afterwards it was maintained at 0.1 mbar. Finally, vacuum was broken using inert gas. The water as condensate and other byproducts were collected in an ice-cooled trap which was connected in series with condenser as shown in figure 2.1. The prepared material (modified GA) was stored in a sealed vial for further use. Similar procedure was followed for the modification of GG, XG and GR. The *oligo*-(L-lactic acid) (OLLA) was also prepared from LA under identical operating conditions.

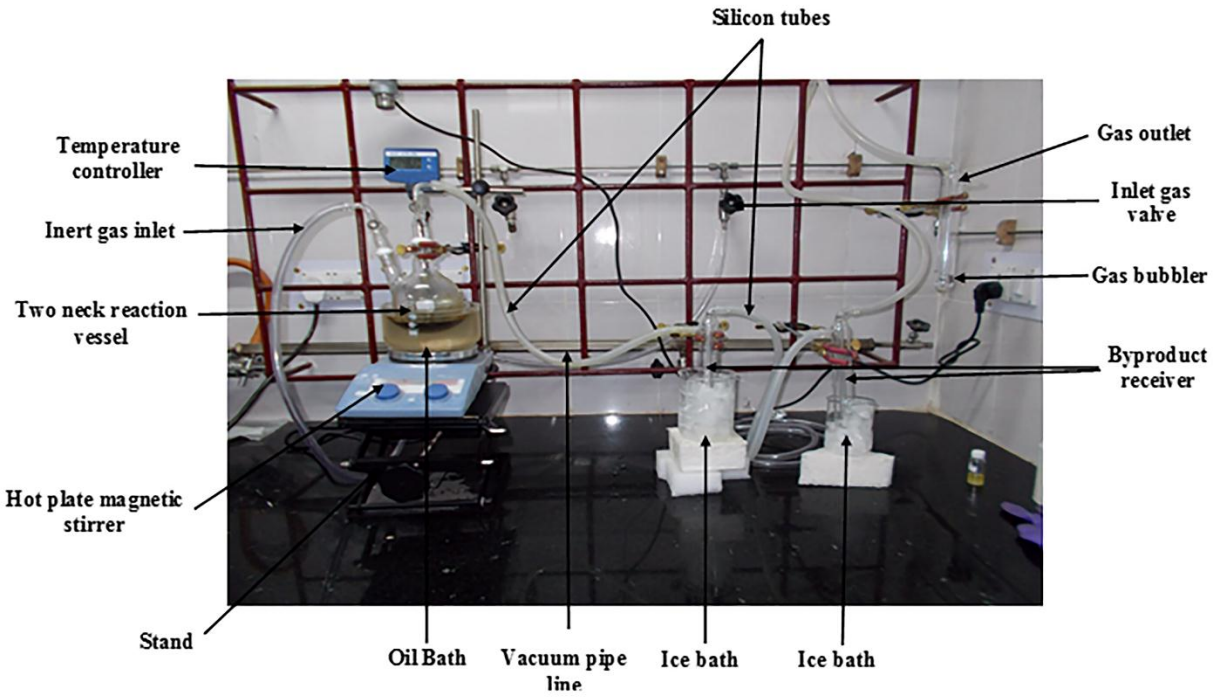

Figure 2.1. Conventional heating setup for modification of the gums.

2.2.2. Microwave initiated synthesis of gums grafted poly l-lactic acid

The in situ polycondensation reaction was performed for the modification of gums such as GA, GG, XG and GR under Argon atmosphere. Initially, LA and gums were manually mixed in the proportion of 10:1 (%, wt/wt) in the RBF. The RBF was fixed in microwave reactor and inert atmosphere was maintained into the RBF under convection cum microwave mode with set temperature of 130 °C for 45 min at 240 watts as shown in figure 2.2. The temperature was maintained at 100 °C between RBF outlet and condenser to avoid clogging of byproducts and subsequently, the condensate (byproducts) was collected in the trap. After completion of reaction, the prepared modified gums were stored in sealed vials for further use. Same operating conditions were followed for the preparation of *oligo*-(L-lactic acid) (OLLA). Similarly, the various concentrations of GA such as 5, 10, 15 and 20 (%,wt/wt) were used to

synthesize different concentrations of GA-*g*-PLA bionanocomposite. Finally, the synthesized GA-*g*-PLA bionanocomposites were kept in sealed vials for further analysis.

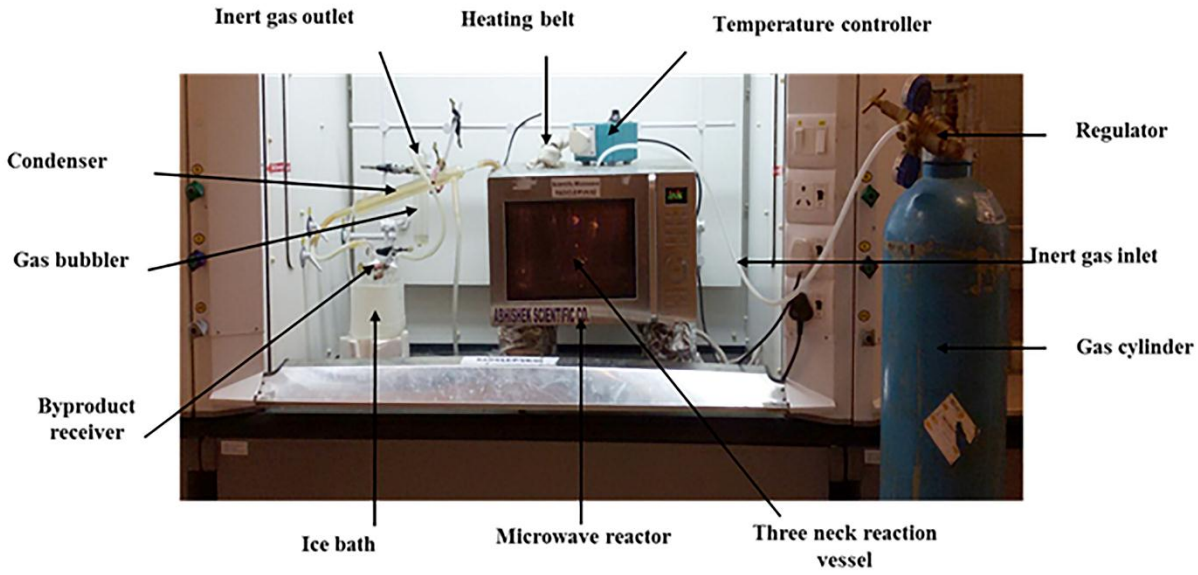

Figure 2.2. Microwave setup for modification of gums.

2.2.3. Fabrication of PLA/modified gums (5%) bionanocomposite films

Pristine PLA, neat gums and PLA/modified gums (5%) based bionanocomposite films were prepared by solution casting method. Solutions of PLA/modified gum were prepared by dissolving modified gums with PLA solution in chloroform with vigorous stirring magnetically at room temperature. The solutions were filtered using filter paper to remove the undissolved part. The solutions were poured into 15 cm diameter teflon Petri dishes to obtain the films after evaporation of solvent. PLA and GR films were also prepared by the same procedure. However, neat GA, GG and XG films were prepared by dissolving the gums in Millipore water. The formed films were peeled off from the Petri dishes after 12 h and further dried in vacuum oven at 40 °C for 12 h to remove the remaining chloroform from the films. Finally, the prepared

films were stored in desiccator for further analysis. The thickness of the different films was determined by thickness meter (indi6156; indi) at ten different locations and the average values were calculated and summarized in table 2.1.

Table 2.1. Composition of PLA/modified gums and thickness of their films.

Codes of film samples	Composition of blends		Film thickness (µm)
	PLA (wt%)	Modified gum (wt%)	
PLA	100	0	97 ± 2
PLA/modified GA(5%)	95	5	94 ± 3
PLA/modified GG(5%)	95	5	102 ± 5
PLA/modified XG(5%)	95	5	112 ± 10
PLA/modified GR(5%)	95	5	96 ± 5

The different concentrations of PLA/GA-*g*-PLA bionanocomposite films were prepared by the same procedure as described above. GA-*g*-PLA(20%) filler at 3, 5 and 10 wt% loading was mixed in PLA matrix to obtain PLA/GA-*g*-PLA(3%), PLA/GA-*g*-PLA(5%) and PLA/GA-*g*-PLA(10%) bionanocomposite films respectively. PLA pellets and GA-*g*-PLA filler were magnetically stirred in chloroform at room temperature for 12 h. The prepared solution was cast onto teflon Petri dishes to fabricate the films of 100 ± 20 µm thickness. Thereafter, chloroform was allowed to evaporate for 12 h in fume hood at room temperature. Neat PLA films were also prepared by the same procedure. After that, the dried films were peeled off from the petri dishes and kept in vacuum oven at 40 °C for 12 h to remove remaining

chloroform entrapped in the films. The thickness of the films was measured at ten different locations. The average values were calculated and summarized in table 2.2.

Table 2.2. Composition of PLA/GA-*g*-PLA and thickness of their films.

Codes of film samples	Composition of blends		Film thickness (µm)
	PLA (wt%)	GA-*g*-PLA (wt%)	
PLA	100	0	100.0 ± 2
PLA/GA-*g*-PLA(3%)	97	3	102.5 ± 3
PLA/GA-*g*-PLA(5%)	95	5	85.8 ± 5
PLA/GA-*g*-PLA(10%)	90	10	89.5 ± 8

2.3. Characterizations

2.3.1. Solubility and grafting calculations

Solubility of all neat gums, OLLA and modified gums was evaluated by dissolving the samples in various solvents such as Millipore water, acetone, chloroform, dichloromethane, methanol and ethyl acetate at a concentration of 20 mg ml^{-1} at room temperature and the solutions were shaken for 10 min by using spinix-vortex shaker (Tarsons). The solutions were then filtered and the residual weight was measured to determine the percentage solubility.

The grafting efficiency and percent grafting were calculated from equations (2.1) and (2.2) respectively.

$$\text{Grafting efficiency } (\%) = \left(\frac{W_1 - W_0}{W_2}\right) \times 100 \quad (2.1)$$

$$\text{Percent grafting } (\%) = \left(\frac{W_1 - W_0}{W_0}\right) \times 100 \quad (2.2)$$

where, W_0: weight of neat gum; W_1: weight of grafted copolymer; W_2: weight of lactic acid.

2.3.2. Fourier transform infrared spectroscopy analysis

Fourier transform infrared spectroscopy (FTIR) of neat gums, OLLA and modified gums was carried out by using IRAffinity-I Shimadzu spectrophotometer. The samples were thoroughly mixed with KBr and homogenous mixtures were prepared in 100:1 ratio. Before analysis, the samples were kept in hot air oven at 60 °C overnight. The spectra were recorded in transmission mode within a wavenumber range of 4000-400 cm^{-1} at averaging a minimum of 20 scans with a resolution of 4.0 cm^{-1}.

Attenuated total reflectance - Fourier transform infrared spectroscopy (ATR-FTIR) was carried out by using IRAffinity-I Shimadzu spectrophotometer. The spectra from PLA, PLA/GA-*g*-PLA(3%), PLA/GA-*g*-PLA(5%) and PLA/GA-*g*-PLA(10%) bionanocomposite films were recorded in transmission mode within a wavenumber range of 4000-600 cm^{-1} at averaging a minimum of 20 scans with a resolution of 4.0 cm^{-1}. Film samples were kept at 80 °C for 2 h in hot air oven before analyzing.

2.3.3. Nuclear magnetic resonance analysis

Proton nuclear magnetic resonance (^{1}H NMR) analysis was performed for OLLA and GA-*g*-PLA samples by using Bruker Ascend^{TM} 600 nuclear magnetic resonance spectrometer. The OLLA and GA-*g*-PLA of ~10 mg ml^{-1} concentration were prepared by dissolving the samples in deuterated chloroform ($CDCl_3$). Before the analysis, GA-*g*-PLA solution was filtered by using 0.45 µm size syringe filter. Further, 2 ml samples were transferred into NMR tubes for analysis at room temperature.

2.3.4. X-ray diffraction analysis

X-ray diffraction (XRD) analysis was carried out by using X-ray diffractometer (Bruker, D8 Advance) using copper Kα-radiation source (λ = 1.54 Å) generated at 40 kV and 40 mA. XRD patterns were observed in the diffraction angle range 2° and 50° (2θ) with scan speed of 2 sec step $^{-1}$ and increment of 0.05 °/sec. The samples were kept in hot air oven at 80 °C for 2 h before analysis.

Segal empirical method was used to calculate the crystallinity index (Cr I) by employing the equation 2.3.

$$\text{Cr I} = \frac{\left(\text{I}_{[110/200]} - \text{I}_{\text{am}}\right)}{\text{I}_{[110]/[200]}} \times 100 \qquad (2.3)$$

where, I is the maximum intensity of the lattice reflection of PLA crystallography at around 2θ = 16.7° and I_{am} is the intensity of diffraction of the amorphous material at minimal intensity **(Segal et al., 1959; Zhao et al, 2011; Park et al., 2010)**.

2.3.5. Gel permeation chromatography analysis

The molecular weight of sample was determined using gel permeation chromatography (GPC) system (Shimadzu, Communications bus module (CBM-20A), Autosampler (SIL-20A HT), Liquid chromatograph (LC-20AD), Degassing unit (DGU-20A_{3R}), Refractive index detector (RID-10A), Column oven (CTO-20A)). Agilent two PL gel 5 micron MIXED-D column in series was used with mobile phase consisted of HPLC grade chloroform. The effluent flow rate of mobile phase was kept at 1.0 ml min^{-1} at column temperature 40 °C. Eight narrow molecular weight standard of polystyrene samples from Mp ~ 144 Da-400 kDa were used for calibration under chloroform as mobile phase.

2.3.6. Differential scanning calorimetry analysis

Differential scanning calorimetry (DSC) was carried out in DSC 204 F1 Phoenix, NETZSCH. The analysis was performed under N_2 atmosphere. Platinum-Rhodium (Pt-Rh) crucible was used for the tests, where reference crucible of same material was placed empty. Samples weighing 5-8 mg were heated from 25 °C to 200 °C at 5 °C min^{-1} heating rate, followed by 2 min. isothermal condition at 200 °C. After erasing the processing history in first heating cycle, samples were again cooled to 25 °C and then second heating cycles were recorded in the same manner.

Differential scanning calorimetry (DSC) was carried out in DSC 1, Star^e System, Mettler Toledo. The analysis was performed under N_2 atmosphere. Aluminium crucibles were used for the tests, where reference crucible was placed empty. Samples were heated from -25 °C to 200 °C at 5 °C min^{-1} heating rate. After erasing the processing history in first heating cycle, samples were again cooled to -25 °C and then second heating cycles were recorded.

2.3.7. Thermogravimetric analysis

The thermal stability of the samples was determined by thermogravimetric analysis (TGA) with a PerkinElmer Thermogravimetric Analyzer (TGA 4000). The analysis was conducted by using 6-10 mg of sample in the temperature range from 30 °C to 600 °C at 20 °C min^{-1} heating rate under inert atmosphere.

The thermal stability of the all film samples was determined by thermo gravimetric analysis (TGA) with a PerkinElmer Simultaneous Thermal Analyzer (STA-8000). The analysis was conducted in the temperature range from 35 °C to 500 °C at 5 °C min^{-1} heating range under inert atmosphere. The analysis was also conducted in the same temperature range at heating rates of 2, 5 and 10 °C min^{-1} for thermal degradation kinetics study.

2.3.8. Thermogravimetric analysis-fourier transform infrared spectroscopy (TGA-FTIR) analysis

Thermogravimetric (TG) analyzer (Perkin Elmer) was hyphenated to FTIR spectrophotometer (Frontier 4000) to investigate the mass loss of PLA and PLA/GA-*g*-PLA based bionanocomposite and on-line evolution of gaseous products. About 10 mg of sample was placed into the crucible and heated from 30 °C to 700 °C at the heating rate of 10 °C min^{-1} under nitrogen atmosphere. The flow rate of nitrogen was 50 ml min^{-1} for maintaining the inert atmosphere for the decomposition. The FTIR connected to TG by a transfer line was preheated to 260 °C to prevent condensation of the produced gases on the tube and cell walls. The scanning range was set to be 4000-450 cm^{-1} at a resolution of 8 cm^{-1} with 4 scans. The start time difference between FTIR and TG was about 2 min which was due to the time required for nitrogen flow to fill the cell volume of the spectrophotometer.

2.3.9. Scanning electron microscopy analysis

The scanning electron microscopy (SEM) analysis was conducted to observe the changes in surface morphology of neat gums, their respective modified gums, all PLA/modified gum films, by scanning electron microscope (LEO, 1430 vp). The morphology of the samples was examined under the exposure of an accelerating voltage of 10 kV. The samples were mounted on aluminium holder with double sided carbon tape. Before analysis, gold coating of 10 nm was done by high vacuum gold sputter module (Quorum, SC7620) on the samples to increase the static charge dissipation.

2.3.10. Field emission scanning electron microscopy analysis

Field Emission Scanning Electron Microscopy (FESEM) analysis was conducted to observe the surface morphology of PLA/GA-*g*-PLA bionanocomposite films at higher magnification by using field emission scanning electron microscope (Σigma, ZEISS). The film samples were fixed on stubs using carbon tape. Sputtering of gold layer on sample surface was done before analysis. This helps in proper conductivity of electrostatic charge during electron irradiation.

2.3.11. Transmission electron microscopy analysis

Transmission electron microscopy (TEM) micrograph of the samples were captured using transmission electron microscope (JEOL, JEM-2100). For preparing the sample, small piece of thin film was dissolved in the HPLC grade chloroform. Then the solution was filtered using Whatman® syringe filter (pore size 0.45 µm). Thereafter, a drop of the filtered solution was put on the copper grid. The solvent was allowed to evaporate for 12 h at room temperature before analysis. The analysis was also used for analyzing GA-*g*-PLA(15%). During sample preparation, a small amount of sample was dissolved in the HPLC grade chloroform followed by filtering by using Whatman® syringe filter (pore size 0.45 µm). Filtered solution was dropped on the copper grid and dried for 12 h at room temperature before analysis.

2.3.12. Contact angle analysis

Contact angle measurements were performed on a KRUSS, Drop Shape Analyzer-DSA25 apparatus with a millipore water drop volume of 4 µL at 23 ± 1 °C by sessile drop method. The analyzed surface of samples were prepared by dissolving the samples in chloroform, filtered all the samples by using Whatman® syringe filter (pore size 0.45 µm). The solutions were uniformly poured on the glass slides followed by overnight drying in an oven at 60 °C.

2.3.13. Single lap shear test analysis of modified gums for adhesive selection

Neat gums and their respective modified gums were explored to check the adhesive strength by single lap shear test. The test was performed by universal testing machine (Kalpak Instruments and Controls, KIC-2-050-C). The two granite rectangular bars of dimensions (80 mm × 40 mm × 9 mm) and glass slides of dimensions (120 mm × 50 mm × 5 mm) were prepared. The single lap shear test of different modified gums was performed by binding glass substrates. The substrates were properly cleaned by acetone and dried completely before analysis. The glass substrates were prepared according to ASTM D 1002 standard. The temperature and relative humidity (%RH) was maintained at 25-28 °C and 50-60 % RH respectively during substrate preparation. The substrate area and shear test speed were maintained at 0.25 mm^2 and 1.3 mm min^{-1} respectively. The modified gums were coated on the glass substrates at 70 °C. The two substrates were joined together at a compression load of 1000 N for 5min. The test was performed at a cross head speed of 1.3 mm min^{-1}. Five test specimens were tested at each condition and average values were reported. Single lap shear tests were performed for various concentrations of gum arabic grafted poly lactic acid (GA-*g*-PLA) samples on glass and granite substrates by using the previously explained instrumentation and procedure. The preliminary observations were conducted to test the adhesive strength of various materials prepared at different conditions. The test was also conducted for different substrates by using GA-*g*-PLA bionanocomposite as an adhesive in order to check the binding strength. The single lap shear test was performed at various GA-*g*-PLA concentrations, compression loads and compression time.

2.3.14. Mechanical properties

A universal testing machine (UTM) (Kalpak Instruments and Controls, model KIC-2-050-C) was used to determine different mechanical properties such as tensile strength (MPa), Young's modulus (MPa) and elongation at break (%). Film samples were cut as strips with 100 mm length and 25.4 mm width according to ASTM D882-02. The samples were equilibrated in an environmental chamber for 48 h at 50 ± 5% relative humidity (RH) and 25 ± 5°C temperature before testing. A 1000 N load cell was used for tensile test. Cross-head speed was 50 mm min^{-1} and the grip separation was set at 50 mm.

2.3.15. Oxygen permeability analysis

Oxygen transmission rate (OTR) measurements were carried out by using an oxygen permeability tester (Labthink, model PERME® OX2/231) according to ASTM standard D3985. The temperature was maintained by using the temperature controller (Labthink, model TC-01). The test was conducted at 25 ± 0.1 °C and 0% relative humidity (RH). The test area considered for analysing the samples was 50 cm^2. While analysing the sample, pure nitrogen (99.9995%) was passed in the lower half of the chamber and pure oxygen (99.95%) was introduced in the upper half of the chamber. Film thickness was measured with digital coating thickness meter (model indi6156; indi). The thickness of each sample was determined at 10 different locations and their average value was considered. The OTR (cm^3 m^{-2} day^{-1}) values were recorded. The tests were performed in duplicate and the average values have been reported. The OTR value obtained from the instrument was multiplied by the average film thickness (e, in mm) for each film, and expressed as OTR × e values (cm^3 mm m^{-2} day^{-1}).

2.3.16. Water vapour transmission rate analysis

Water vapour transmission rate (WVTR) of the films was calculated according to the ASTM E398 by water vapour permeability tester (Mocon, PERMATRAN-W® 1/50G). Prior to the analysis, the sample was conditioned at 25 ± 1 ºC and 50% RH for 48 h. The test was conducted for exposure area of 50 cm^2 at 37.8 ± 0.5 ºC and 100% RH. Nitrogen gas (99.9% purity) was purged through the films during the analysis. The test was performed at continuous mode. The test readings were noted down after reaching the saturation point of WVTR value. The tests were performed in triplicate and the average values have been reported. The WVTR value obtained from the instrument was multiplied by the average film thickness (e, in mm) for each film, and expressed as WVTR × e values (cm^3 mm m^{-2} day^{-1}).

Chapter 3

Selection of Gum Grafted Poly L-Lactic Acid for Adhesive and Food Packaging Application

The chapter focuses on selection of the polysaccharide gum among gum arabic, guar gum, xanthan gum and gum rosin for the desired applications. The monomer lactic acid has been used to graft with the polysaccharide gums by conventional heating and microwave heating method. The grafted composites have been tested as an adhesive for structural applications and food packaging applications. The preliminary tests have been conducted by the two synthesis methods and the grafting in the composites have been studied. The synthesized composites have been tested for the preliminary critical properties of both the applications.

3.1. Introduction

For the development of new products, raw materials need to be graft modified for various end uses. Among the various grafting processes, chemical grafting has proved to be one of the most effective method for increasing the compatibility between synthetic and natural polymers. In the process, monomers attach on the polymer backbone for the desired characteristic properties. The work involves the two heating methods for modification of raw materials namely, conventional heating method and microwave heating method. In the conventional heating method, competing homopolymerization results in lowering the copolymer yield (figure 3.1a). Furthermore, maintaining the inert atmosphere during conventional grafting is

also required. The recent interest in using microwave irradiation for the synthesis of copolymer is increasing since last two decades, as it involves clean and green environment friendly chemistry. The use of microwave irradiation for the synthesis of copolymer is increasing due to its instantaneous 'in core' heating of materials in a homogeneous and selective manner **(Singh et al., 2006)**. The grafting process using microwave irradiation has proved to be a powerful tool for developing tailor made products. Moreover, significant reduction in use of toxic solvents, high yield, product selectivity, reaction time and clean product formation are its benefits. The microwave irradiation results in high yield due to its favored reaction (figure 3.1b). Some of the few benefits of microwave heating over conventional heating are stated in table 3.1. Hence the microwave methodology proved to be a cheaper, quicker, simpler and safer over conventional heating process **(Singh et al. 2012)**.

Table 3.1. Advantages of microwave over conventional heating.

Property	Conventional heating	Microwave heating
Rxn. time	Long time	Short time
Pressure	High pressure rxns. for long duration: more dangerous	High pressure rxns. for short duration: less dangerous
Heating rate	Slow	Fast
Homogeneity of heating	Low; "wall effect" cannot be prevented	High; no "wall effect"
Yield	Low	High
Amount of secondary products	High	Low
Reproducibility	Low	High

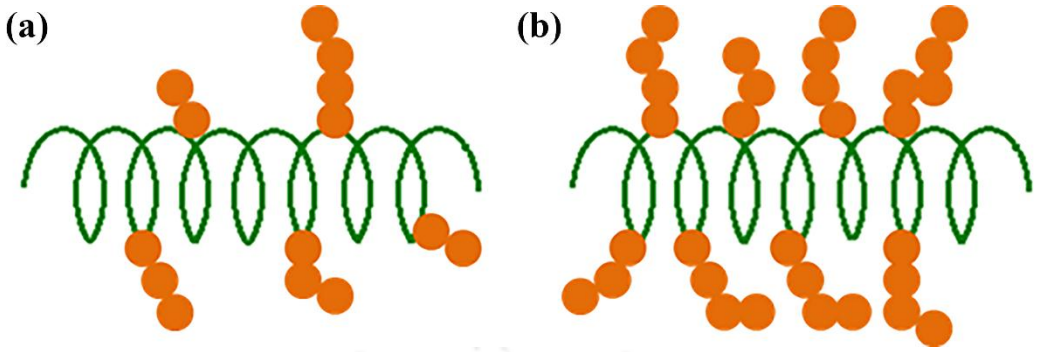

Figure 3.1. Schematic representation of grafting in (a) conventional heating and (b) microwave heating.

The current work was focused on two applications (1) formulation of adhesive (2) fabrication of films for food packaging. The adhesives and sealants have many commercial applications, as it is a 20 million ton global industry having $20 billion sales value. The adhesives seems to be a less significant product for our modern society, however it plays a very important role in assembling millions of parts available in the market and affects the performance of products. It also plays critical role in maintaining the safety and quality of food. The adhesives have various field of applications such as product assembly, transportation, medical, packaging and labelling, construction, textiles and carpets. Nowadays, the major concerns in using adhesives are pollution, toxicity and flammability. Hence, people are getting more inclined towards developing bio-based adhesives having comparable properties with that of petroleum based adhesives. The strength of the adhesives can be checked by various methods. One of the important one for structural adhesives is single lap shear test.

In general, there are three criteria by which adhesive performance can be tested. On performing the test, we come across three failure modes to confirm the binding strength of the adhesives (figure 3.2). In adhesive failure mode, adhesive bond fails if adhesive separates from the

substrate. In cohesive failure, cohesion or attraction of particles within the adhesive fails to hold the adhesive mass together fails. The highest strength of the adhesives is achieved if adhesive and cohesive strengths of the adhesive is more than the strength of the substrate which results in substrate failure **(Dunn, 2003)**.

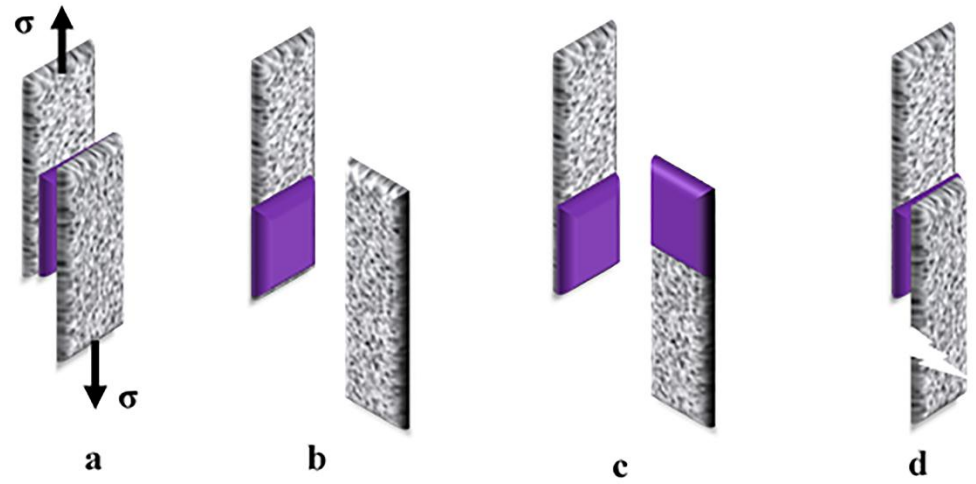

Figure 3.2. Modes of adhesive failure (a) single lap shear joint, (b) adhesive failure, (c) cohesive failure, (d) substrate failure.

3.2. Results and Discussion

3.2.1. Conventional heating method for the synthesis of gums grafted poly l-lactic acid

Lactic acid was mixed with gum (10wt/wt%) in RBF in inert atmosphere. The reaction mixture was kept at 150 °C under the stirring rate of 450 rpm. During synthesis, the bubbling in the reaction mixture was observed that signifies the formation of water molecules which was condensed out in the condenser. After 150 min, formation of brown color in all the gums except gum rosin was observed. The byproduct (lactide) removal was also observed after 150 min under vacuum. During the conventional heating process, the free radicals were generated on polar groups of the polysaccharide gum backbone and LA monomer. As the free radical sites

were generated on the molecules, the grafting between the reactants started. The LA and OLLA active sites reacted on the gum backbone. After removal of around 30 wt% of water, a viscous dark brown colour grafted material of lactic acid and gum was formed (figure 3.3). Scheme 3.1, 3.2 and 3.3 show the proposed reaction pathways of GA, GG and XG during reaction which occurred in OH group. The free hydroxyl groups in GA, GG and XG molecules which were grafted with the reducing end groups of the LA molecules. No reaction took place in case of GR because of absence of active functional groups required for the reaction. The proposed scheme 3.1 also shows the reaction of free amino groups in GA with LA molecules. The synthesis of modified gums under conventional heating conditions was a time consuming process with less yield. The process of removing water and producing modified gums under conventional heating took more than 480 min.

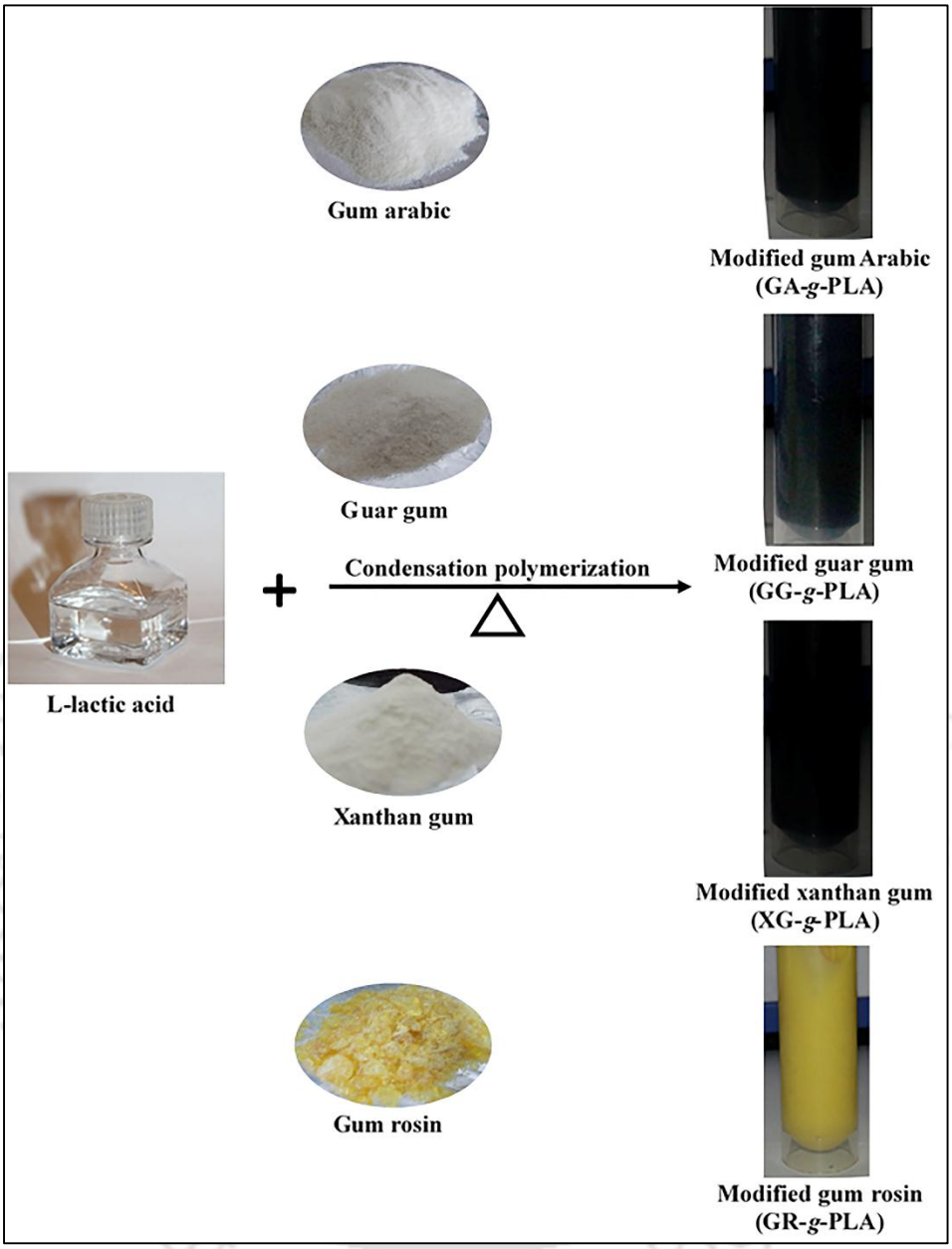

Figure 3.3. Layout of prepared modified gums.

3.2.2. Microwave initiated synthesis of gums grafted poly l-lactic acid

The modified gums were also synthesized by using microwave irradiation. The synthesis was based on free radical mechanism, in which free radicals were generated on polysaccharide gums backbone because of microwave irradiation. In the process, LA molecules were grafted

on gum backbone in the presence of microwave irradiation. During the reaction, microwave radiations irradiate polar molecules of water which leads to generation of heat. The free radical sites were also generated on polar groups of the polysaccharide gum backbone and LA monomer on exposure of microwave radiation. When the free radical sites were produced on gum backbone, LA monomer gets attached and propagation of the monomeric molecules started on the active sites. The brown color was developed in the reaction mixture within 30 min and around 30 wt% of water was removed from the reaction as a byproduct. In microwave irradiation process also, no modification was observed for gum rosin. The proposed reactions are explained in scheme 3.1, 3.2 and 3.3 for GA, GG and XG gums respectively.

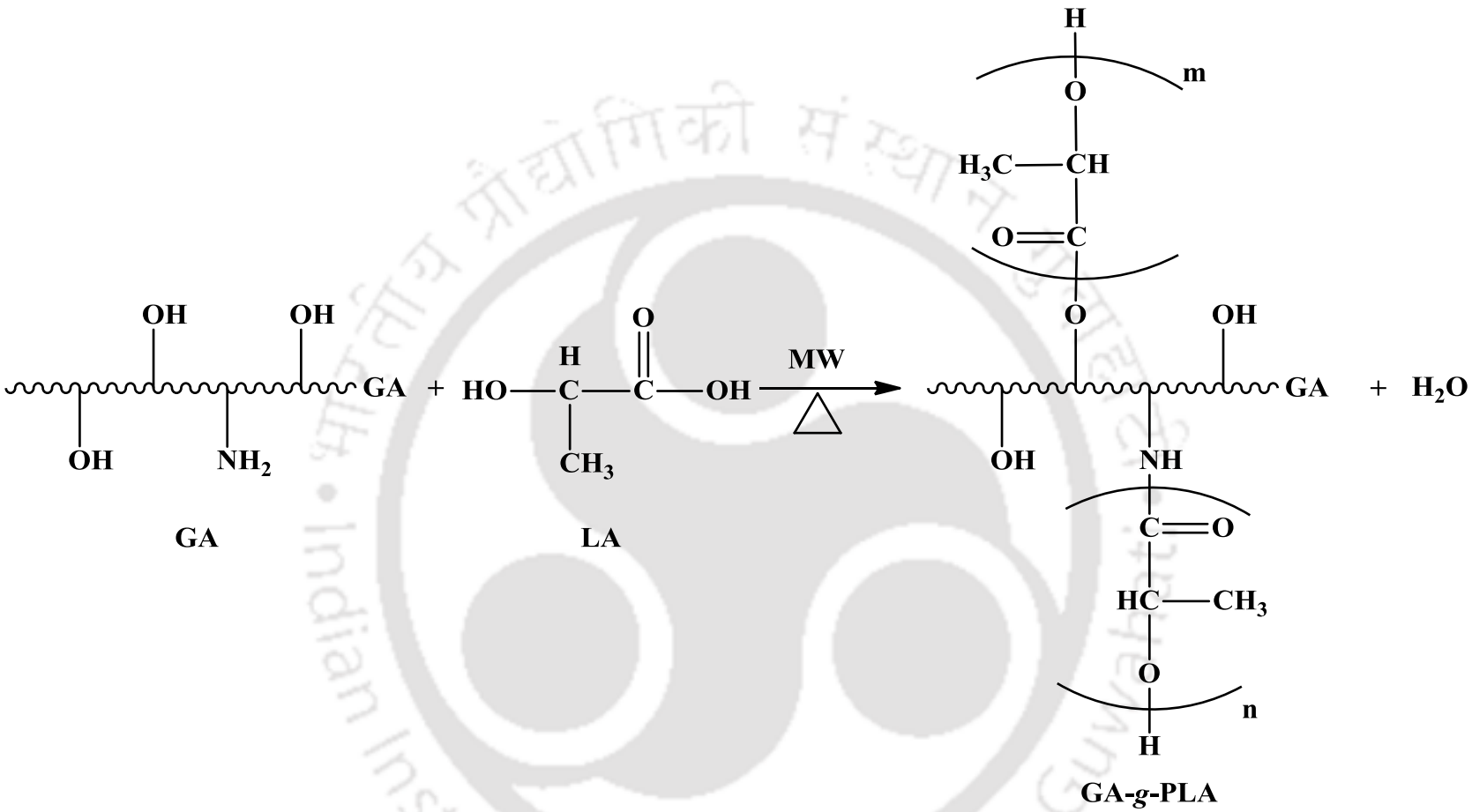

Scheme 3.1. Reaction pathway for the modification of gum arabic.

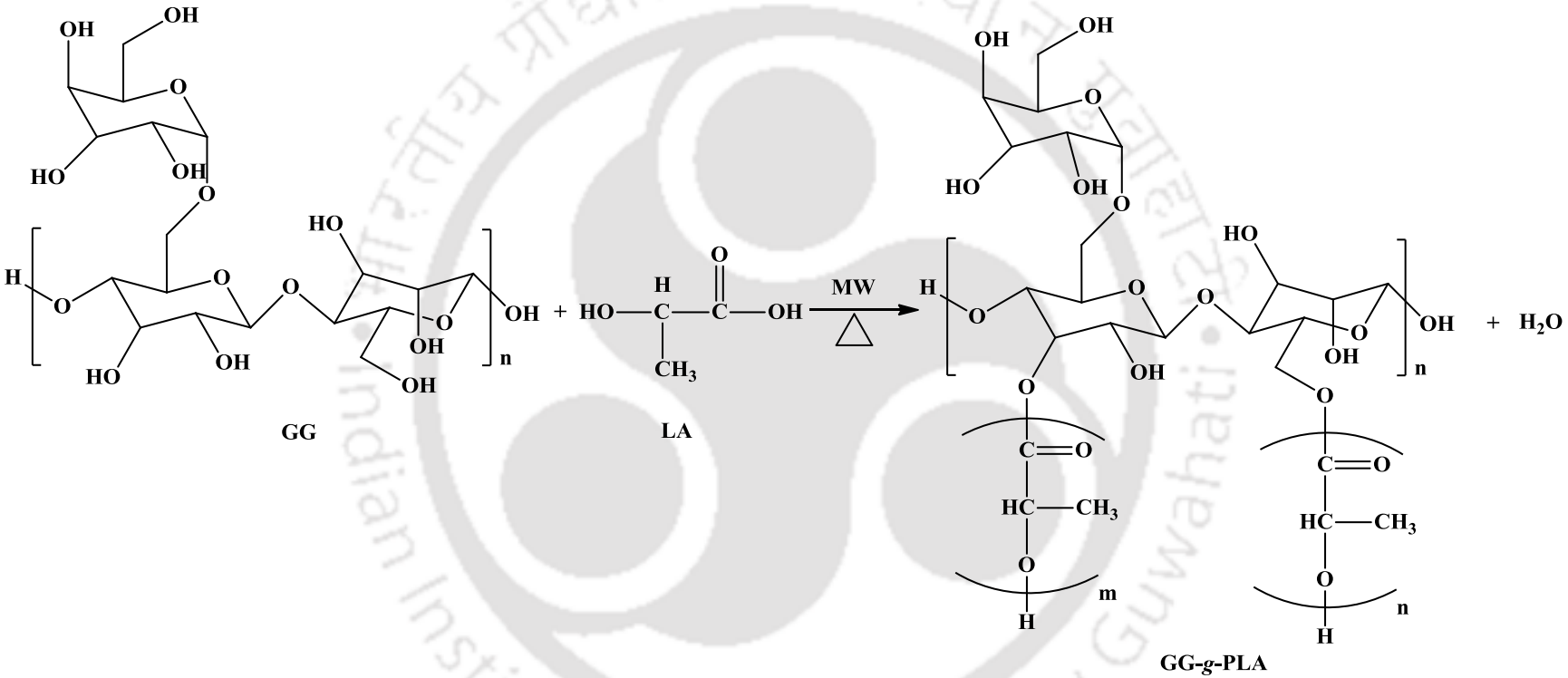

Scheme 3.2. Reaction pathway for the modification of guar gum.

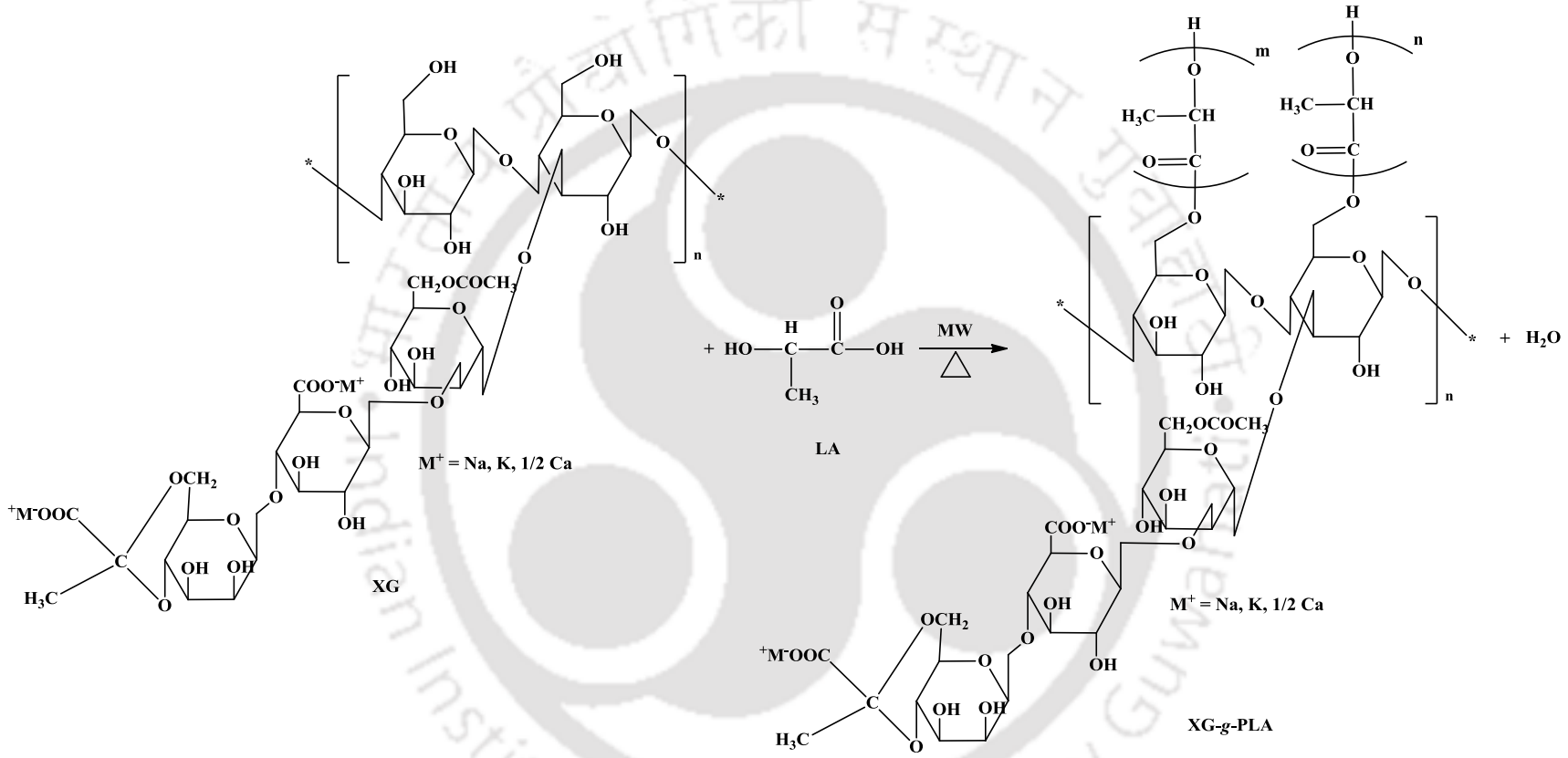

Scheme 3.3. Reaction pathway for the modification of xanthan gum.

3.2.3. Grafting by FTIR analysis

Intermolecular interaction and grafting were proved by comparing FTIR spectra of neat gums, OLLA and their respective modified gums as shown in figure 3.4. The clear changes in molecular structure of modified gums was noticed from the FTIR spectra. Figure 3.5 (a) & (b) exhibit the FTIR spectra of GA, OLLA and GA-*g*-PLA(10%) prepared by microwave heating method. The IR spectra of GA showed the broad absorption band at 3350 cm^{-1} due to the overlapped stretching vibrations of OH group, N-H group and glucosidic ring. The same broad vibration was found narrow in the case of OLLA and narrower in the case of GA-*g*-PLA(10%) samples. The peak also shifted towards higher wavenumber and found at 3636 cm^{-1} and 3641 cm^{-1} for OLLA and GA-*g*-PLA(10%) respectively. It suggested that the grafting was happened at both OH and N-H groups. The peak at 2920 cm^{-1} suggested the stretching vibrations of C-H group in pure GA. The sharp and intense Peak at 1750 cm^{-1} attributed to -C=O (carbonyl) stretching vibrations which was present in the spectra of OLLA and GA-*g*-PLA(10%) but not in the spectra of GA. A peak at 1600 cm^{-1} in GA attributed to the COO- asymmetric stretching which was not present in modified GA. The regular peaks at 1133 cm^{-1}, 1204 cm^{-1}, 1094 cm^{-1} and 1045 cm^{-1} confirmed the -C-O- stretching in OLLA and GA-*g*-PLA samples. The Peak 1455 cm^{-1} attributed to $-CH_3$ bending in OLLA and GA-*g*-PLA bionanocomposite. A broad vibration was observed at 1016 cm^{-1} in pure GA which is the finger print spectra of carbohydrates present in the sample. The same peak was also observed at 1045 cm^{-1} in GA-*g*-PLA which was merged with -C-O- stretching. Hence, the OLLA chains were grafted on GA backbone at OH and N-H functional groups as shown in scheme 3.1 **(Almuslet et al., 2012)**.

The FTIR spectra of GG, OLLA and GG-*g*-PLA(10%) was shown in figure 3.4 (c) & (d). It was observed that a broad peak was identified at 3630 cm^{-1} in OLLA which signified the presence of

stretching vibrations of OH group. This peak was absent in GG and GG-*g*-PLA(10%) samples which suggested that the samples were completely dried and moisture free. A tiny peak was observed in pure GG at 2965 cm^{-1} which attributed to the C–H stretching vibrations. A little shift towards higher wavenumber at 2970 cm^{-1} was observed in this peak in GG-*g*-PLA(10%) sample. All other regular significant peaks were observed at same position in OLLA as in figure 3.4(b). But all the regular peaks shifted towards lower wavenumber with reduced intensity in the case of GG-*g*-PLA(10%) which suggested the consumption of functional groups during grafting. The bands at 1024 cm^{-1} and 803 cm^{-1} were assigned to C–O–C stretching vibrations in pure GG which were absent in GG-*g*-PLA(10%). Hence, the shifting and reduction in peak intensities confirmed grafting of OLLA chains on GG backbone at OH groups as shown in scheme 3.2 **(Sen et al., 2010; Likhitha et al., 2014; Yan et al., 2012)**.

The FTIR spectra of XG, OLLA and XG-*g*-PLA(10%) was shown in figure 3.4 (e) & (f). IR spectrum of XG showed a broad peak at 3483 cm^{-1} due to hydrogen bonded O-H stretching vibration. But the same peak was observed at 3636 cm^{-1} in OLLA which was absent in XG-*g*-PLA(10%) sample. It is the most significant observation which suggested that the grafting was done mostly at OH groups. The small peak at 2890 cm^{-1} indicated the presence of C-H stretching of alkyl group in pure XG spectra. All other regular peaks were observed at same position in OLLA spectra but all the peaks shifted towards lower wavenumber in the case of XG-*g*-PLA(10%). Two peaks at 1638 cm^{-1} and 1014 cm^{-1} were attributed to stretching vibrations of COO- group and OH bending vibrations respectively which was absent in the case of modified XG. Hence, the shifting of regular peaks and absence of OH peak from the spectra confirmed the grafting of OLLA chains on XG backbone as shown in scheme 3.3 **(Pandey et al., 2011; Mundargi et al., 2007; Kumar et al., 2009)**.

The FTIR spectra of GR, OLLA and GR-*m*-PLA(10%) was shown in figure 3.4 (g) & (h). In the IR spectrum of GR, a broad peak at 3427 cm^{-1} was observed due to stretching vibrations of O-H group. The broad peak of OH vibrations was also present in GR-*m*-PLA(10%) sample which suggested that the grafting phenomena was unsuccessful at OH groups of GR backbone. All other regular peaks were observed at same position in OLLA and a shifting towards lower wavenumber was observed in GR-*m*-PLA(10%) also. In the spectra of pure GR, a carbonyl band at 1692 cm^{-1} was observed which attributed to the hydrogen bonded acid dimers. This peak was broader in the case of GR-*m*-PLA(10%). Hence, it was confirmed that the grafting phenomena was not happened at OH groups of GR backbone **(Gutierrez et al., 2014)**.

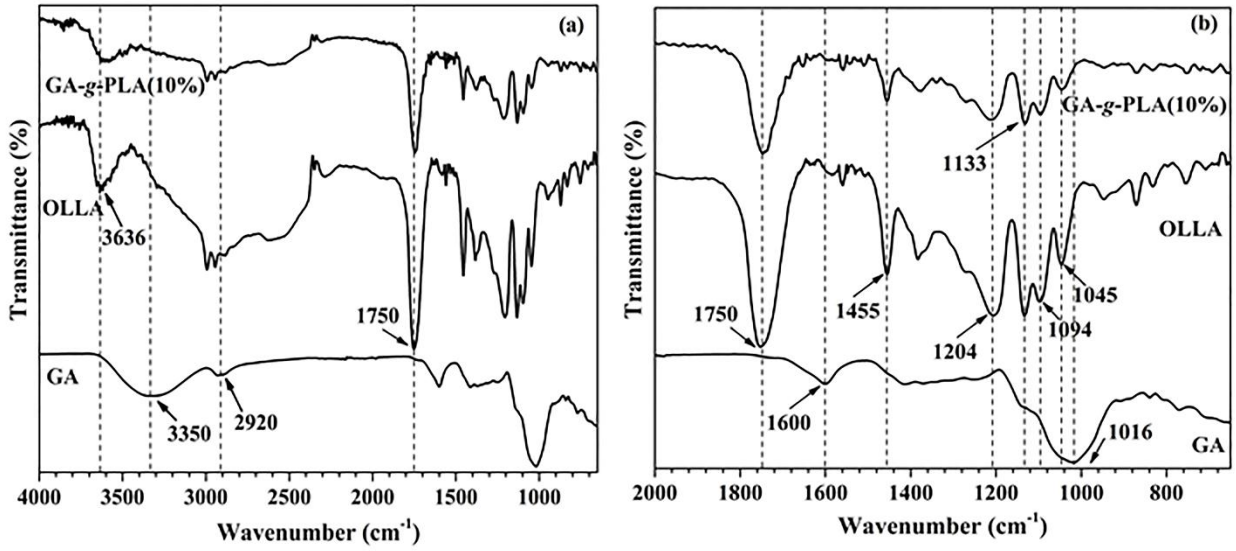

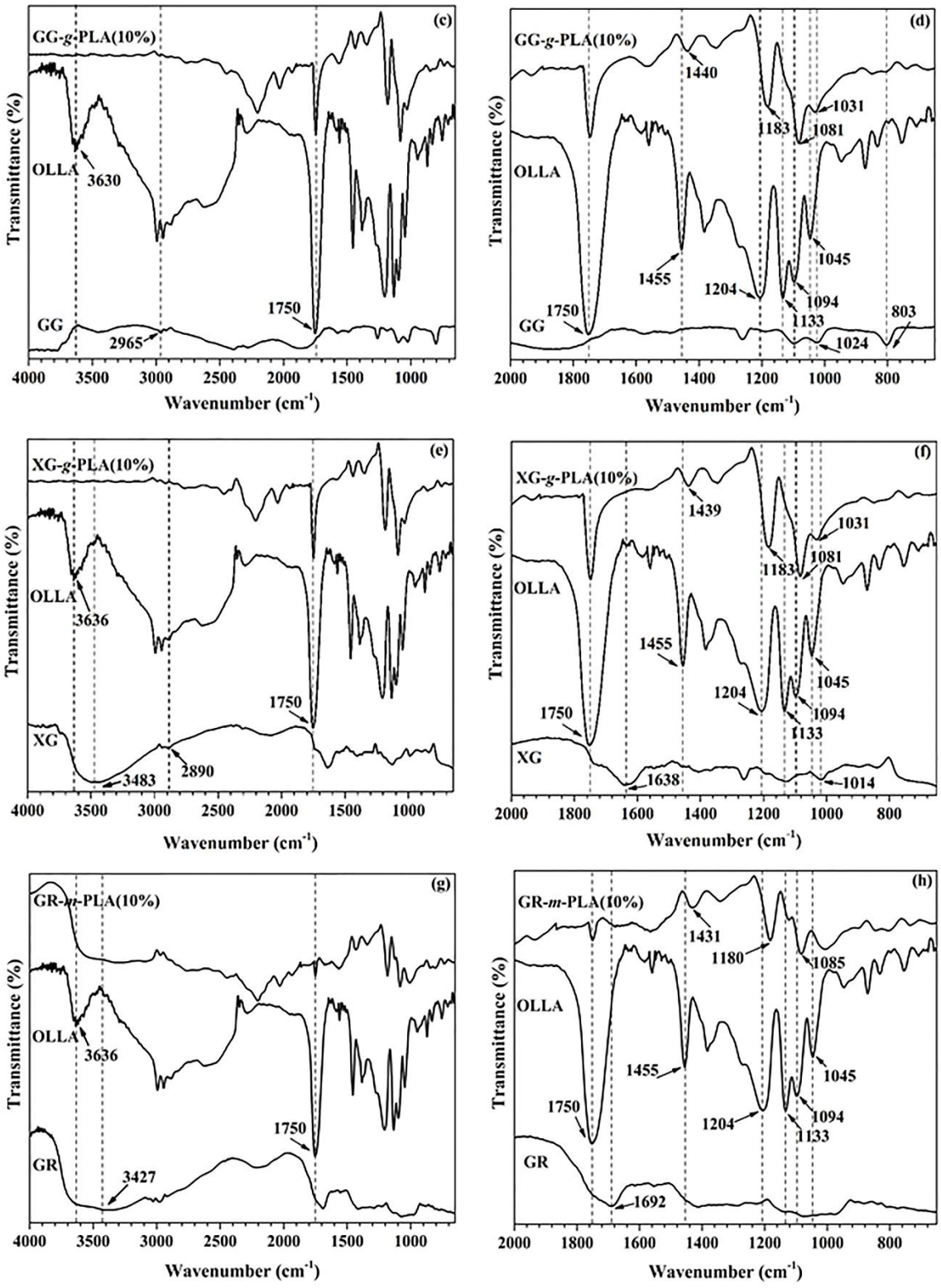

Figure 3.4. FTIR: gums, OLLA & modified gums; (a & b) GA, (c & d) GG, (e & f) XG, (g & h) GR.

3.2.4. Scanning electron microscopy analysis

The surface topography of neat gums and modified gums was examined successfully by SEM analysis. A comparison was made between neat gums and modified gums as shown in figure 3.5. The outer surface of GA-*g*-PLA was appeared to be fluffy and quite different from neat GA. In both the cases, the architecture of particle was similar but the grafted particles were more compact than neat GA. The particles of neat GA were not uniform in size whereas, grafted GA particles were of uniform size. Hence, the surface evidence confirmed the grafting phenomena on GA **(Tiwari et al., 2008)**. The surface morphology of GG and grafted GG was observed at same conditions and found a clear difference in grafted GG than that of neat GG. The flaky and more evenness was observed in grafted GG surface than that of neat GG. Neat GG has granular structure. It confirmed the grafting phenomena on GG backbone **(Wan et al., 2011, Sinha et al., 2013)**. The SEM images of grafted XG showed the grafting of OLLA chains on XG backbone which changed the surface structure of XG completely. The surface of grafted XG was smoother and homogeneous than that of neat XG which confirmed the grafting phenomena **(Vijan et al., 2012)**. Even though the surface of GR was changed than that of grafted GR. But no grafting was observed in GR according to FTIR analysis.

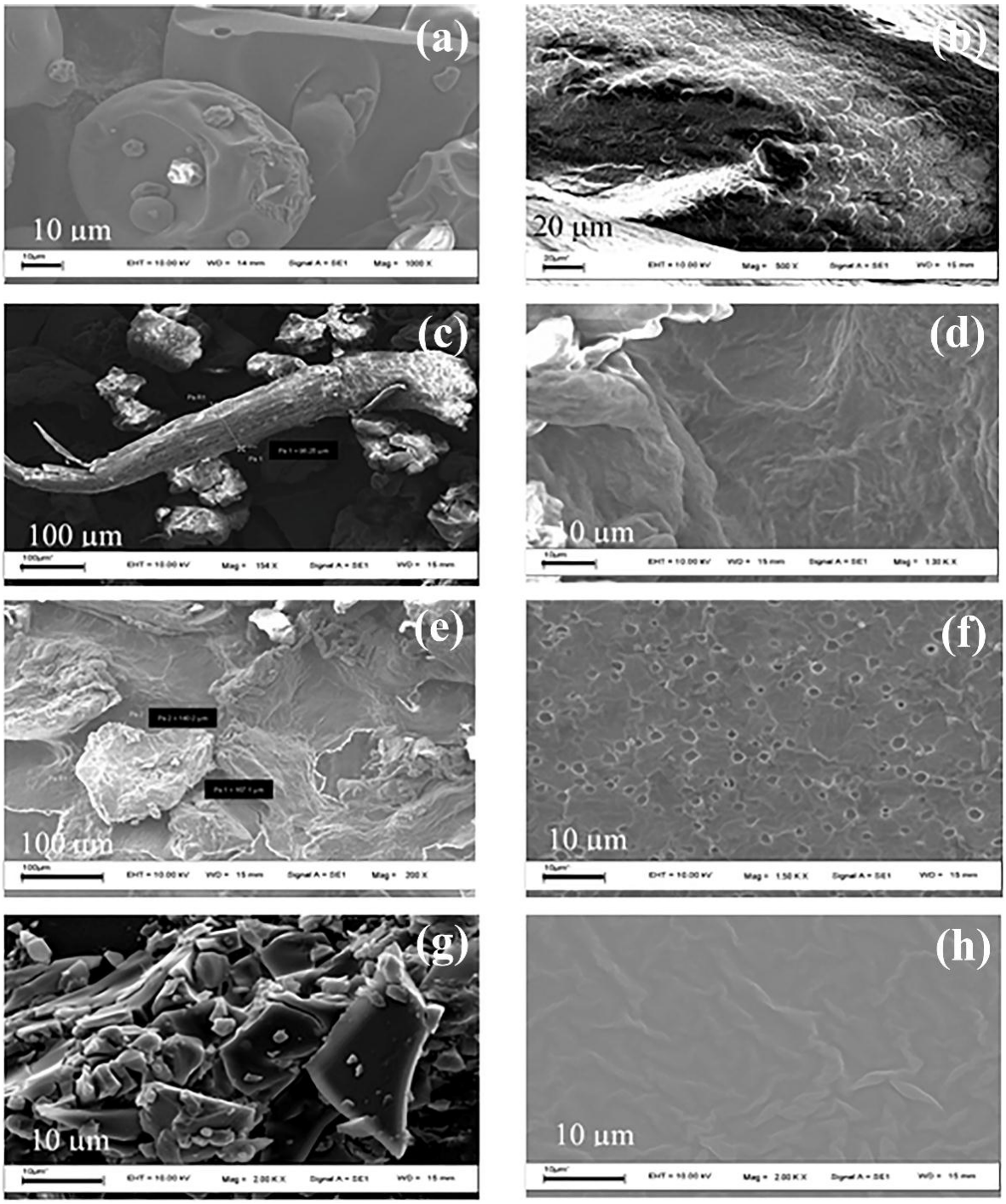

Figure 3.5. Surface morphologies of neat and modified gums: (a) GA, (b) GA-*g*-PLA, (c) GG, (d) GG-*g*-PLA, (e) XG, (f) XG-*g*-PLA, (g) GR, (h) GR-*m*-PLA.

3.2.5. Solubility

Solubility test of all neat gums, OLLA and modified gums was performed in a series of solvents such as water, acetone, chloroform, dichloromethane, methanol and ethyl acetate as presented in table 3.2. It can be observed that the solubility of GA, GG and XG was different from that of the modified ones. Neat gums i.e. GA, GG and XG were completely soluble in millipore water. However, insolubility of GA-*g*-PLA, GG-*g*-PLA and XG-*g*-PLA in water was observed as the polar groups present in gums were converted into non-polar groups or, the polar groups were replaced by long hydrophobic alkyl groups after modification. The strong intra-molecular hydrogen bonding was also one of the important factor for insolubility of modified gums in water. The difference in solubility confirms that the chemical modification occurred on GA, GG and XG backbone. Whereas, no change in solubility was observed for GR, as it was completely soluble in organic solvents but not soluble in water, which confirms no modification occurred after the reaction. Therefore, for further studies, GR-*g*-PLA was not used.

Table 3.2. Solubility of neat polysaccharide gums and gums-*g*-PLA.

Solvent	Before reaction				After reaction							
					Conventional heating method				Microwave heating method			
	GA	**GG**	**XG**	**GR**	**GA-*g*-PLA**	**GG-g-PLA**	**XG-g-PLA**	**GR-g-PLA**	**GA-*g*-PLA**	**GG-g-PLA**	**XG-g-PLA**	**GR-g-PLA**
Water	Yes	Yes	Yes	No	No	No	No	No	No	No	No	No
Chloroform	No	No	No	Yes	Yes	Yes	Yes	Yes	Yes	Yes	Yes	Yes
Di-chloroform methane	No	No	No	Yes	Yes	Yes	Yes	Yes	Yes	Yes	Yes	Yes
Acetone	No	No	No	Yes	Yes	Yes	Yes	Yes	Yes	Yes	Yes	Yes
Ethyl acetate	No	No	No	Yes	Yes	Yes	Yes	Yes	Yes	Yes	Yes	Yes
Methanol	No	No	No	Yes	Yes	Yes	Yes	Yes	Yes	Yes	Yes	Yes

3.2.6. Single lap shear test of modified gums for adhesive selection

The single lap shear test was conducted to check the bonding strength of the modified gums. The 5% concentration of all the modified gums were applied on the two glass surfaces. The compression load of 1000 N was applied on the glass-modified gum joint so that the bonding between the adherent and adhesive can be done. After applying the load for 5 min the joint was tested to check the binding. Although, no adherent-adhesive bonding was observed (Table 3.3.).

Table 3.3. Adhesive selection among prepared LA-*g*-gums(5%).

Sample name	**Shear strength (MPa) ± Std. dev.**
GA-*g*-PLA(5%)	No adhesion
GG-*g*-PLA(5%)	No adhesion
XG-*g*-PLA(5%)	No adhesion
GR-*m*-PLA(5%)	No adhesion

However, as the higher concentration modified gums that is 10 % was synthesized and the adhesive strength was checked, it showed some adhesive binding between adherent-adhesive bonding. The same procedure was followed to prepare the glass laminated using all the 10% modified gums as explained in section 3.3.4. The single lap shear test was conducted for GA-*g*-PLA(10%), GG-*g*-PLA(10%), XG-*g*-PLA(10%) and GR-*g*-PLA(10%). Among the all four samples, it was observed that GR-*g*-PLA(10%) was not able to bind the glass substrates. The modified gums GA-*g*-PLA(10%), GG-*g*-PLA(10%) and XG-*g*-PLA(10%) were able to bind the glass substrates. However, the highest shear strength was achieved by GA-*g*-PLA(10%) (figure 3.6). Hence, it was concluded that among all the four modified gums, GA-*g*-PLA(10%) can be selected for further studies.

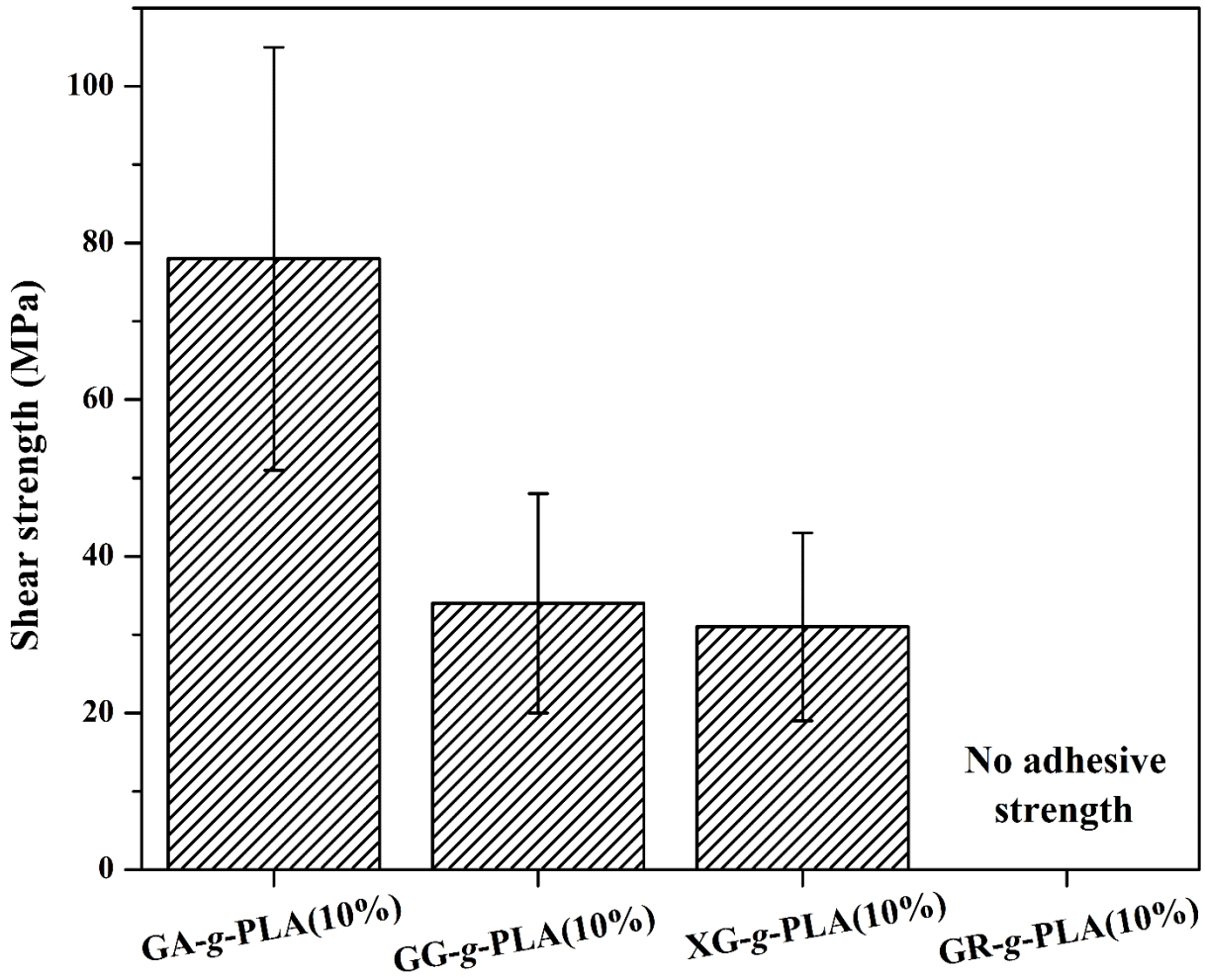

Figure 3.6. Single lap shear test of modified gums.

3.2.7. Fabrication of PLA/modified gums (5%) bionanocomposite films

From the preparation of various films by solution casting method, it was observed that PLA film can be made homogeneous and uniform by the dispersion of PLA granules in chloroform but not in water due to its hydrophobic nature as shown in figure 3.7. By the visual inspection of the film, the transparency was quite good which is sufficient for food packaging. The film can easily be peeled off from the petri dish which supports easily handing of such film. Whereas, the neat gum films (GA, GG, XG and GR) can only be prepared by dissolving it into millipore water due to hydrophilic nature. All the prepared neat gum films were very brittle except neat GA film. It was

very difficult to peel off the films from petri dish due to brittleness. Even though it was very difficult to handle neat GA film. On the other hand, the films were easily prepared by PLA and modified gums together. The modified gums were hydrophobic in nature and become soluble in chloroform and hence, compatible with PLA. In such films, PLA was used as matrix and modified gums were used as filler or reinforcement material. The prepared PLA/modified gum films were translucent and easy to handle as PLA.

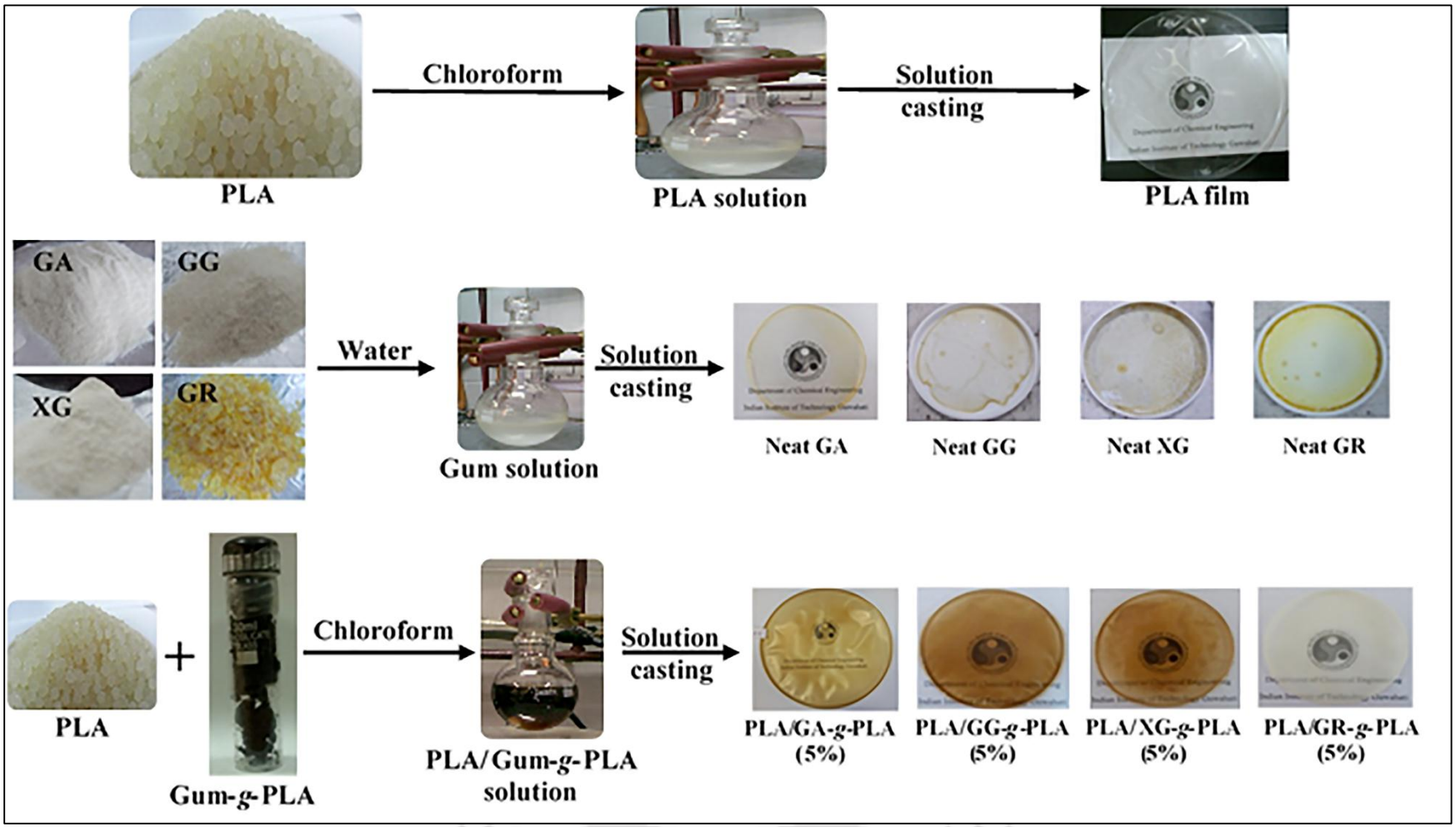

Figure 3.7. Layout of prepared films by solution casting method.

3.2.8. Scanning electron microscopy of PLA/modified gum films

SEM analysis of all PLA/modified gum films was performed to choose the best film which can be further used in food packaging application. As shown in figure 3.8, as the modified gums were introduced into PLA films in the ratio 1:20, change in the surface morphology in films were observed. The uniform and homogenous micro & nano-spheres in PLA/GA-*g*-PLA films were observed. However in PLA/GG-*g*-PLA films, only micro-spheres were observed which were not homogeneously distributed. The non-uniform matrix of the PLA/GG-*g*-PLA films were also observed. In PLA/XG-*g*-PLA films, non-uniform spheres of different sizes showed the less compatibility of the masterbatch in PLA matrix than that of PLA/GA-*g*-PLA films and PLA/GG-*g*-PLA films. The presence of several pits and cavities in PLA/GR-*g*-PLA films were observed which are also not required in films for packaging application. From the findings, it was concluded that among all the modified gum films, modified GA film proved to be the best for selection for food packaging applications among the rest modified gum films.

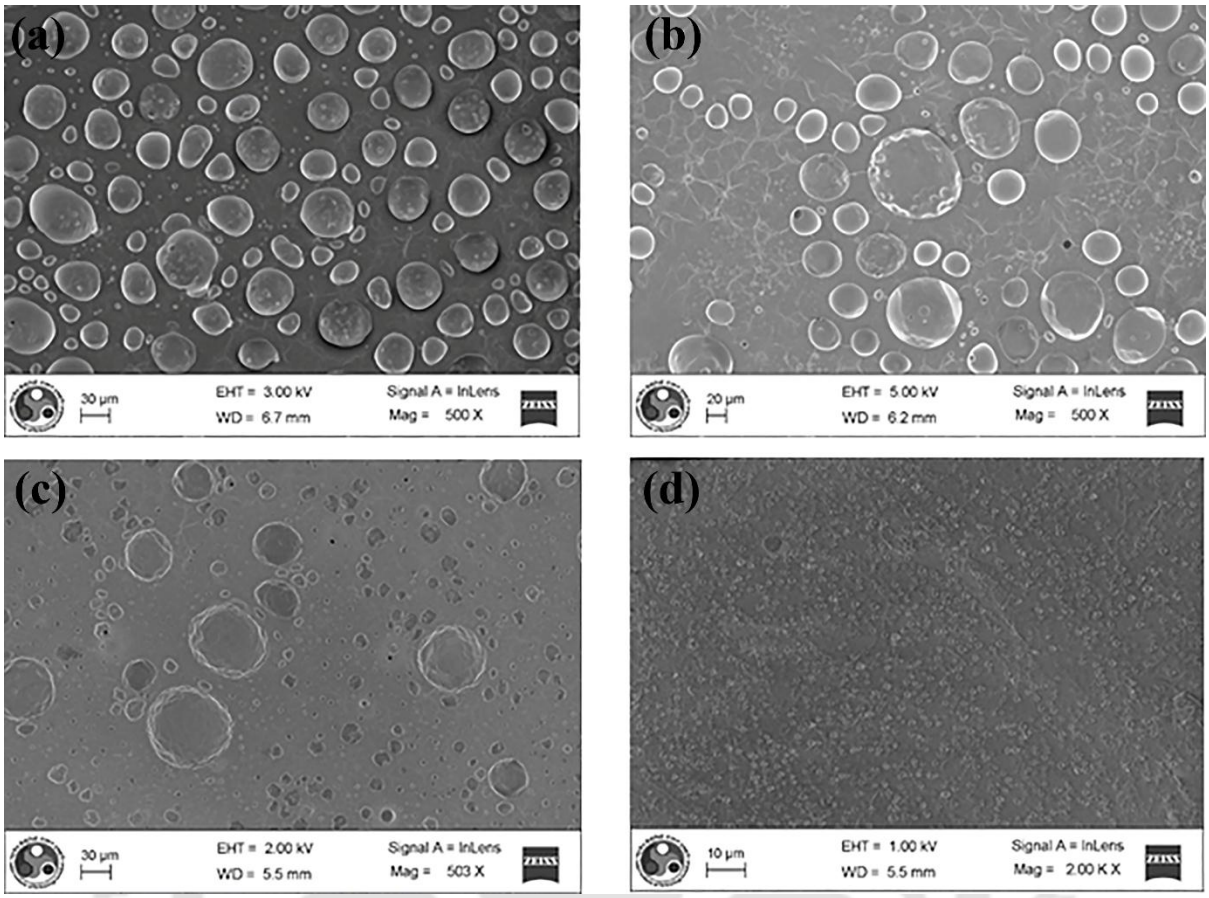

Figure 3.8. Modified gum 5% films: (a) PLA/GA-*g*-PLA, (b) PLA/GG-*g*-PLA, (c) PLA/XG-*g*-PLA, (d) PLA/GR-*g*-PLA.

3.3. Summary

The four polysaccharide gums were selected and modified by the grafting process. The grafting was conducted by the conventional as well as microwave heating method based on the reaction time, grafting and solubility. The microwave heating method was better than that of conventional heating process. During the analysis, LA molecules were grafted on the polysaccharide gums backbone. After the grafting process the hydrophilic GA, GG and XG were converted to hydrophobic material. However, no change in solubility was observed for

GR. The modified gums were tested to check the adhesive strength. From the single lap shear test of all the four modified gums, it was inferred that the GA-*g*-PLA(10%) showed the best binding strength of glass substrates. The films were also prepared using the modified gums by solution casting method. The modified gums were used as filler in PLA matrix. The surface morphology of the films showed that GA-*g*-PLA can prove to be the best filler for food packaging application. Hence, it can be concluded that GA-*g*-PLA should be used for both the applications that is as an adhesive for binding glass and similar objects and as filler in food packaging application.

Chapter 4

Synthesis and Characterization of Microwave Initiated Gum Arabic Grafted Poly L-Lactic Acid Bionanocomposite

The chapter presents the investigation on gum arabic (GA) grafted poly l-lactic acid (PLA) bionanocomposite [GA-g-PLA] which has been synthesized by using microwave heating in which the hydrophilic GA has been grafted with in-situ grown lactic acid oligomer. The grafting at $O-H$ and $N-H$ groups in GA backbone with oligo-(L-lactic acid) (OLLA) chains has been confirmed by FTIR and NMR analyses. XRD, TGA, SEM and TEM analyses supports uniform dispersion of GA in OLLA due to effective grafting reaction. The prepared bionanocomposite has been found to be amorphous in nature which has been proved by XRD and DSC analyses due to unavailability of crystallization peak and broad peak of heat of fusion.

4.1. Introduction

The natural polysaccharides have many advantages over synthetic polymers such as low cost, easy availability, nontoxicity and biodegradability. Among the different polysaccharides, gums have tremendous applications in many fields. Due to its emulsifying and stabilizing properties, it is used in beverages, paints, cosmetics and pharmaceutical industries. Among the various polysaccharides, Gum Arabic (GA) is a complex polysaccharide derived from an exudate of Acacia trees namely *Acacia senegal* and *Acacia seyal*. The molecular structure of GA has three

main fractions such as arabinogalactan (AG), arabinogalactan-protein (AGP) and glyco-protein (GP). It has approximately 90% AG fraction with very little associated protein, ~ 10% AGP fraction with ~10% of protein component, and about 1% GP fraction with ~20-50% of protein component. GA has proteinaceous molecules as an integral part of the structure. Many researchers carried out studies on grafting of GA with different materials such as polyaniline **(Tiwari et al., 2008)**, acrylonitrile **(Thota et al., 2012; Abdel-Razik et al., 2013)**, soy protein isolate **(Mu et al., 2010)** using different processes.

Many modifications of polysaccharides have also been made to achieve the desired physical, chemical and biological properties. The polysaccharides can be modified by many ways such as derivatization of functional groups, etherification, hydrolytic degradation, oxidative degradation or grafting of polymeric chains **(Setia et al., 2014)**. Among the different methods, grafting is one of the promising method for polymer modification of which has gained much attention recently. According to the literature, the graft copolymers can be defined as a long chain of polymer backbone having branched polymer side chains **(Rani et al., 2013; Rani et al., 2013)**. The graft copolymer can be synthesized by using the external agent for creating the free radical sites on which the grafted chains get attached and added up on the polymer backbone through chain propagation step **(Mahto et al., 2014)**. It should be noted that the external agent should not rupture the structural integrity of the preformed polymer chain **(Mahto et al., 2014)**. Graft copolymerization can be mainly conducted by chemical initiation and radiation techniques **(Setia et al., 2014)**.

Recently great interest has been increasing on the synthesis of graft copolymers by microwave radiation due to its ease of operation, high reproducibility and less reaction time **(Rani et al., 2013)**. The 'selective excitation' caused by microwave radiations leads to the rupture or

cleavage of polar bonds which results in the formation of free radical sites at the points of radiation exposure however the structural integrity of the backbone is not affected by the microwave radiation because of the non-polar 'C-C' bonds **(Rani et al., 2013; Rani et al., 2013)**. The synthesis of graft copolymers in the presence of microwave radiation can be basically classified into two types namely microwave assisted and microwave initiated synthesis. In microwave assisted synthesis, grafting is initiated by chemical free radical initiator and microwave radiation. Whereas in microwave initiated synthesis, grafting is only initiated by microwave radiation for creating the free radical sites on polysaccharide.

In the present work, the modification in GA molecule was conducted by L-lactic acid (LA) (2-hydroxy propanoic acid) by microwave initiated method. LA is also a bio-based material which is produced by fermentation of naturally occurring renewable sources such as corn, sugarcane, sweet potato etc. LA has bifunctionality as it has hydroxyl and carboxyl functional groups which promotes intermolecular esterification and grafting.

Hitherto, no report has been found on the microwave initiated synthesis of GA grafted PLA. In this work, the effect of GA concentration was investigated on different properties. FTIR, NMR, XRD, GPC and contact angle analyses were conducted to determine different properties of the synthesized bionanocomposite. The thermal properties of the bionanocomposite were studied by DSC and TGA analyses. SEM and TEM analyses were carried out to study surface morphology.

4.2. Results and Discussion

4.2.1. Microwave initiated synthesis of gum arabic grafted poly l-lactic acid (GA-*g*-PLA)

In the process LA molecules were grafted on GA backbone on exposure of the microwave irradiation. The microwave setup for synthesis of GA-*g*-PLA bionanocomposite is shown in

figure 4.1. During the reaction, microwave radiations have irradiated the small polar molecules of water which resulted in generation of heat. The free radical sites were also generated on polar groups of the polysaccharide GA backbone and LA monomer on exposure of microwave radiation. When the free radical sites were produced on GA backbone, LA monomer was attached and added up on the GA backbone **(Sen et al., 2010)**. The brown color was developed when the reaction mixture was heated for certain time when grafting have taken place due to Maillard-type reaction.

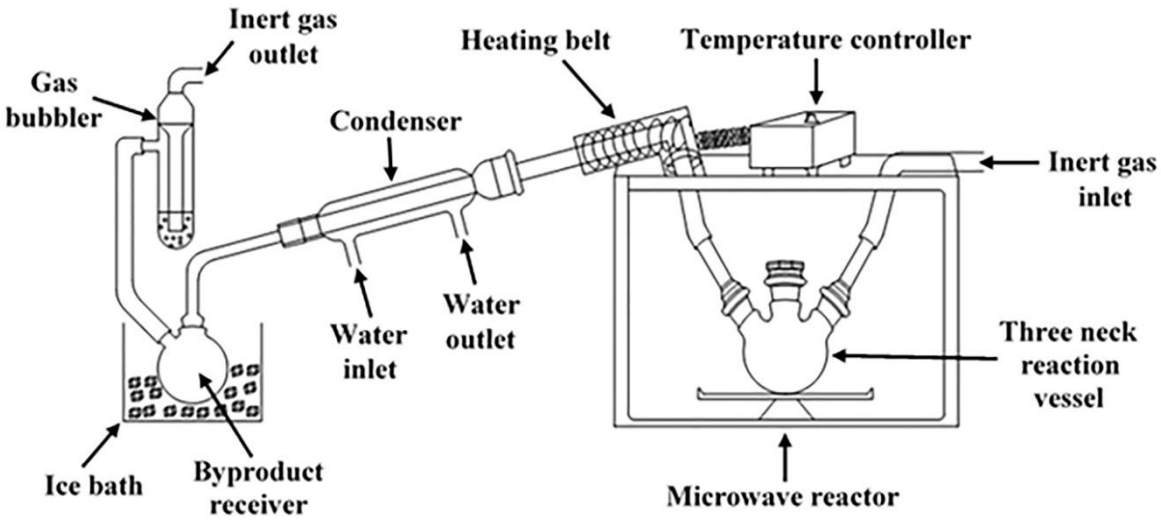

Figure 4.1. Microwave setup for synthesis of GA-*g*-PLA bionanocomposites.

The reaction occurred between the free amino groups of protein in GA which were grafted with the reducing end groups of the polysaccharide or LA molecules **(Guan et al., 2011; Guan et al., 2006)**. The percentage grafting (%G) and percentage grafting efficiency (%GE) were evaluated and have been shown in table 4.1.

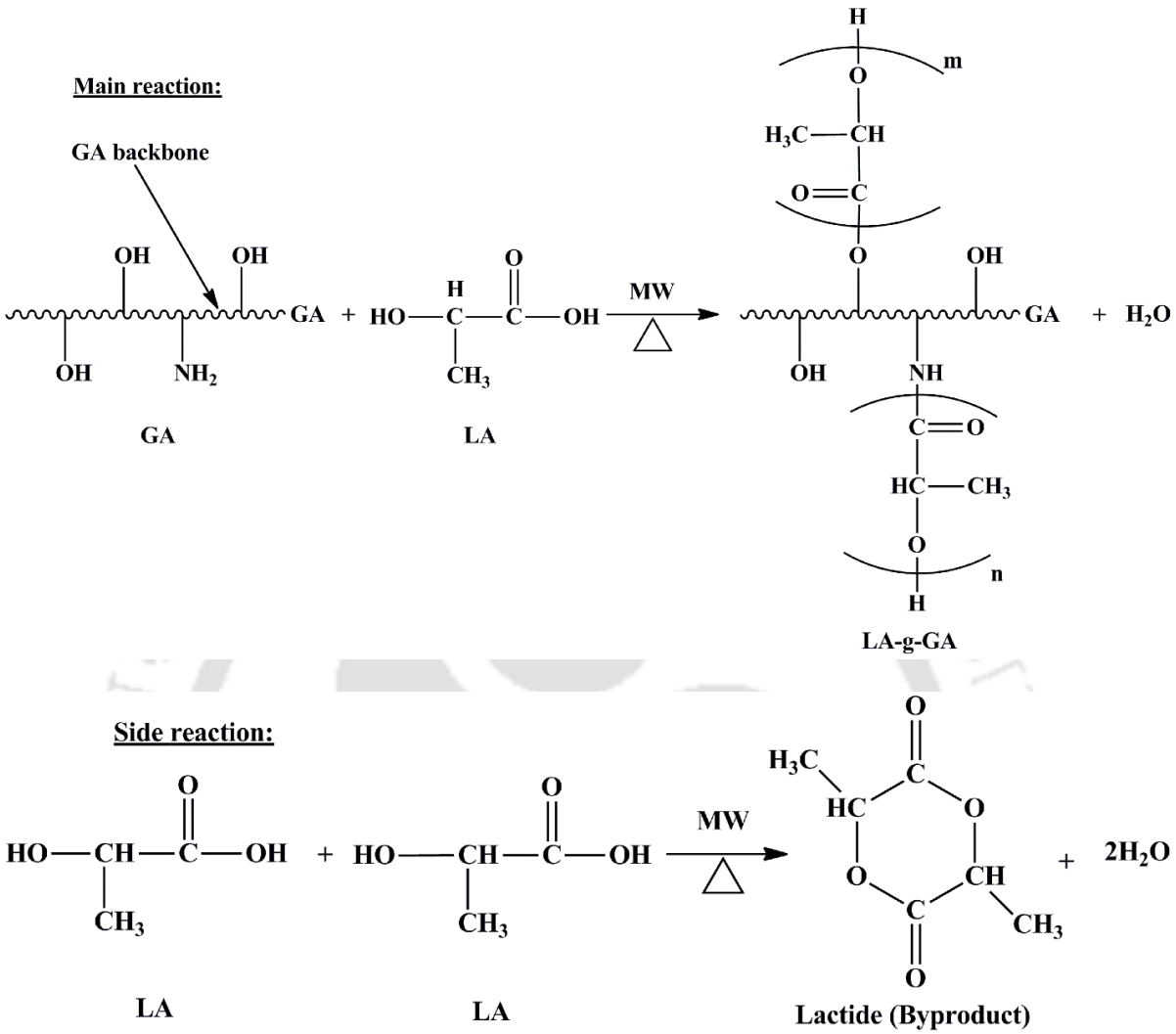

Scheme 4.1. Synthesis of GA-*g*-PLA bionanocomposite.

4.2.2. Solubility and grafting calculations

The solubility of GA, OLLA and synthesised grafted samples was checked in chloroform and millipore water as shown in table 4.1. It is clearly observed from the table that the solubility of OLLA and grafted samples are completely different from GA. Neat GA powder was soluble in water but not soluble in chloroform whereas, OLLA and grafted samples were soluble in chloroform but not in water. This change in solubility confirmed that the chemical modification

on GA backbone occurred. Both the grafting efficiency (%) and percentage grafting were decreased on increasing the GA concentration. The decrease in grafting efficiency (%) is due to the unavailability of LA monomers for chain propagation. So, all the available active sites of GA molecules were not consumed by LA. Whereas, in the case of percentage grafting, the possible reason of reduction is due to the formation of more homopolymer through competing reaction process **(Mishra et al., 2011; Alfaifi et al., 2014)**.

Table 4.1. Various properties of GA, OLLA and bionanocomposites.

Sample Name	Solubility		Grafting efficiency (%)	Percent grafting (%)	Contact angle (deg.) ± Std. Dev.
	Water (%)	Chloroform (%)			
GA	100	0	-	-	20 ± 2
OLLA	0	100	-	-	29 ± 2
GA-*g*-PLA(5%)	0	95	64.35	1287	54 ± 2
GA-*g*-PLA(10%)	0	82	51.50	515	76 ± 2
GA-*g*-PLA(15%)	0	71	41.80	279	80 ± 2
GA-*g*-PLA(20%)	0	66	34.78	174	58 ± 2

4.2.3. Fourier transform infrared spectroscopy analysis

FTIR analysis was conducted for investigating intermolecular interaction and to predict the possible changes in the grafted samples. Figure 4.2 shows FTIR spectra of GA, LA, OLLA and GA-*g*-PLA bionanocomposites. The peaks at 1133 cm^{-1}, 1204 cm^{-1}, 1094 cm^{-1} and 1045 cm^{-1} represents $-C-O-$ stretch in the samples. Peaks at 1750 cm^{-1} and 1454 cm^{-1} attributes to $-C=O$ carbonyl stretching and $-CH_3$ bending respectively. The decrease in the

peak intensity in GA-*g*-PLA samples at 1750 cm^{-1} was observed with increase in loading of GA reflects grafting phenomena. It was also observed that the peak at 3635 cm^{-1} of OLLA was shifted to 3641 cm^{-1} in GA-*g*-PLA bionanocomposites. Furthermore, the reduction in intensity was also detected which suggested grafting occurred at $O-H$ and $N-H$ groups on GA backbone with OLLA molecular chains.

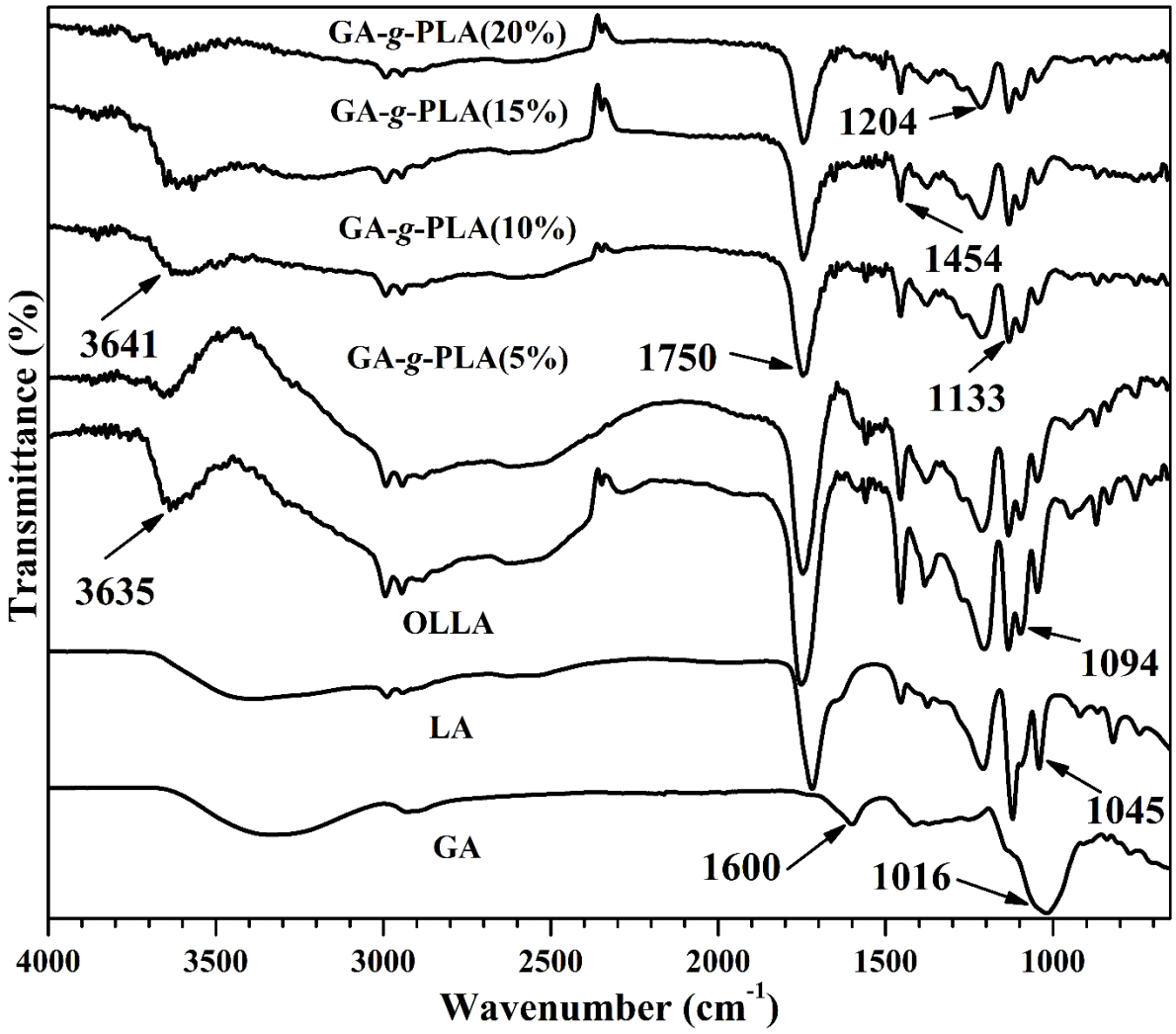

Figure 4.2. FTIR spectra of GA, LA, OLLA, GA-*g*-PLA(5%), GA-*g*-PLA(10%), GA-*g*-PLA(15%) and GA-*g*-PLA(20%) bionanocomposites.

4.2.4. Nuclear magnetic resonance analysis

The ^{1}H-NMR of OLLA and GA-*g*-PLA was conducted to study the grafting as shown in figure 4.3. The OLLA peaks were observed at 1.4, 4.3 and 5.2 ppm which were present because of the methyl protons of the OLLA side chain, terminal $-C(CH_3)H-$ group and $-CH-$ hydrogen of lactyl moiety respectively. The presence of the GA results in reduction of the intensity at 4.37 ppm in bionanocomposite which confirmed the grafting of *oligo*-(lactic acid) on $-NH_2$ group of GA backbone. Furthermore, shift in the peak intensity was observed from 3.8 to 3.4 ppm confirmed grafting at $-OH$ group.

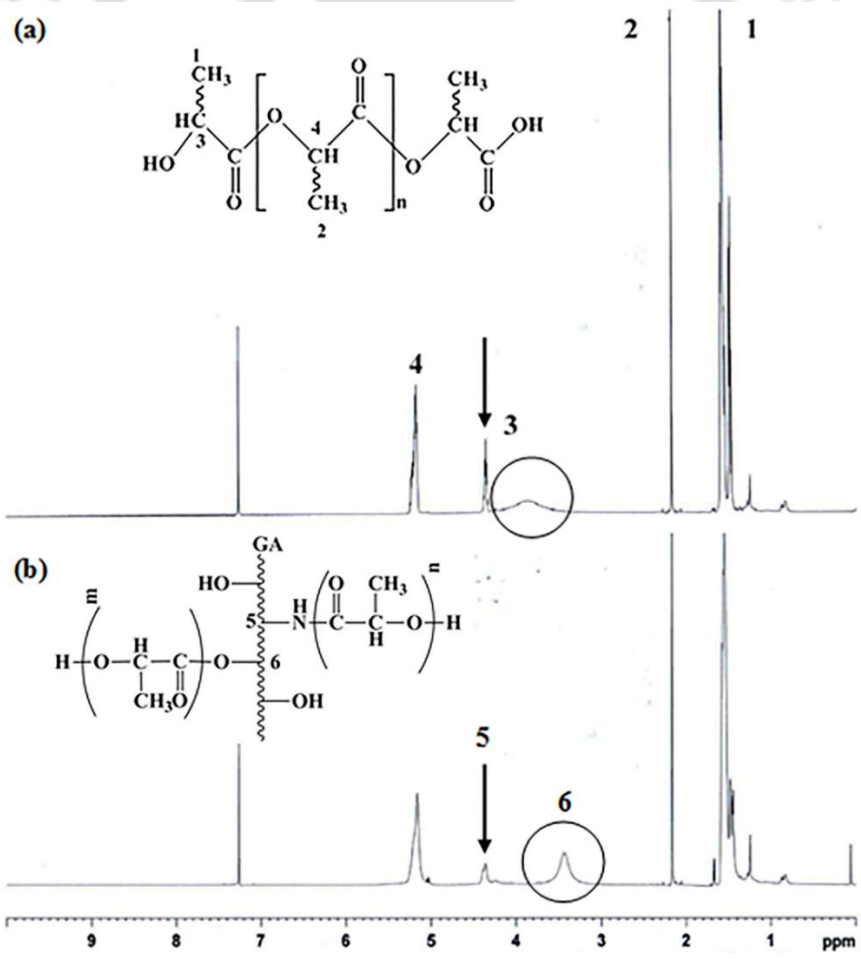

Figure 4.3. ^{1}H NMR spectra of (a) OLLA and (b) GA-*g*-PLA(15%) bionanocomposite.

4.2.5. X-ray diffraction analysis

XRD patterns of GA, OLLA and GA-*g*-PLA bionanocomposites are compared in figure 4.4. GA showed a broad intensity or a hump with a maximum intensity at approximately 19.5° indicating the amorphous structure. Furthermore, no such hump or any peak was observed in the synthesized GA-*g*-PLA bionanocomposites. It was explained by the fact that randomness of amorphous phase in the graft copolymers was enhanced by the grafting of LA on GA backbone, which gave rise to a disruption of long-ranged spacing between the molecular chains. This suggested that amorphous nature increased after grafting and modification occurred in bionanocomposite.

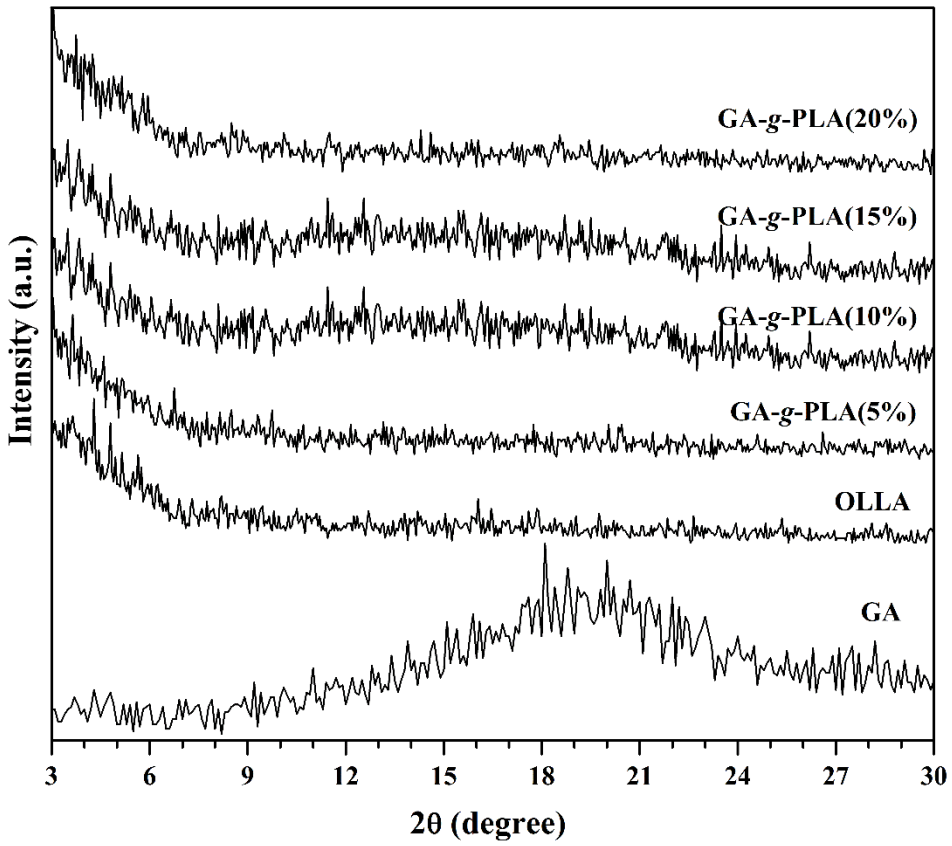

Figure 4.4. XRD pattern of GA, OLLA and GA-*g*-PLA bionanocomposites.

4.2.6. Gel permeation chromatography analysis

GPC analysis was performed for OLLA, GA-*g*-PLA(5%), GA-*g*-PLA(10%), GA-*g*-PLA(15%) and GA-*g*-PLA(20%) samples. It was observed that the number average (M_n) and weight average (M_w) molecular weights for OLLA were 700 and 850 g mol^{-1} respectively (table 4.2).

Table 4.2. GPC analysis of OLLA and GA-*g*-PLA bionanocomposites.

Sample	Molecular weight		Poly dispersity index (PDI)
	M_n (g mol^{-1})	M_w (g mol^{-1})	
OLLA	700	850	1.21
GA-*g*-PLA(5%)	1130	1990	1.76
GA-*g*-PLA(10%)	1060	2520	2.38
GA-*g*-PLA(15%)	1140	2470	2.16
GA-*g*-PLA(20%)	1100	2570	2.33

This low molecular weight of OLLA confirms that the oligomerization occurred in maintaining these reaction parameters. The poly dispersity index (PDI) was observed as 1.21 which means that the prepared OLLA was bifunctional. The M_n and M_w values of the grafted samples were found in the range of 1060-1140 g mol^{-1} and 1990-2570 g mol^{-1} respectively which are higher than that of OLLA as shown in figure 4.5. The PDI was also found in the range of 1.76 to 2.38 which confirms the improvement in functionality and supports the grafting phenomena.

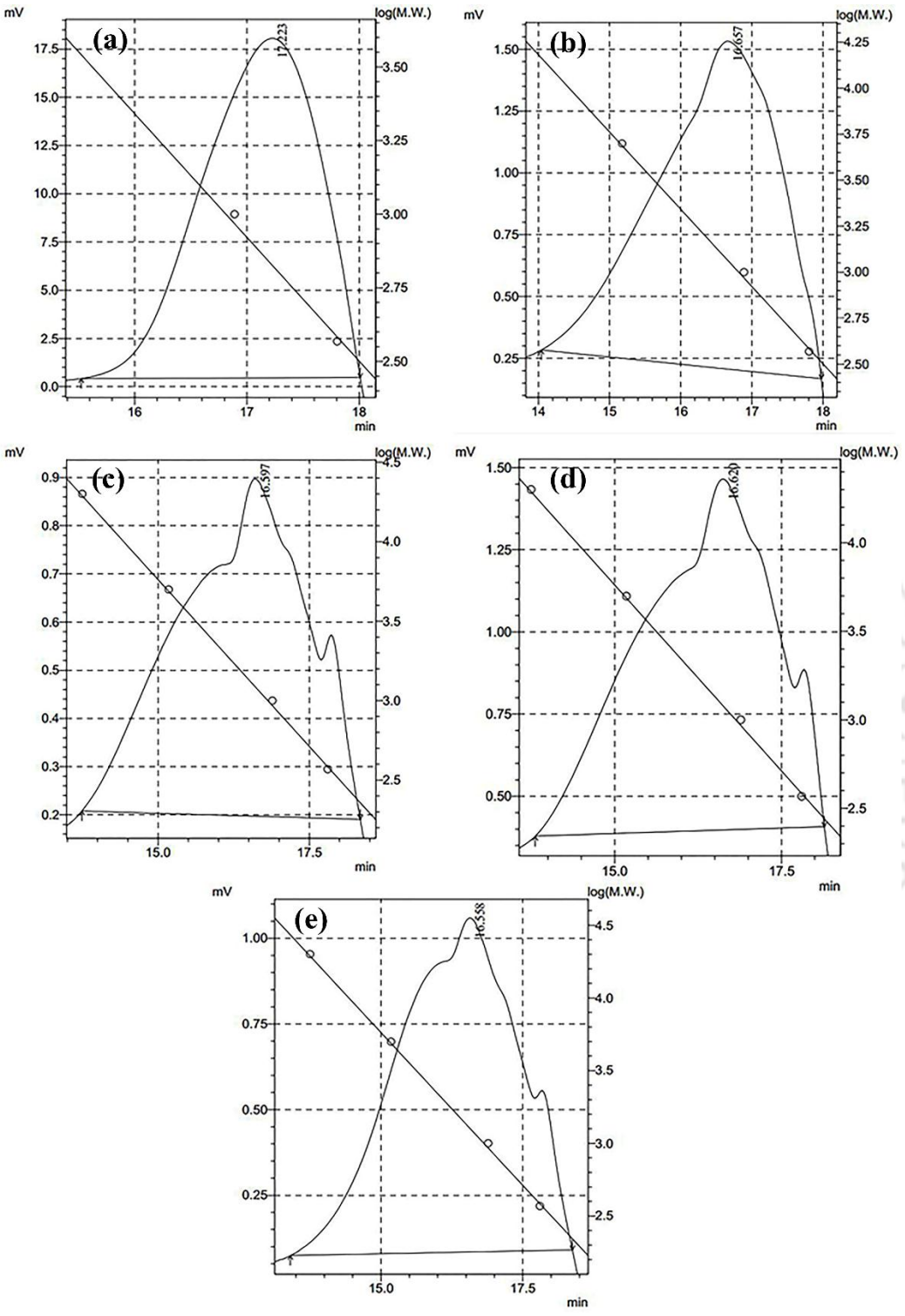

Figure 4.5. GPC curves of (a) OLLA, (b) GA-*g*-PLA(5%), (c) GA-*g*-PLA(10%), (d) GA-*g*-PLA(15%) and (d) GA-*g*-PLA(20%).

4.2.7. Differential scanning calorimetry analysis

DSC thermograms of the samples are shown in figure 4.6. In the first heating cycle, a very broad endothermic peak was observed around 56 °C for GA (precisely designating thermal transitions is difficult) **(Ganie et al., 2015)**. The resulted broad peak was due to the melting and partial thermal decomposition of the complex polysaccharide **(Ahmad et al., 2013)**. **Zohuriaan et at. (2004)**, reported that transition is due to dehydration from hydrophilic functional group. Figure 4.6 (a) and (b) do not showed T_c and T_m peaks in bionanocomposites, suggests that either amorphous segment does not crystallize itself or they do not have well-ordered hard domain (arranged molecular chains).

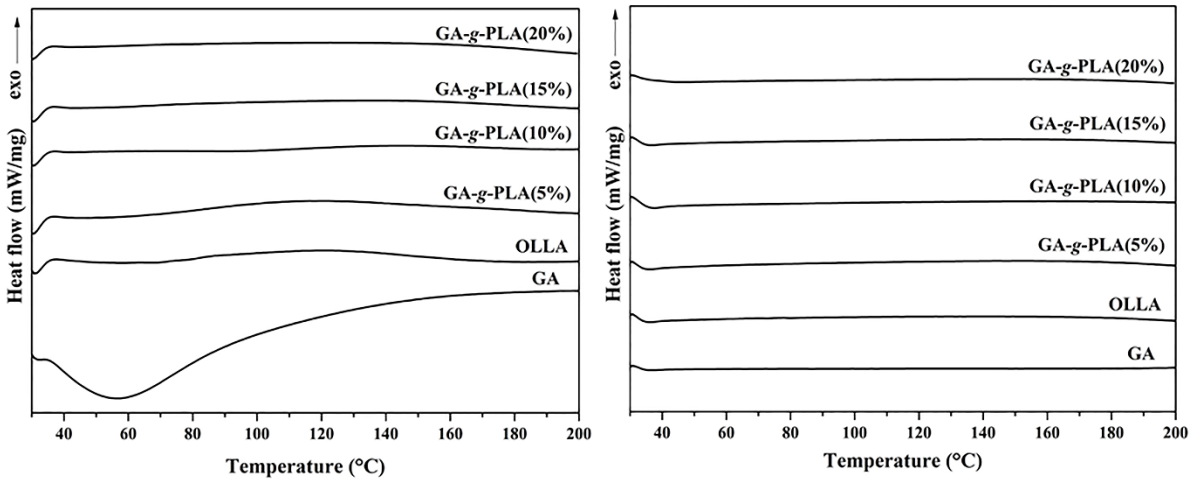

Figure 4.6. DSC thermograms (exo up) for (a) first heating scan and (b) second heating scan of GA and GA-*g*-PLA bionanocomposites.

4.2.8. Thermogravimetric analysis

Thermogravimetric analysis (TGA) have been conducted for GA, OLLA and GA-*g*-PLA bionanocomposite at a heating rate of 20°C min^{-1} under inert atmosphere. Two significant

peaks were observed at different temperature ranges for GA powder which denote the different weight losses during heating. The first broad peak in the temperature range of 35-162 °C denotes the removal of unbound and bound and unbound moisture as shown in figure 4.7. Whereas, no such peaks were observed for OLLA and GA-*g*-PLA samples in this temperature range, shows hydrophobic nature. The single degradation peak or peak temperature (T_p), was observed in the bionanocomposites suggested that the grafting occurred between LA and GA. The T_p was observed at 327 °C, 276 °C, 282 °C, 285 °C and 296 °C for GA, GA-*g*-PLA(5%), GA-*g*-PLA(10%), GA-*g*-PLA(15%) and GA-*g*-PLA(20%) respectively as shown in table 4.3. The increment in T_p was observed with increase in GA concentration in bionanocomposites due to the presence of more entangled GA-*g*-PLA oligomer chains. Whereas, two degradation peaks of OLLA were observed at 197 °C and 266 °C due to the presence of two different molecular weights of OLLA formed during microwave irradiation. The onset and offset temperature for GA powder were observed at 243 °C and 388 °C respectively. The onset-offset range for the samples are listed in table 4.3. Henceforth, it is confirmed that the thermal stability increases with increase in GA concentration in bionanocomposites.

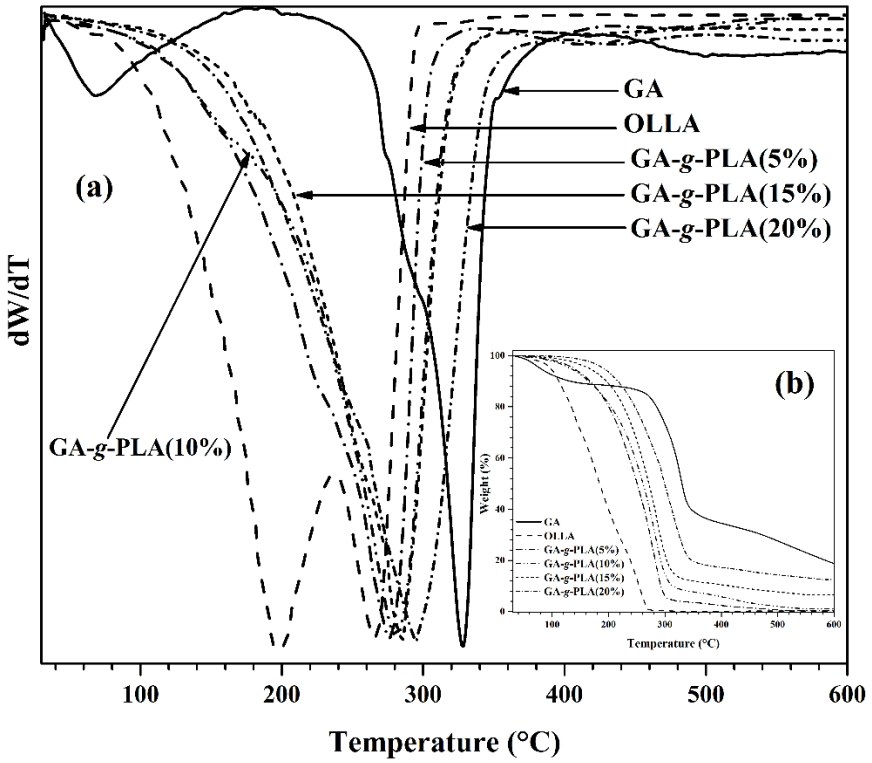

Figure 4.7. TGA and DTG thermograms of GA, OLLA and bionanocomposites.

Table 4.3. Thermogravimetric analysis of GA, OLLA and bionanocomposites.

Sample name	T_{on} (°C)	T_p (°C)	T_{off} (°C)
GA	243	327	388
OLLA	81	197, 266	298
GA-*g*-PLA(5%)	114	276	317
GA-*g*-PLA(10%)	115	282	334
GA-*g*-PLA(15%)	122	285	337
GA-*g*-PLA(20%)	126	296	367

4.2.9. Surface morphology

The surface morphology of GA and GA-*g*-PLA was determined by SEM, as shown in figure 4.8(a) and (b). The smooth granular structure of GA was significantly changed to closely packed particles of GA-*g*-PLA which appeared to be quite different from that of parent GA which resulted because of the grafting of oligomeric chains of LA on GA backbone. Hence, it is evident from the micrographs that the significant change in surface morphology occurred which confirmed grafting **(Tiwari et al., 2008; Thota et al., 2012)**. Homogenous dispersion of nano size grafted GA particles have been observed in TEM analysis. However, the agglomeration of GA nanoparticles were also observed from figure 4.8(c).

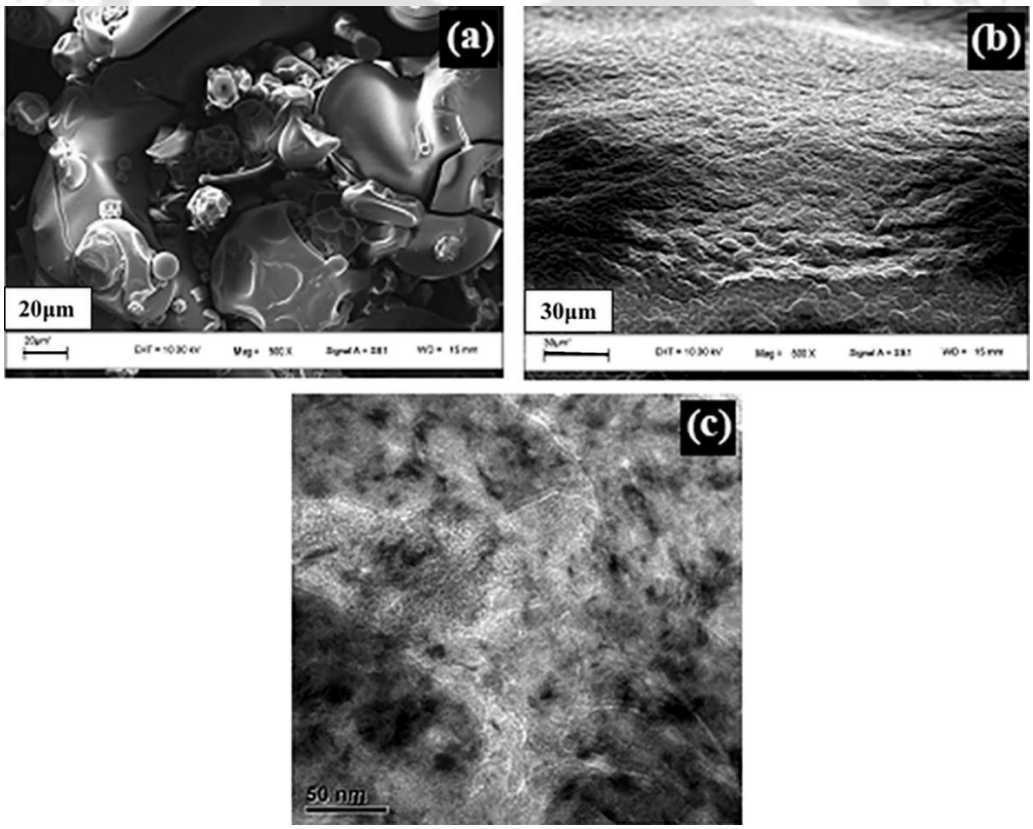

Figure 4.8. (a), (b) SEM images of gum arabic, GA-*g*-PLA(15%) and (c) TEM image of GA-*g*-PLA(15%) bionanocomposite.

4.2.10. Contact angle analysis

By static contact angle measurement, hydrophilic/hydrophobic character of the surface was evaluated. Table 4.1 shows the water contact angles for the samples. It was observed that with increase in loading concentration of GA i.e. for 5, 10 and 15%, reduction in contact angle was observed due to reduction in –COOH and –OH group present in GA backbone. The hydrophobicity of GA-*g*-PLA was also significantly improved by the substitution of the hydrophilic polar groups of GA with hydrophobic ester groups of OLLA. This confirmed that the grafting process replaced polar groups on the surface of GA backbone and conferred a more hydrophobic character to the GA-*g*-PLA. However at 20% concentration, reduction in contact angle was observed due to the unreacted GA groups in bionanocomposite which resulted in increase in polar groups on the surface. The polar groups consecutively give rise to a more wettable surface, as indicated in figure 4.9.

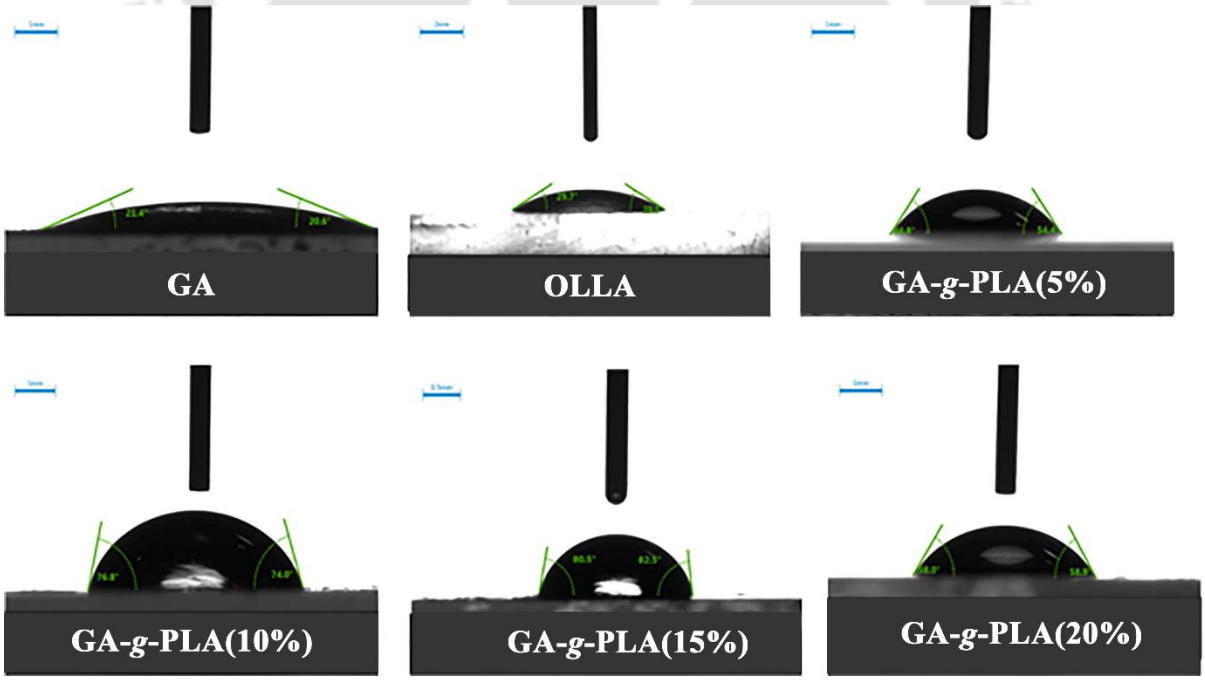

Figure 4.9. Contact angle analysis of GA, OLLA and GA-*g*-PLA bionanocomposites.

4.3. Summary

The synthesis of gum arabic grafted poly lactic acid (GA-*g*-PLA) was conducted by microwave initiated polycondensation method. The synthesis of GA-*g*-PLA samples resulted in the conversion of hydrophilic GA to hydrophobic bionanocomposite. The change in the grafting efficiency was observed with change in the GA concentration. The FTIR and NMR analyses confirmed that the grafting of *oligo*-(lactic acid) on GA backbone occurred at $-OH$ and $-NH$ groups. The XRD analysis revealed that the synthesized bionanocomposite is amorphous in nature. The M_n of the bionanocomposites were in the range of 1060 to 1140 g mol^{-1} which was determined by GPC. No T_c and T_m were obtained in DSC analysis suggested that well-ordered molecular chains are not present in the bionanocomposites. On increasing the concentration of GA, thermal stability enhanced due to increase in entanglement of molecular chains. Significant change in the surface morphology was observed by SEM analysis which also supports grafting. The presence of GA nanoparticles were observed in TEM images. The surface characteristics on the bionanocomposites were observed by contact angle analysis. The improvement in hydrophobicity occurred with increase in GA concentration confirmed the reduction in polar groups due to grafting. The shear test parameters were optimized to check the adhesive strength of the synthesized bionanocomposites for glass as well as granite substrates. The single lap shear test for the adhesive resulted in substrate failure. The prepared bionanocomposite was proved to be remarkable adhesive with respect to the present bio-based adhesives.

Chapter 5

Microwave Initiated Gum Arabic Grafted Poly L-Lactic Acid Bionanocomposite: Adhesive Application

The chapter presents the performance of microwave initiated gum arabic grafted poly l-lactic acid bionanocomposite for adhesive application. The single lap shear test has been performed to check the binding ability of the synthesized bio-based adhesive. The various parameters of the adhesive have been tested such as compression load, compression time and the effect of concentration of GA in the composite. The bio-based adhesive showed excellent adhesive strength for glass and granite substrates.

5.1. Introduction

Adhesives are very important materials that we encounter in our everyday life. It can be used in wide and diversified fields such as packaging, automobiles, medical, household etc. Adhesive is defined as a material which bonds together the surfaces of two substrate materials. Hence, the selection of adhesive must be based on its bonding capability of other surface either by physical or chemical bonds. Surfaces bind with chemical bonds are permanent in nature than bonding via van der Waals forces in case of physical bonding. Adhesives are further preferred in day to day life due to its ability to join thinner materials, better stress distribution over joint area with improved joint strength and ability to join dissimilar materials. Application of adhesive may minimally change the aesthetic appearance of joint substrate.

Presently, most of the adhesives are prepared from precursors obtained from non-renewable resources such as crude oil. In most of the adhesives, petroleum based volatile organic compounds (VOCs) are also used which evaporate from the adhesive compositions and cause environmental pollution. The efforts have been made to identify the bio feedstock based sustainable adhesives which can be used to replace conventional ones. As per the available literature, we could not find sufficient information in this field. However, some of the bio-based polymers such as starch, soy-proteins, lignin, vegetable oils and their derivatives are in process of exploring its application towards adhesive. For examples, many companies like Cargill (Minneapolis, MN, USA), Henkel (Düsseldorf, Germany), 3M and others, have started research on development of non-toxic adhesives. These adhesives are obtained from corn and soybean which are used in paper bags, wallpaper, furniture, plywood and pharmaceutical preparations **(Imam et al., 2013)**. Such adhesives can be possible candidates for the proposed research work. One of the important bio-based precursors that have been identified based on its characteristics is lactic acid. Other component(s) will be directly used as extracted from plant sources such as polysaccharide gums. Further to improve the performance of adhesives, the use of concepts of nanotechnology will be explored to develop adhesives for fixing structural substrates.

Hitherto, no report has been found on the adhesive application of GA grafted PLA, synthesized by microwave initiated method. In this work, the effect of GA concentration was investigated on different properties. Adhesive property of the bionanocomposite was analyzed by single lap shear test.

5.2. Results and Discussion

5.2.1. Substrate lamination protocol

Slabs of glass and granite were cleaned properly using acetone & dried to remove acetone. Before applying adhesive on both end/area of the substrates, pieces were heated at around 70-90 °C. These pair of substrates were placed between the compression plates on one another and a fixed load was applied for a fixed time. When the pieces got stuck to each other, single lap shear test was performed.

5.2.2. Single lap shear test

5.2.2.1. Adhesive performance at various substrates

The adhesive strength of GA-*g*-PLA(10%) was checked for different samples at room temperature and 50-60% RH. The sample was melted and applied on the surface of the substrates at 70 C°. The laminates were prepared by applying the compression load of 1000 N for 10 min. The selected adhesive that is GA-*g*-PLA(10%) was also tested for other substrates apart from glass and granite, as shown in table 5.1. The results confirmed that the adhesive has the capability to bind only silica based substrates such as glass and granite. No adhesive strength was observed for any other substrates (table 5.1).

Table 5.1. GA-*g*-PLA(10%) adhesive for different substrates.

Test no.	Adhesive	Substrate	Shear strength (MPa)	Adhesion
1	GA-*g*-PLA(10%)	Paper	N/A	No
2		Aluminium foil	N/A	No
3		Wood	N/A	No
4		Metals	N/A	No
5		PET	N/A	No
6		**Glass**	90	**Yes**
7		**Granite**	80	**Yes**

5.2.2.2. Adhesive performance prepared at various conditions

The results present the single lap shear test before modification of GA. The adhesive strength of the different combinations of LA, GA and OLLA was checked to get the best adhesive strength for glass substrates (table 5.2). Among all the trials it was concluded that the best adhesive can only be achieved after the polycondensation of LA-GA system in microwave. Henceforth, the polycondensation process was followed for the preparation of adhesive.

Table 5.2. Adhesive tests at various substrates.

Test no.	Sample (GA, OLLA, LA)	Conditions	Shear strength (MPa)	Adhesive?
1	GA	Sample & glass **heated** till 200 °C	N/A	No
2	LA	Sample & glass **heated** at 70 °C & compressed	N/A	No
3	OLLA	Sample & glass **heated** at 70 °C & compressed	10.2	No
4	Stirred GA & OLLA (15%)	Applied on glass at **room temperature** & compressed	3.2	No
5		Sample & glass **heated** at 70°C & compressed	4.7	No
6	GA & OLLA (15%) reacted at **160°C for 2 h.**	Applied on glass at **room temperature** & compressed	6.5	No
7		Sample & glass **heated** at 70°C & compressed	6.7	No
8	Stirred GA & LA (15%)	Sample & glass **heated** at 70 °C & compressed	32.2	No
9	GA & LA (15%) reacted at **160°C for 2 h**.	Applied on glass at **room temperature** & compressed	43.9	No
10		Sample & glass **heated** at 70 °C & compressed	252.8	No

5.2.2.3. Adhesive performance for glass substrates

Different parameters such as compression load, compression time and adhesive concentration are responsible for adhesive strength. All these three parameters were optimized as per the table 5.3 in which 2000 N, 10 min. and GA-*g*-PLA(15%) were selected as optimized compression load, compression time and adhesive concentration respectively. The study was investigated to check the adhesive properties of GA-*g*-PLA by single lap shear test. The substrates were bind together using synthesized adhesive by applying the adhesive on both the surfaces of the laminates and then applying load to the joint for binding the substrates together. The effect of this compression load was also checked by varying the load and compression time. The effect of 10 and 15 wt.% of GA in bionanocomposite was analyzed for investigating adhesive strength. The experimental run for optimizing the parameters to get the best adhesive strength are systematically shown in table 5.3.

Table 5.3. Experimental run protocol for optimizing adhesive parameters for single lap shear test.

Experiment No.	Adhesive concentration (%)	Compression load (N)	Compression time (min)
1	GA-*g*-PLA(10%)	200 1000 2000	10
2	GA-*g*-PLA(10%)	Best compression load	2 5 10
3	GA-*g*-PLA(10%) GA-*g*-PLA(15%)	Best compression load	Best compression time

Optimization of parameters

Compression Load

One of the relevant parameter for determining the adhesive strength is compressive pressure applied during the cure of the adhesive. The compressive pressure was increased from 200 to 2000 N for conducting the test. Figure 5.1 shows the results of tensile lap-shear tests for GA-*g*-PLA(10%) with varying compression load. The average adhesive strength of 93, 111.5 and 230.5 MPa was calculated for compression load at 200, 1000 and 2000 N respectively.

On analyzing the bond stress-slip relations in figure 5.1 (i), (ii) and (iii); the behaviour of the adhesive describes that after an initial linear branch, the trend become nonlinear which confirmed the nonlinear behaviour of the GA-*g*-PLA(10%) adhesive **(Khshain et al., 2015)**. From the trend in figure 5.1 (i)-(iii), it was observed that the adhesive GA-*g*-PLA(10%) has elastic properties. After reaching the maximum load, the initiation of damage in the bond line starts. No cracking in the bond line was observed from the plots was confirmed as after reaching the maximum load, sudden decrease in shear stress was observed with displacement **(Chataigner et al., 2011)**. The adhesive shear stress reaches close to zero within 3 to 10 min which depends on the test conditions. From the results, it was concluded that the best adhesive strength was achieved at 2000 N compression load.

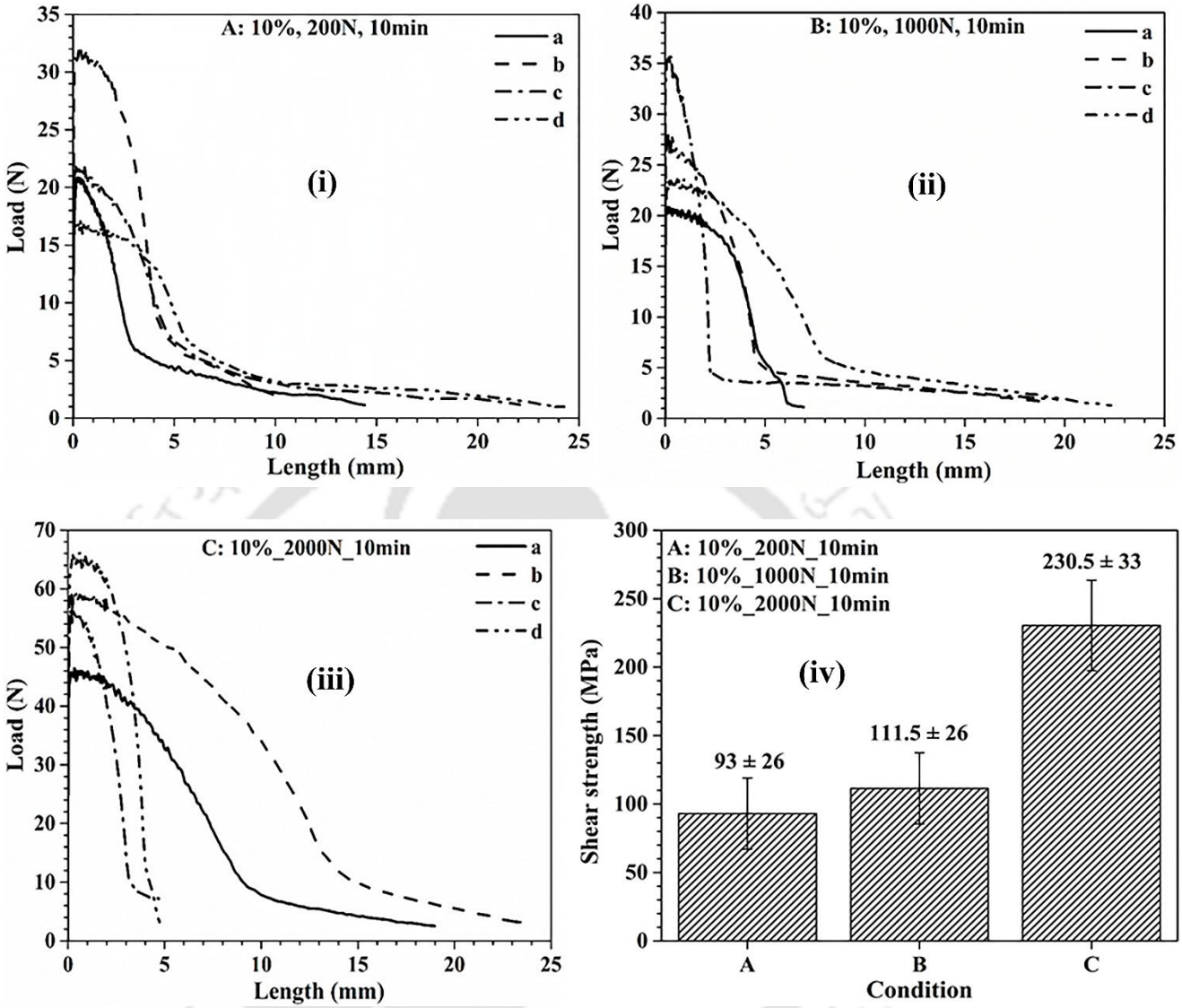

Figure 5.1. Optimization of compression load at (i) 200 N, (ii) 1000 N, (iii) 2000 N, (iv) comparison of shear strength at different compression loads.

Compression time

The single lap shear tests at various compression time are presented in this section. For GA-*g*-PLA(10%), the debonding mechanism at interface was observed by the load versus length graphs. The range of the amount of adhesive retained in the adhesive line is between 50 to 90 mg. The shear test was conducted for 2, 5 and 10 min compression time. On increasing

the compression time beyond 10 min, no increase in shear strength was achieved as the curing of the adhesive was completed within 10 min. From the results it was determined that the 10 min of compression time for the adhesive system gives the highest shear strength.

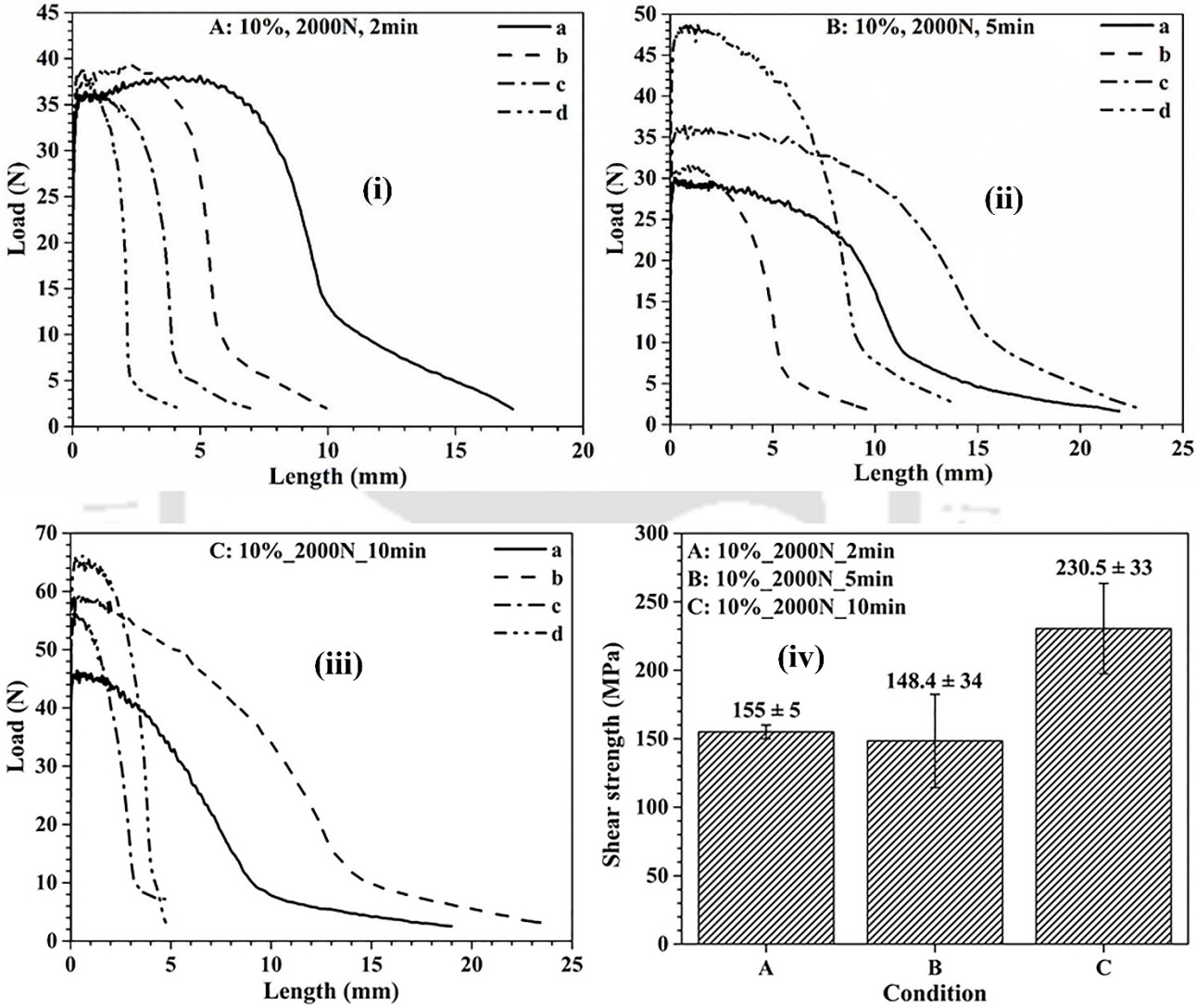

Figure 5.2. Optimization of compression time for (i) 2 min, (ii) 5 min, (iii) 10 min, (iv) comparison of shear strength at different compression time.

Adhesive concentration

Other important parameter optimized was the concentration of GA in composite. The 10 and 15 % was compared and the adhesive strength was determined. The debonding between the GA-*g*-PLA(10%) adhesive-glass substrate occurred resulted in cohesive failure. The best shear strength was obtained for GA-*g*-PLA(15%) on applying 2000 N compression load for 10 min. This proved to be the best combination of concentration and compression load which has ability to increase the joint rigidity drastically. Hence, for this combination adhesive has the capability to develop its full resistance capacity. For GA-*g*-PLA(15%), it was observed that, when the shear stress increases, the shear cracks develop on the substrate resulting in substrate failure. However, the adhesive bond line was intact and no deformation was observed in it. The substrate failure was observed for GA-*g*-PLA(15%), as the shear strength of the adhesive was larger than the tensile strength of the substrate. The adhesive strength was not obtained for 20% composites, because the high viscosity decreased the surface wettability.

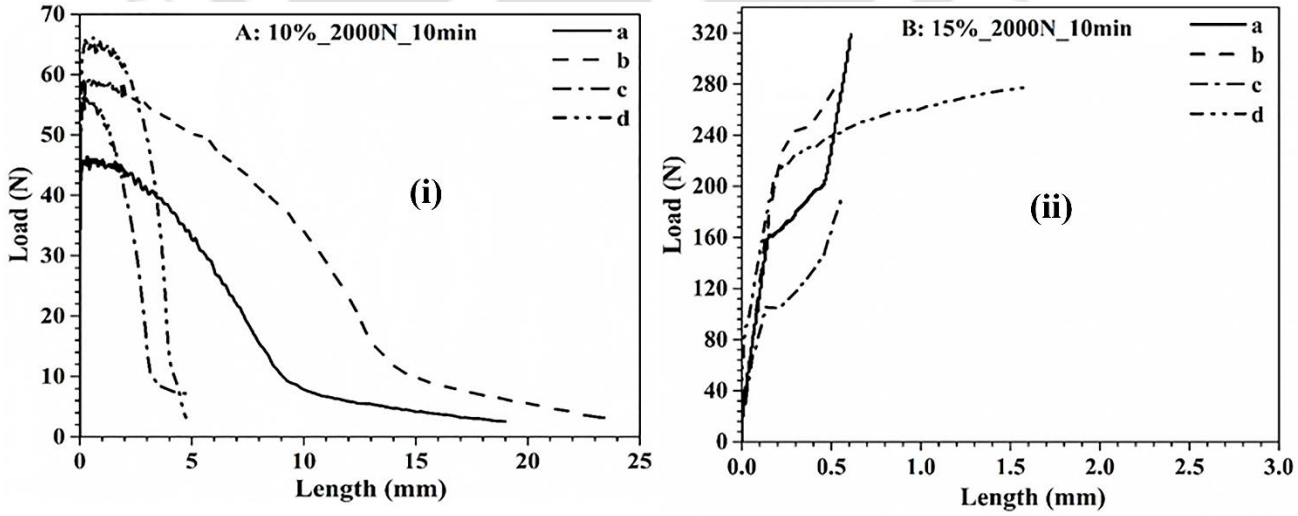

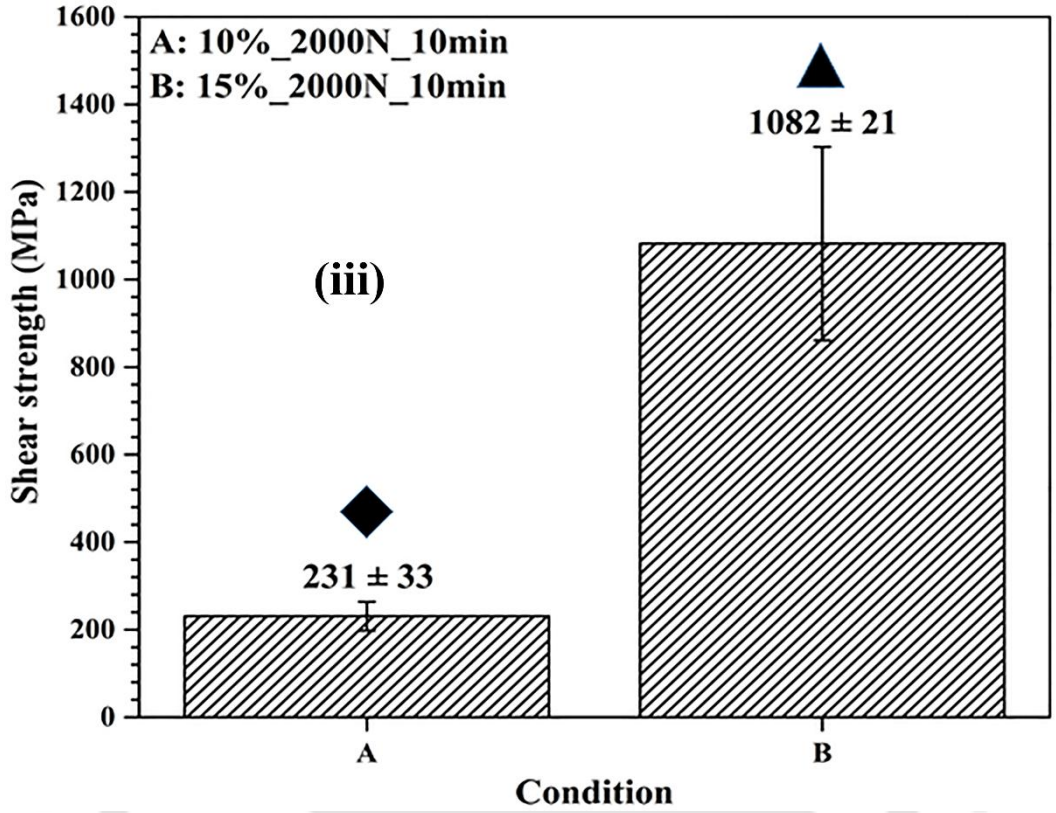

Figure 5.3. Optimization of GA concentration for (i) 10%, (ii) 15%, (iv) comparison of shear strength at different GA concentration (♦ represents cohesive failure, ▲ represents substrate failure).

The adhesion property of the prepared adhesive is due to the chain entanglement of GA-*g*-PLA molecules. The significant improvement in the shear strength of GA-*g*-PLA(10%) adhesive was observed with increase in the compression load and compression time as shown in figure 5.1 and 6.2. Whereas, the adhesive strength was improved drastically only by increasing the adhesive concentration from GA-*g*-PLA(10%) to GA-*g*-PLA(15%) as shown in figure 5.3. The GA-*g*-PLA(15%) showed the maximum adhesive strength which resulted in substrate failure due to more entanglement of GA-*g*-PLA molecular chains which leads to more adhesive power.

From the results, we have concluded that the adhering capacity is basically dependent on the adhesive concentration. Figure 5.4 shows the substrate failure during analysis for GA-*g*-PLA(15%) adhesive concentration, when the laminates were prepared by applying 2000N compression load for 10 min. It was also concluded that the active sites created on the GA backbone increased with increase in GA concentration during reaction which leads to more points of linkages between adhesive and adhering surface. Similarly, the single lap shear test was conducted for granite substrates at optimized conditions as shown in figure 5.4 (b). Hence, the prepared bionanocomposite proved to be excellent adhesive for glass as well as granite substrates.

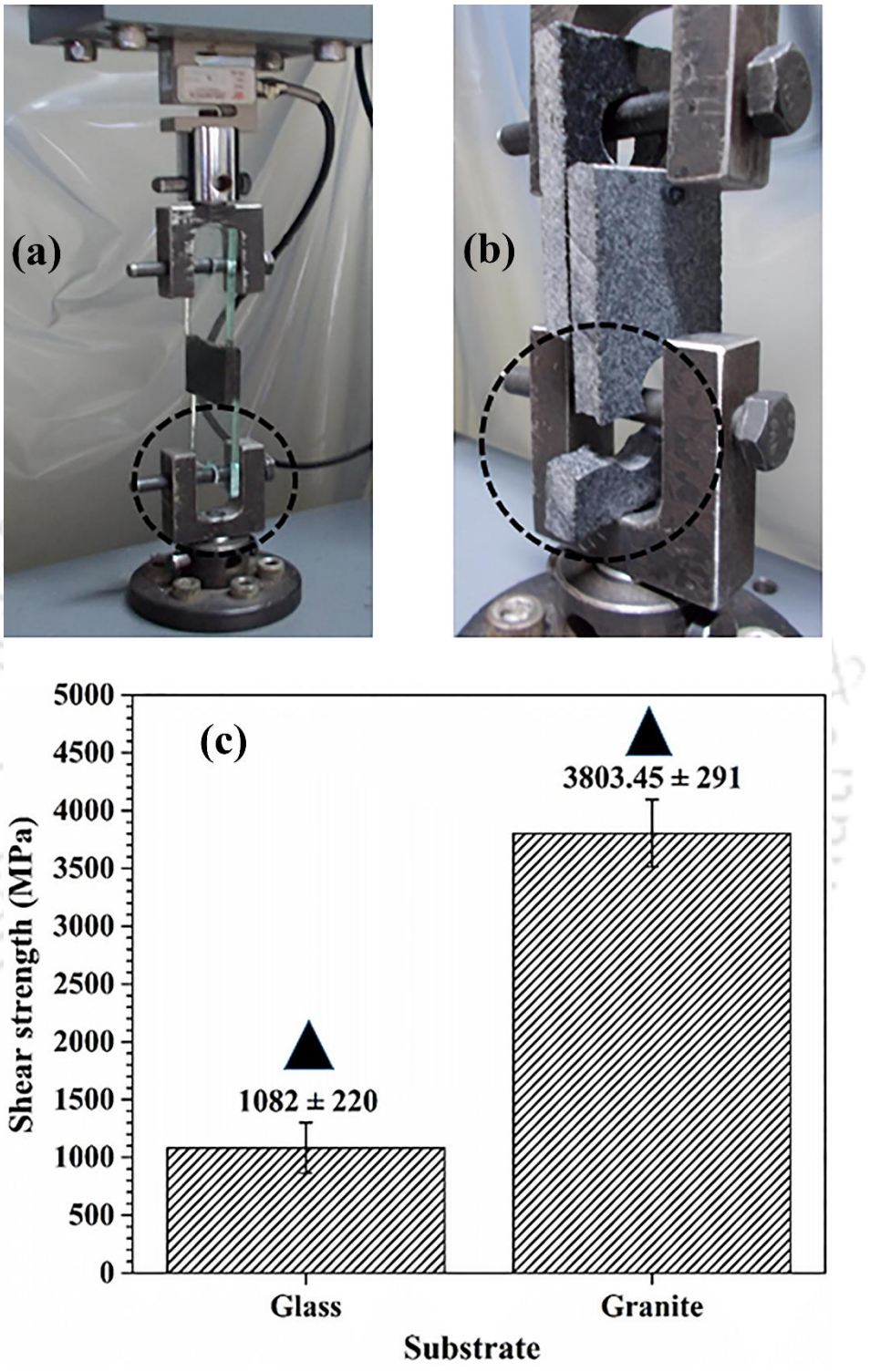

Figure 5.4. Substrate failure occurred in (a) glass laminates, (b) granite laminates

(c) comparison of adhesive shear strength between glass and granite substrates.

5.3. Summary

At higher loading of GA that is GA-*g*-PLA(20 %) has not showed adhesive characteristics and was not able to bind the substrates as the high viscosity reduces the substrate wettability with the adhesive. From the different trials of experiment it was confirmed that without modification of the gum doesn't showed any adhesive properties. The modified GA showed adhesive strength for glass and granite substrates only. The single lap shear test was conducted and optimized at different conditions to achieve maximum shear strength. The best adhesive strength was achieved at 15% GA concentration in composite when the compression load was applied at 2000N for 10 min. Hence, it was concluded that the adhesive has the excellent capability to bind glass and granite substrates.

Chapter 6

PLA/Functionalized-Gum Arabic Based Bionanocomposite Films for High Gas Barrier Applications

The chapter presents the microwave synthesis of gum arabic-grafted-poly l-lactic acid (GA-g-PLA) by polycondensation reaction and its influence as an additive to improve the gas barrier properties of poly (lactic acid) (PLA) films, prepared by solution casting method. It has been observed that during the synthesis of GA-g-PLA, hydrophilic gum has been converted into hydrophobic material due to grafting of in situ grown hydrophobic oligo-(lactic acid), as shown in Scheme 6.1. Subsequently, PLA/GA-g-PLA bionanocomposite films have been fabricated and characterized for structural, thermal, mechanical and gas barrier properties. Significant reduction in oxygen permeability (OP) of ~10 folds is achieved in case of PLA films containing GA-g-PLA as filler. However, water vapour transmission rate (WVTR) has been reduced upto 27% after 5 wt% addition of filler. Reduction in OP of this order of magnitude enable the PLA to compete with PET in terms of enhancing shelf life and maintaining the food quality.

6.1. Introduction

The use of plastics in packaging applications is increasing day by day. Among the different types of packaging materials, food packaging materials play a vital role in extending shelf-life and for maintaining the quality of food.

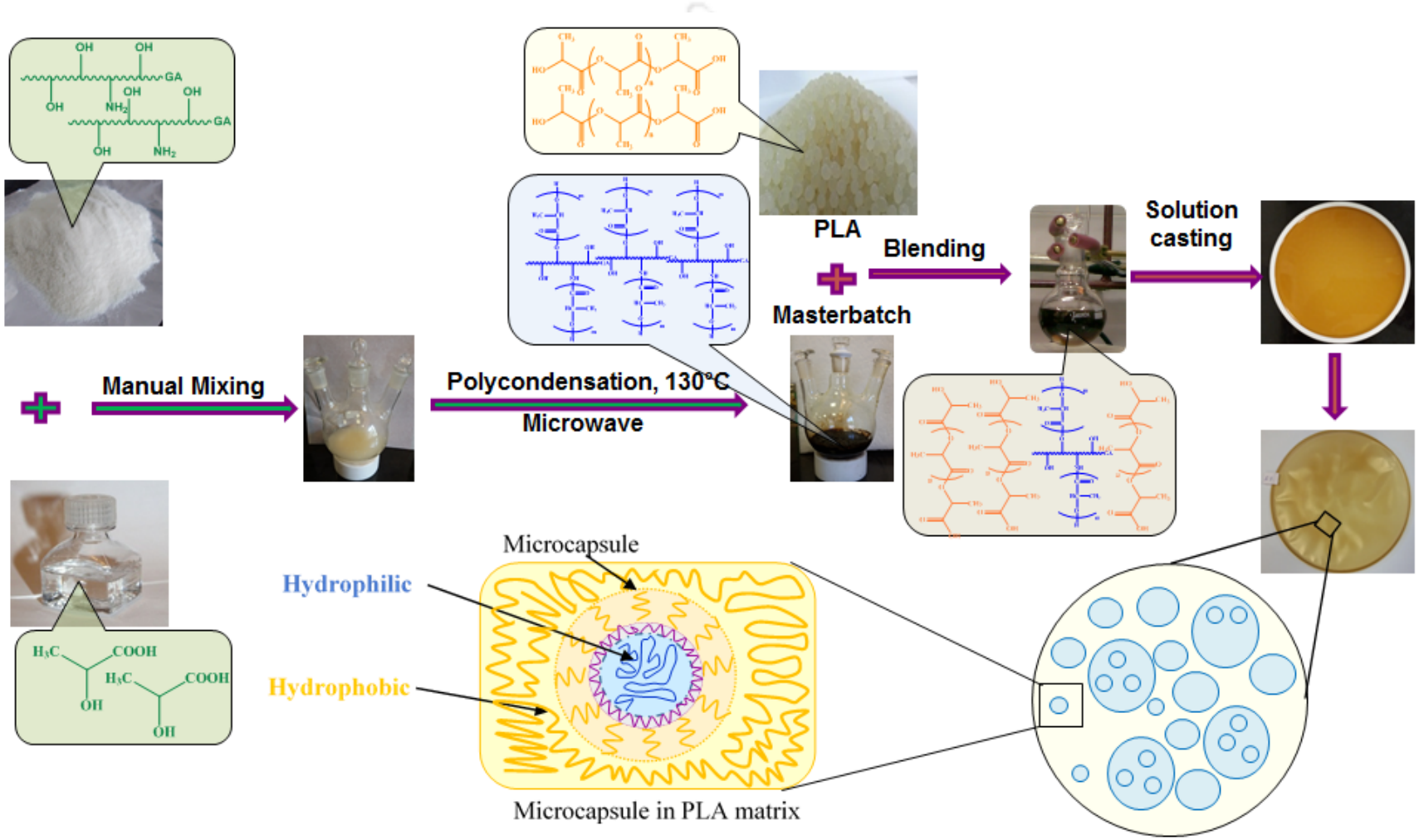

Scheme 6.1. Synthesis of GA-*g*-PLA and PLA/(GA-*g*-PLA)bionanocomposite film preparation.

Most of the food packaging materials are made from the petroleum-based polymers due to their large scale availability, good gas barrier and mechanical properties. In spite of several advantages, these petroleum-based polymeric materials have certain limitations such as poor biodegradability and non-renewability **(Sevigne-Itoiz et al., 2015; Gonzalez et al., 2013)**. To overcome such limitations, development of bio-based, renewable and biodegradable packaging materials have been emerging day by day.

Bio-based polymers based on their origin of raw materials and synthesis process can be classified into three categories namely (i) extracted from biomass, (ii) synthesized from bio-derived monomers and (iii) produced from microorganisms **(Rhim et al., 2013; Cutter, 2006)**. These polymeric materials can be degraded after their service life.

GA is a non-toxic hydrophilic biopolymer in its natural form which has good emulsion and encapsulation properties **(Tsai et al., 2014)**. It can also be used as a filler with some modifications in its structural properties for decreasing the gas-transport through the films. The gas-transport process is defined by permeability, diffusion and solubility coefficients. At steady state, permeability can be expressed by the product of diffusion and solubility coefficients. The initial increment in permeability values with time is only governed by diffusion process which decreases with increase in tortuosity and the increase in tortuosity is due to the incorporation of filler in polymer matrix. Hence, increase in tortuosity has the great impact on increasing the shelf-life of the products in food packaging applications **(Duncan, 2011)**. Oxygen permeability depends on many interrelated factors such as hydrogen bonding characteristics, degree of branching or cross-linking between polymeric chains, molecular weight, polarity and structural features of polymeric side chains, processing methodology, degree of crystallinity and method of synthesis.

Literature survey reveals that none of the articles have demonstrated the blends of PLA and GA-*g*-PLA for film preparation for packaging application. It might be due to incompatibility of pristine PLA which is hydrophobic whereas GA is hydrophilic in nature. Hence in the present study, PLA is blended with varying proportions of hydrophobic GA-*g*-PLA (also referred as filler) were used for the preparation of 'green' films by solution casting approach. Various analyses such as structural, thermal, mechanical, surface morphology and barrier properties of films were studied in detail. One of the major objectives of the present investigation is to develop a novel and ecofriendly packaging material with improved gas barrier properties.

6.2. Results and Discussion

6.2.1. Chemical interaction analysis

ATR-FTIR spectra of neat PLA and PLA/GA-*g*-PLA films with varying loadings of GA-*g*-PLA were recorded, as shown in figure 6.1. In the spectrum of neat PLA films, the peak at 869 cm^{-1} assigned to $-C-C-$ stretch; and peaks at 1083 cm^{-1}, 1130 cm^{-1} and 1182 cm^{-1} assigned to $-C-O-$ bond stretching of $-CH-O-$ group. The peaks at 1359 cm^{-1}, 1382 cm^{-1} and 1454 cm^{-1} were attributed to $-CH_3$ angular deformation, $-CH-$deformation (including symmetric and asymmetric bend) and $-CH_3$ bend respectively. The band originated from $-C=O$ stretching vibration of carbonyl is situated at 1747 cm^{-1}. In the spectra of PLA/GA-*g*-PLA films, a new peak originated at 1755 cm^{-1} also corresponds to $-C=O$ stretching vibration due to oligomer molecules **(Haafiz et al., 2013)**. It was observed that with increase in the concentration of GA-*g*-PLA, peak intensity at 1747 cm^{-1} decreased.

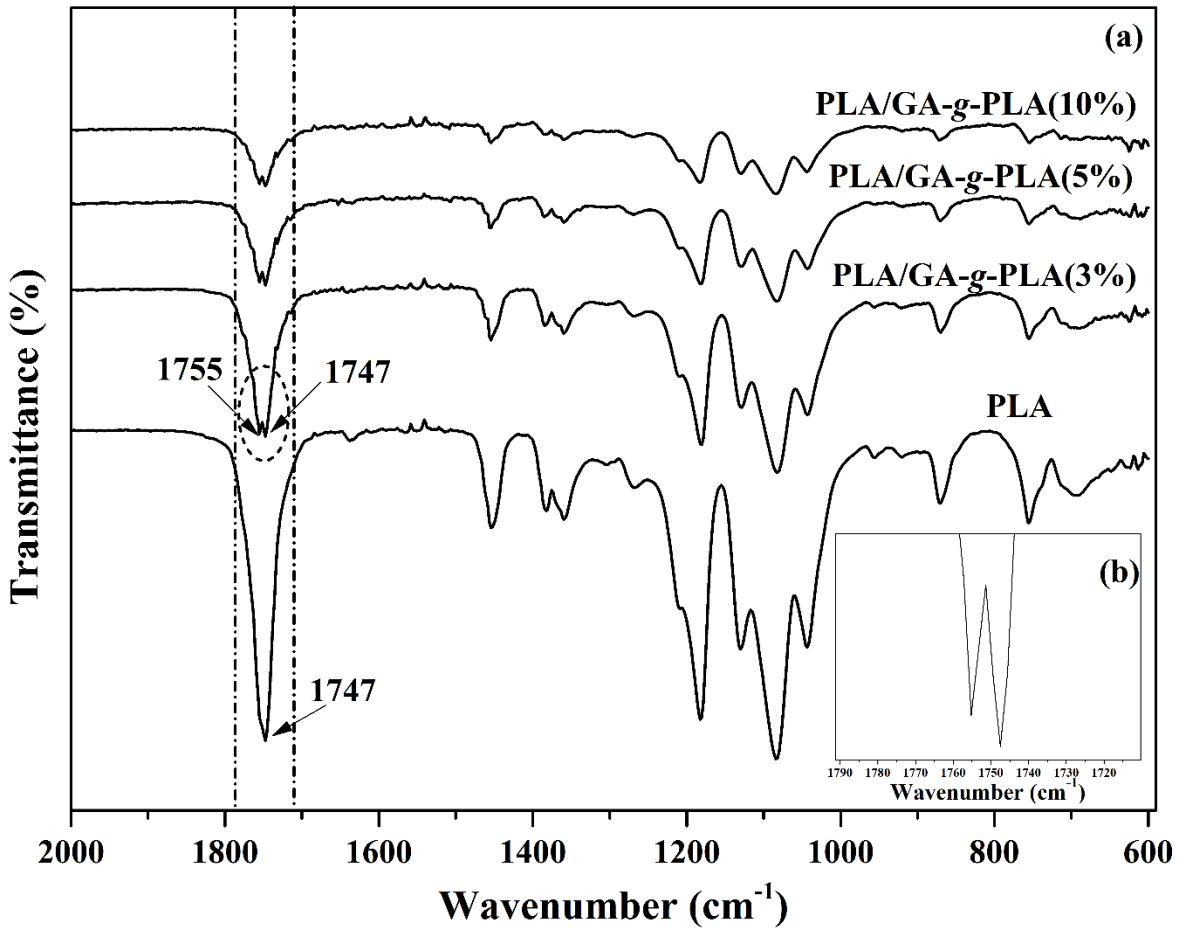

Figure 6.1. FTIR spectra of (a) PLA, PLA/GA-*g*-PLA(3%), PLA/GA-*g*-PLA(5%), PLA/GA-*g*-PLA(10%) bionanocomposite films (b) carbonyl peak at 1755 cm^{-1} [PLA/GA-*g*-PLA(3%) film].

6.2.2. Crystal structure analysis

Figure 6.2 showed the diffraction patterns of all the four film samples [PLA, PLA/GA-*g*-PLA(3%), PLA/GA-*g*-PLA(5%) and PLA/GA-*g*-PLA(10%)]. For neat PLA film, crystalline peaks were observed at 2θ = 14.9, 16.7, 19.1 and 22.3 which attributed to [0 1 0], [1 1 0] / [2 0 0], [2 0 3] and [0 1 5] reflections respectively. The maximum intensity of peak at ~16° corresponds to the α-form of crystals which confirmed that an ordered structure was still

retained in all the film samples. The decrease in peak intensity was observed for PLA/GA-*g*-PLA(3%) ($I_{max\ at\ 16.75°}$ = 403) and PLA/GA-*g*-PLA(5%) ($I_{max\ at\ 16.75°}$ = 737) films with respect to neat PLA film ($I_{max\ at\ 16.7°}$ = 996). Further, the values of Cr I for PLA, PLA/GA-*g*-PLA(3%), PLA/GA-*g*-PLA(5%) and PLA/GA-*g*-PLA(10%) films as calculated by using equation 2.3 were 87.95, 81.89, 86.43 and 88.34% respectively. On comparing the XRD patterns of PLA/GA-*g*-PLA(3%), PLA/GA-*g*-PLA(5%) and PLA/GA-*g*-PLA(10%) films, increase in peak intensity was observed with increase in filler loading. This increase in peak intensity could be attributed to the increase in crystallinity caused due to nucleating effect of GA-*g*-PLA filler in the film samples. The peak obtained in the XRD pattern of PLA/GA-*g*-PLA(10%) showed higher intensity, with respect to PLA film, suggested that oligomer promoted crystallization without changing the crystal structure.

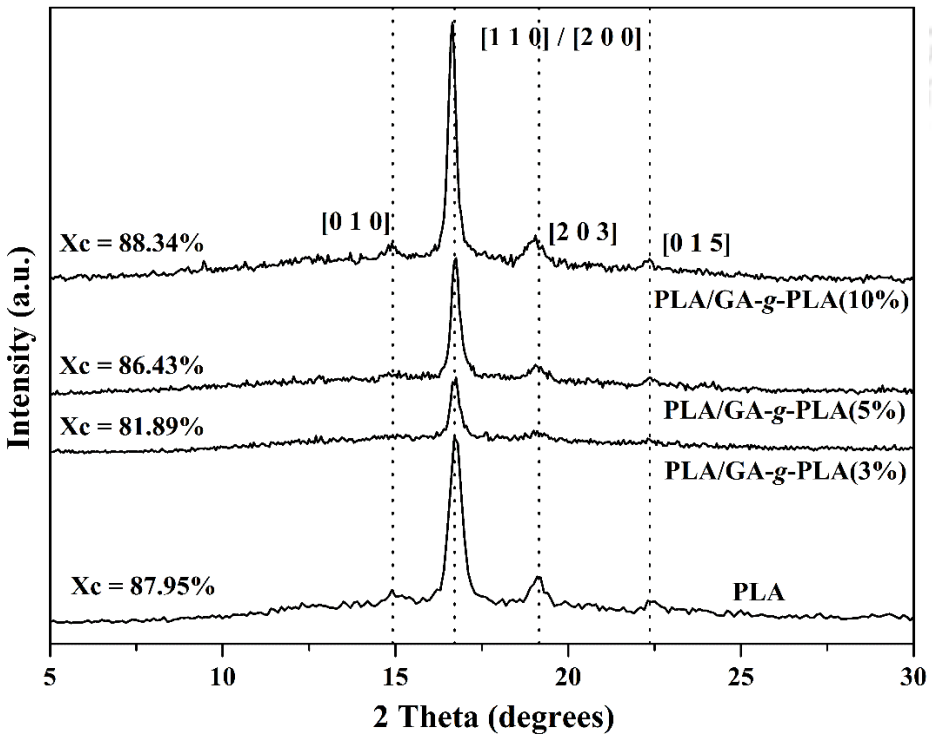

Figure 6.2. XRD patterns for PLA, PLA/GA-*g*-PLA(3%), PLA/GA-*g*-PLA(5%) and PLA/GA-*g*-PLA(10%) bionanocomposite films.

6.2.3. Thermal analysis

TGA was conducted for PLA, PLA/GA-*g*-PLA(3%), PLA/GA-*g*-PLA(5%) and PLA/GA-*g*-PLA(10%) films under inert atmosphere. In the derivative thermogravimetric (DTG) curves, two peaks were observed at different temperatures for neat PLA films which denote the different weight losses during heating at different temperatures. In neat PLA film, the first broad peak in the temperature range of 75-155 °C indicated the removal of unbound moisture. No such peak was observed upto 150 °C in any PLA/GA-*g*-PLA films which confirmed that bound and unbound moisture were negligible therein. However, the second prominent peak as observed in neat PLA film at 230-440 °C was found in all the samples of PLA/GA-*g*-PLA films also with varying heights indicative of their thermal stability. Highest thermal stability was observed for neat PLA films, and on increase in the loading of the filler, decrease in the thermal stability was observed. This could be attributed to the presence of low molecular weight species of oligomer in PLA/GA-*g*-PLA films. The onset and offset temperatures for neat PLA films were observed at 315 °C and 375 °C. The onset-offset temperature ranges for PLA/GA-*g*-PLA(3%), PLA/GA-*g*-PLA(5%) and PLA/GA-*g*-PLA(10%) were 171-356 °C, 177-346 °C and 157-338 °C respectively. The weight loss percentage in these temperature range was approximately 73%, 93%, 93% and 92% for PLA, PLA/GA-*g*-PLA(3%), PLA/GA-*g*-PLA(5%) and PLA/GA-*g*-PLA(10%) films respectively, as shown in figure 6.3(a). The maximum peak temperature was 359 °C, 336 °C, 328 °C and 307 °C for PLA, PLA/GA-*g*-PLA(3%), PLA/GA-*g*-PLA(5%) and PLA/GA-*g*-PLA(10%) respectively, as shown in figure 6.3(b) which indicated the reduction in thermal stability with increase in the loading of GA-*g*-PLA. The weight loss (%) at the corresponding temperatures was approximately 37%, 70%, 72% and 68% for PLA, PLA/GA-*g*-PLA(3%), PLA/GA-*g*-

PLA(5%) and PLA/GA-*g*-PLA(10%) respectively. The huge weight loss in blend films was observed as compared to that of neat PLA films which confirmed the reduction in thermal stability due to incorporation of short chain GA-*g*-PLA in the PLA matrix. The residual weight percent for PLA, PLA/GA-*g*-PLA(3%), PLA/GA-*g*-PLA(5%) and PLA/GA-*g*-PLA(10%) was observed as 0.6%, 3.54%, 3.52% and 3.19% respectively. For the PLA/GA-*g*-PLA films around 3% residual weight was observed because of the presence of salts and minerals in GA **(Ali et al., 2009)**. It was also observed that the degradation temperatures in all the PLA/GA-*g*-PLA films were around 300 °C which was higher than the processing temperature of neat PLA film. Thus, PLA/GA-*g*-PLA films could be processed at the same temperature as neat PLA films.

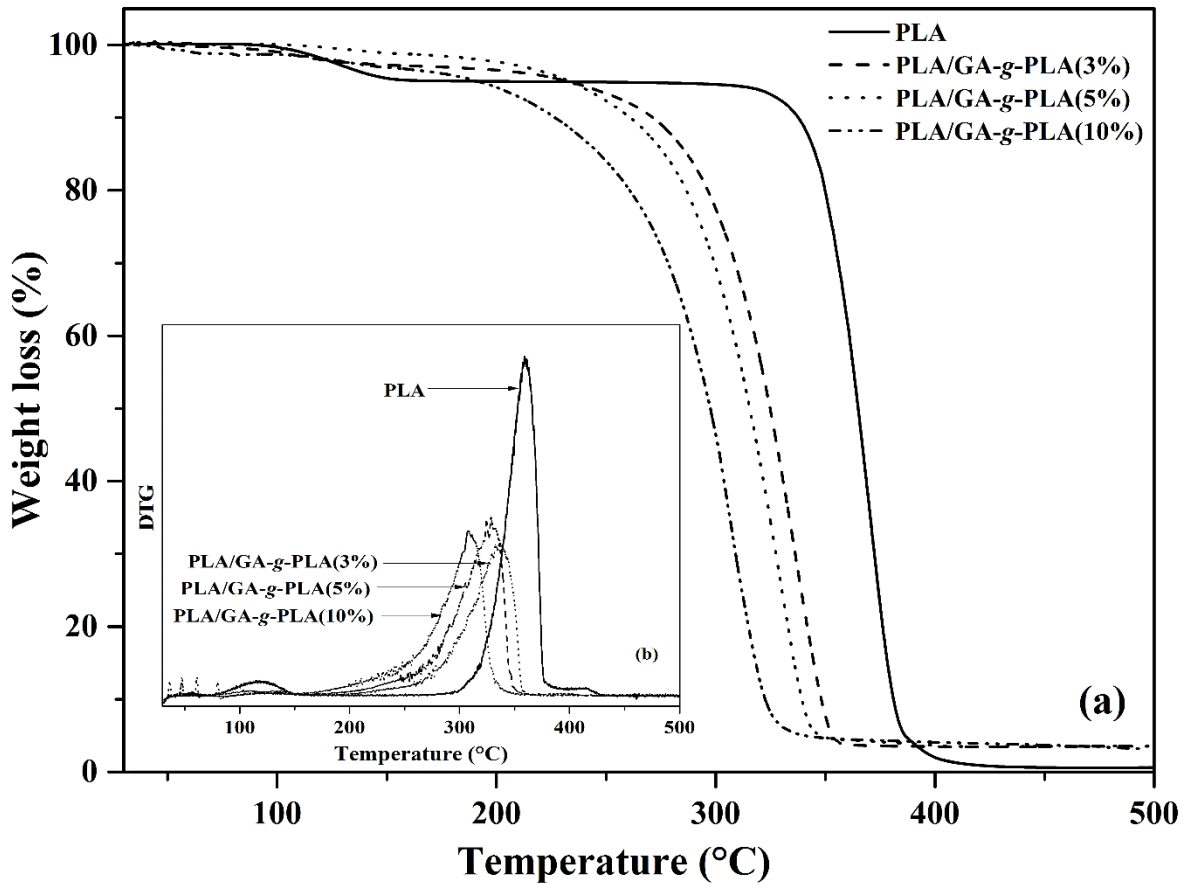

Figure 6.3. (a) TGA thermograms and (b) DTG curves of PLA and PLA/GA-*g*-PLA bionanocomposite films.

Through DSC studies, structural arrangement and torsion oscillation of molecular backbone of polymers can be explained by T_g. Figure 6.4 presents the thermogram for second heating cycles. The observed T_g for PLA, PLA/GA-*g*-PLA(3%), PLA/GA-*g*-PLA(5%) and PLA/GA-*g*-PLA(10%) were found to be 64.8 °C, 46.4 °C, 41.8 °C and 41.0 °C respectively. The DSC thermogram shows that the reduction in T_g took place as the filler concentration was increased. With increase in concentration of the oligomer, magnitude of plasticizing effect

increased which was due to enhancement in molecular segmental mobility resulting in reduction in T_g values.

In addition, reduction in regularity and crystalline growth was found hindered. This was because of small and irregular branching of GA-*g*-PLA molecules. Single T_g was observed in all the film samples that suggested a good compatibility of GA-*g*-PLA (filler) with PLA. As the filler was incorporated in the PLA matrix, an increase in free volume resulted in reduction in T_g values of blend films with respect to neat PLA film. The cold crystallization temperature (T_{cc}) for neat PLA film was observed to be at 107 °C and the same for PLA/GA-*g*-PLA films was found to be at 106.99 °C. With increase in the concentration of oligomer molecular chains, broadness of cold crystallization peak increased. The endothermic peak for PLA, PLA/GA-*g*-PLA(3%), PLA/GA-*g*-PLA(5%) and PLA/GA-*g*-PLA(10%) were observed at 153 °C, 149 °C, 143 °C and 143 °C respectively. In the PLA/GA-*g*-PLA films, two distinct peaks were observed which indicated the presence of less ordered crystal structures. Thus, at lower temperatures, peaks were formed because of thinner crystalline lamella and at higher temperatures, sharper peaks confirmed about the melting of more perfect crystals. Figure 6.5 also suggests that as the oligomer concentration increased, the peaks became broader and shifted towards lower temperature which confirmed the increase in irregularity in crystals.

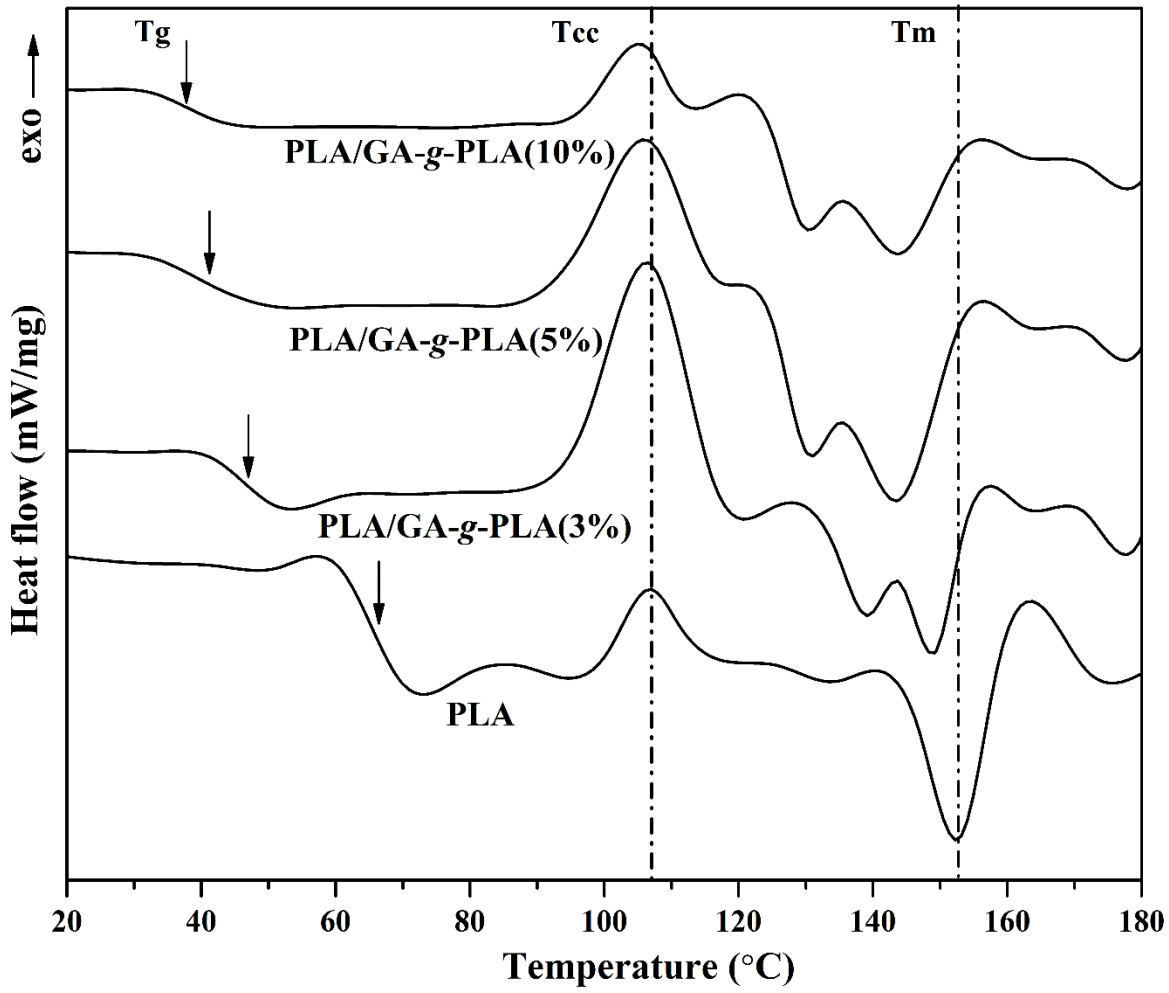

Figure 6.4. DSC themograms of PLA and PLA/GA-*g*-PLA bionanocomposite films during second heating at 5 °C min^{-1}.

6.2.4. Surface morphology

Transmission electron microscopy (TEM) was conducted to analyze the dispersion of nanoparticles in the matrix as shown in figure 6.5. Nicely and homogenously dispersed nanometer range particles were observed in the PLA matrix which resulted in drastic enhancement of the oxygen barrier property.

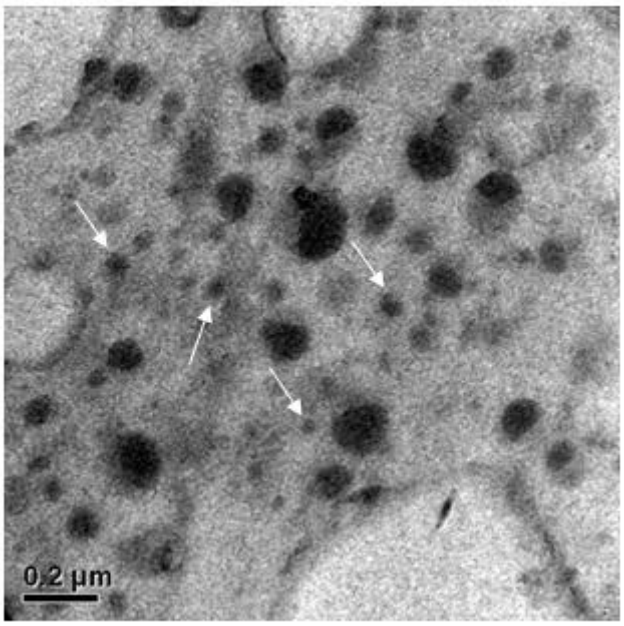

Figure 6.5. Representative TEM micrograph of PLA/GA-*g*-PLA(5%) bionanocomposite film.

6.2.5. Mechanical properties

The mechanical properties of PLA and PLA/GA-*g*-PLA films were evaluated for tensile strength, elongation at break and Young's modulus, and their values have been presented as in figure 6.6. The obtained values of tensile strength, elongation at break and Young's modulus were 40.9 MPa, ~9% and 541.91 MPa respectively for neat PLA films. It was observed that with increase in the filler concentration, reduction in tensile strength of the films occurred [Figure 6.6(a)]. In PLA/GA-*g*-PLA(3%) films, 14% reduction in tensile strength with respect to neat PLA films was observed. This could be due to the presence of short oligomer chains in PLA matrix and GA-*g*-PLA filler which are contributing towards poor interaction due to reduction in chain entanglement effect with PLA interphase, as shown in figure 6.6(a) **(Chou et al., 2012; Silverajah et al., 2012)**.

The enhancement of 16% in elongation at break (ε_b) was observed for PLA/GA-*g*-PLA films with respect to neat PLA films. Addition of 3 wt% filler loading reduced intermolecular forces which increased the flexibility of PLA/GA-*g*-PLA(3%) films due to the plasticizing effect of oligomers as shown in figure 6.6(b). On further addition of oligomer concentration, 7% and 50.5% reduction in elongation at break were observed for PLA/GA-*g*-PLA(5%) and PLA/GA-*g*-PLA(10%) films respectively. Thus, as small molecules of the oligomer interact with long chain of polymer molecules, 'free volume' was generated between the long polymer chains. Such interaction results in weakening intermolecular forces between the polymer chains or decreased in entanglement in molecular chains of the neat PLA matrix. These small molecules of oligomer were responsible for increase in the distance between two polymer chains. This could also be ascribed to phase separation between the oligomer and PLA matrix. Young's modulus was reduced by 28.2, 32.8 and 40.7% on addition of 3, 5 and 10% GA-*g*-PLA filler respectively as shown in figure 6.6(c). Furthermore, with increase in the filler concentration, reduction in polymer homogeneity leads to reduction in tensile strength and Young's modulus in PLA/GA-*g*-PLA films. Thus, increase in oligomer concentration reduced the stiffness of the films.

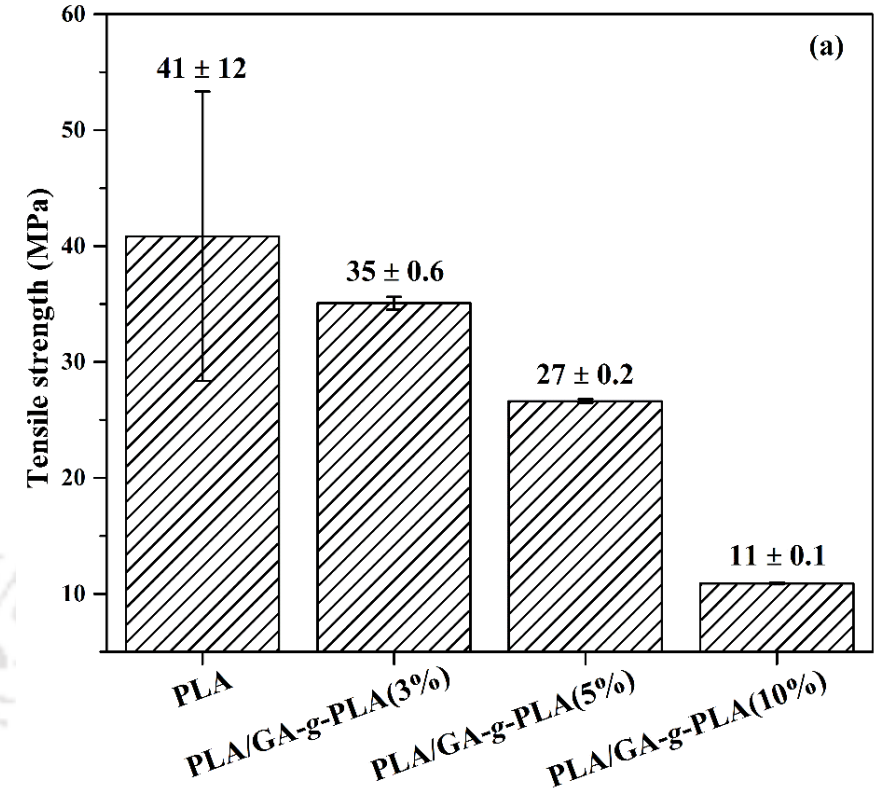

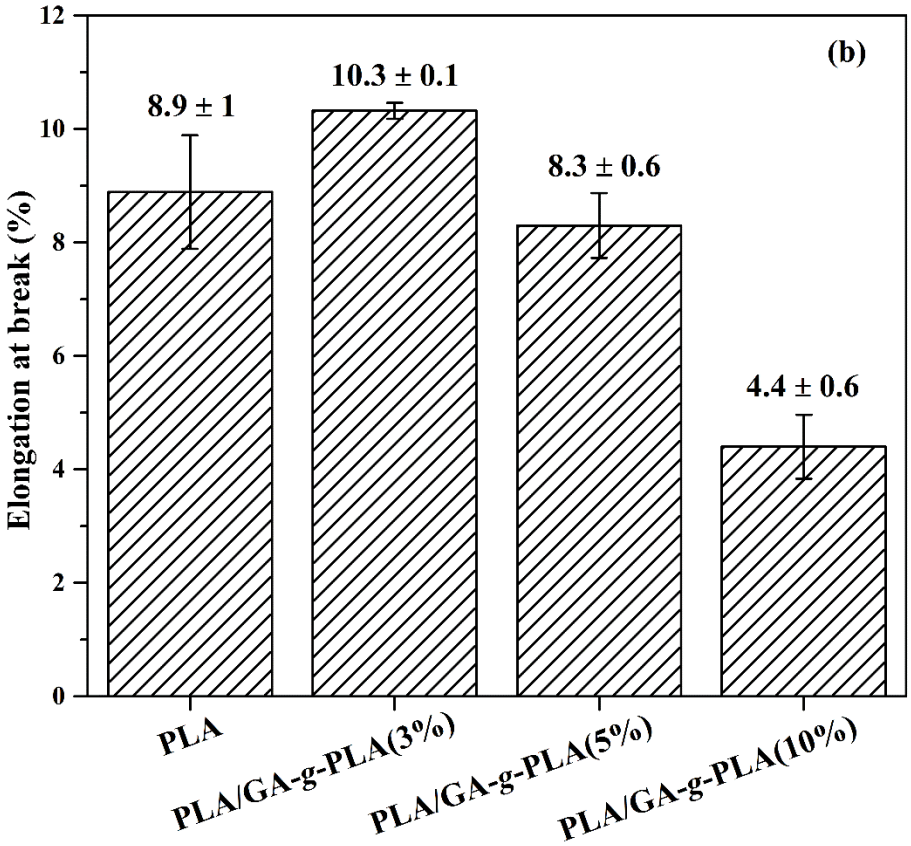

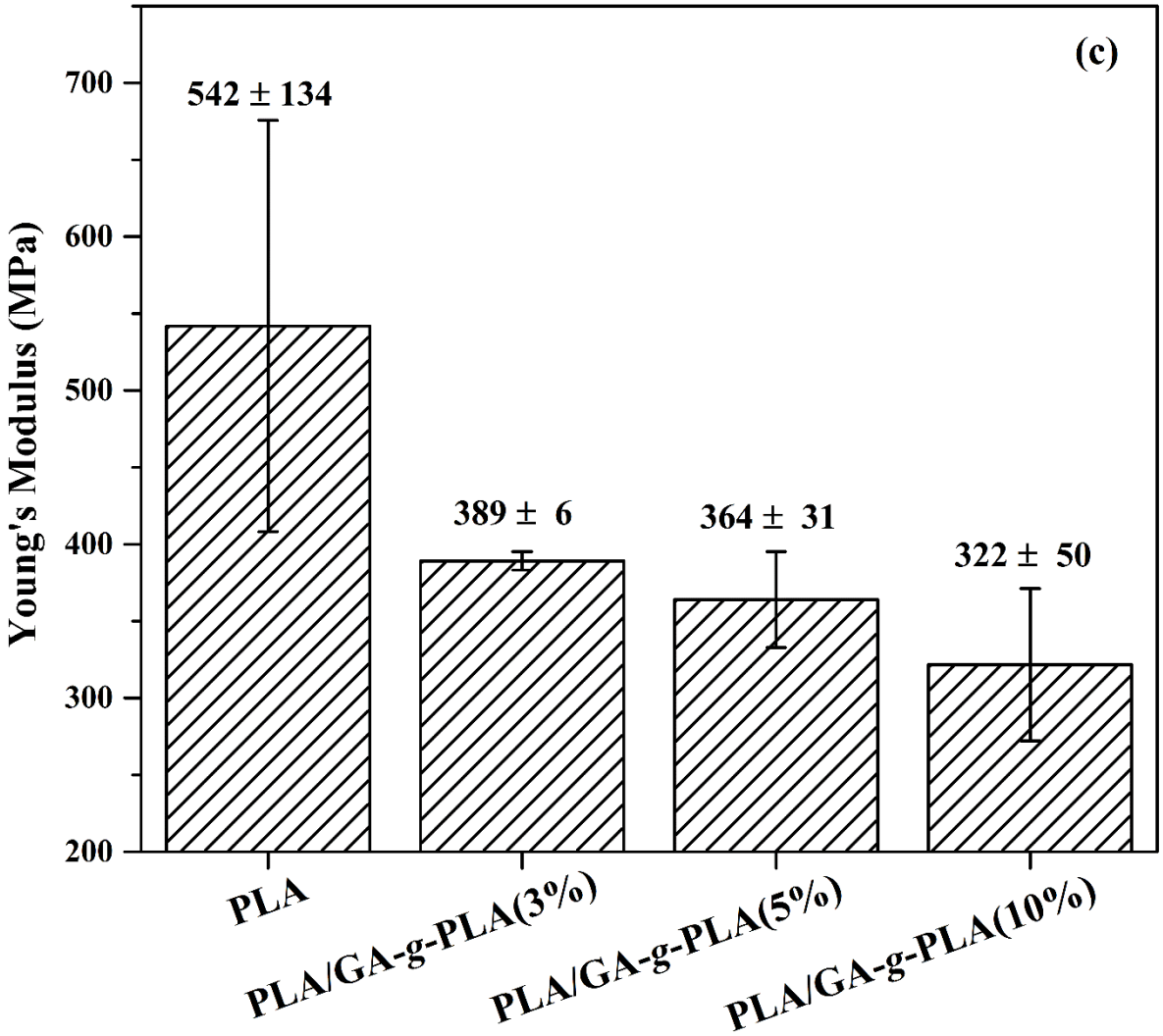

Figure 6.6. Mechanical properties of film samples (a) tensile strength, (b) elongation at break and (c) Young's modulus (The error bars represent standard deviations).

6.2.6. Oxygen permeability

Figure 6.7 presents the oxygen transmission rate (OTR); OTR × e values obtained for PLA and PLA/GA-*g*-PLA films. A very significant decrease in OTR values was observed when oligomer was added to the polymer matrix. The PLA/GA-*g*-PLA films showed an enhanced barrier effect due to their good dispersion as shown in figure 6.5. PLA/GA-*g*-PLA films with

3%, 5% and 10% loading showed 88.3, 90.3 and 89.1% reduction in OTR × e values respectively, with respect to the PLA films. This was in accordance with the results obtained in surface morphology, where it was observed that the presence of microspheres causes discontinuity in the film matrix and increase the tortuosity in the probable oxygen path to prevent permeation of gas molecules. It is noteworthy to mention here that due to uniform dispersion of GA-*g*-PLA in the PLA matrix, it reduces the solubility of oxygen molecules in the bionanocomposites and hence, the combine effect of tortuosity and solubility leads to the significant reduction in oxygen permeability. However, it was possible to observe that, in PLA/GA-*g*-PLA(10%) film, the oxygen permeation increased slightly which could be attributed to agglomeration of microspheres that lead to reduction in tortuosity.

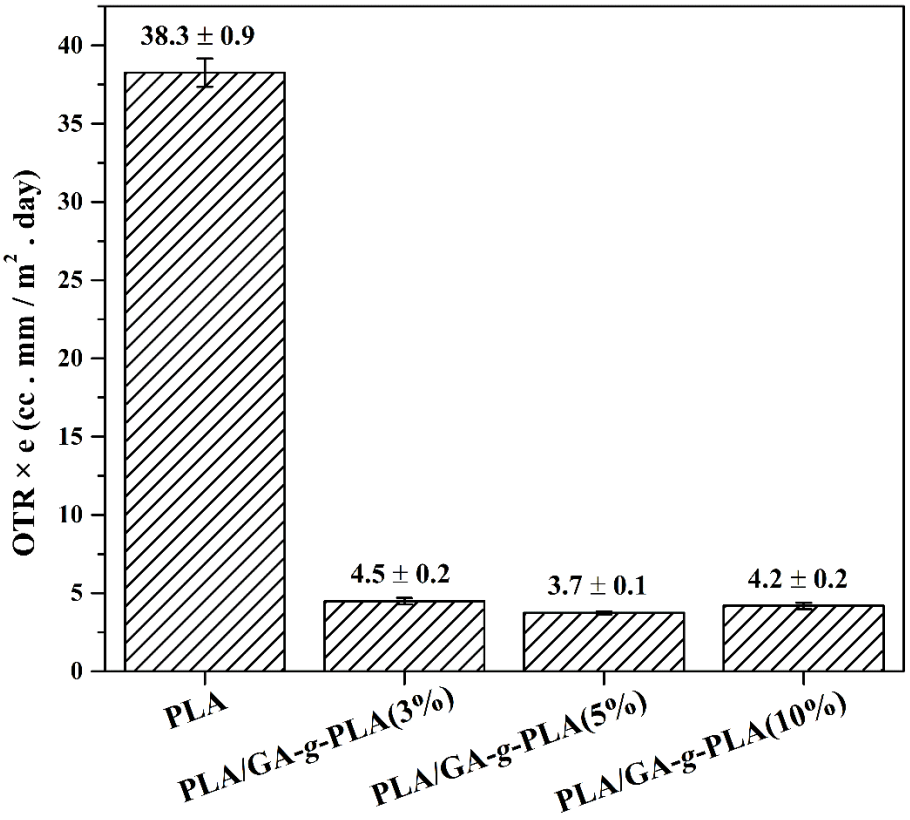

Figure 6.7. Oxygen transmission rate (OTR × e) value of neat PLA and PLA/GA-*g*-PLA bionanocomposite films.

A few recent OTR investigations were also conducted by using argon (Ar) as a carrier gas (99.999% purity) instead of nitrogen (N_2) (99.999% purity) as carrier gas. It has been noticed the effect of selection of carrier gas on the permeability. The analysis was conducted in a temperature range of 15 to 45 ± 0.1ºC and 0% RH for 6 h so as to reach OTR value at steady state. The oxygen volumetric flow rate can be measured using equation (6.1).

$$\text{OTR (t)} = \frac{Pp}{l}[1 + 2\sum_{n=1}(-1)^n \exp(-\frac{D^2 n^2 t}{l^2})] \quad (6.1)$$

where P, p and l are oxygen permeability, oxygen partial pressure and film thickness respectively. The half time ($t_{1/2}$) was defined as the time at which OTR values reached 50% of steady state value. The diffusion coefficient (D) and solubility coefficient (S) of oxygen in bionanocomposite films were calculated by using equations (6.2) & (6.3). The tests were conducted in triplicate and average values have been reported.

$$\text{D} = \frac{l^2}{7.199\ t_{1/2}} \quad (6.2)$$

$$\text{P} = D \times S \quad (6.3)$$

A better understanding was developed about the effect of variation in temperature on gas transport properties of bionanocomposite films by using Arrhenius expression as shown in equation (6.4).

$$P = P' e^{\frac{-\text{E}_P}{RT}} \quad (6.4)$$

where P', E_P, R and T are pre-exponential factor (cc.mm/m^2.day), activation energy for permeation (kJ mol^{-1}), universal gas constant (8.3145 J mol^{-1} K^{-1}) and absolute temperature (K) respectively. Table 6.1 shows permeability coefficient, oxygen permeability, 'D' and 'S' values of PLA/GA-*g*-PLA bionanocomposite films, calculated at 25 ± 0.1°C and 0% RH. The

oxygen permeability and solubility coefficient were reduced upto ~81% and ~43% respectively by the addition of 5 wt% of filler. Whereas, the maximum reduction in diffusivity coefficient was observed ~77% only by adding 3 wt% of filler. It was clearly observed that the reduction in solubility coefficient was more responsible for decrease in gas barrier property because more active sites in PLA matrix were occupied due to the presence of filler. Hence, the physical interaction of polymer with oxygen molecules was less due to less availability of active sites. This significant lack of active sites in bionanocomposite films is due to the chemically bonded PLA and GA molecules. It also helps to increase the resistance to the diffusion of oxygen molecules in PLA matrix.

Table 6.1. Oxygen barrier properties of PLA and PLA/GA-*g*-PLA films at 25 ± 0.1°C and 0%RH

Sample	Permeability coefficient (cc.mm/m^2.day)	Permeability (cc.mm/m^2.day.kPa)	% Reduction	Diffusivity (m^2/sec)×10^{-12}	Solubility (g/g.Pa)×10^{-5}
PLA	19.97	9.98	0	3.25	3.56
PLA/GA-*g*-PLA (3%)	4.13	2.1	78.96	0.75	3.2
PLA/GA-*g*-PLA (5%)	3.84	1.92	80.76	1.1	2.03
PLA/GA-*g*-PLA (10%)	9.86	4.93	50.60	2.66	2.15

The OTR values were recorded for PLA/GA-*g*-PLA bionanocomposite films at 15ºC, 25ºC, 35ºC and 45ºC as shown in figure 6.8(a). The OTR values were continuously increased with increase in temperature due to the increment in diffusion rate of oxygen in polymeric chains at higher temperatures. The rate of change in OTR values with respect to temperature was also increased with increase in operating temperature as shown in figure 6.8(b). It describes about the change in slope becomes higher at higher temperatures due to the chemical interaction between GA and OLLA, GA-*g*-PLA and PLA. It restricts the molecular motion of polymeric

chains which results the reduction in OTR values with increase in filler loading. However, at 10 wt% filler loading, the OTR values increased and found more than that of 3 wt% loading. This was due to the agglomeration of the filler in PLA matrix. Figure 6.8(c) explains about the temperature dependence of permeation rate for various GA-*g*-PLA loadings in PLA matrix.

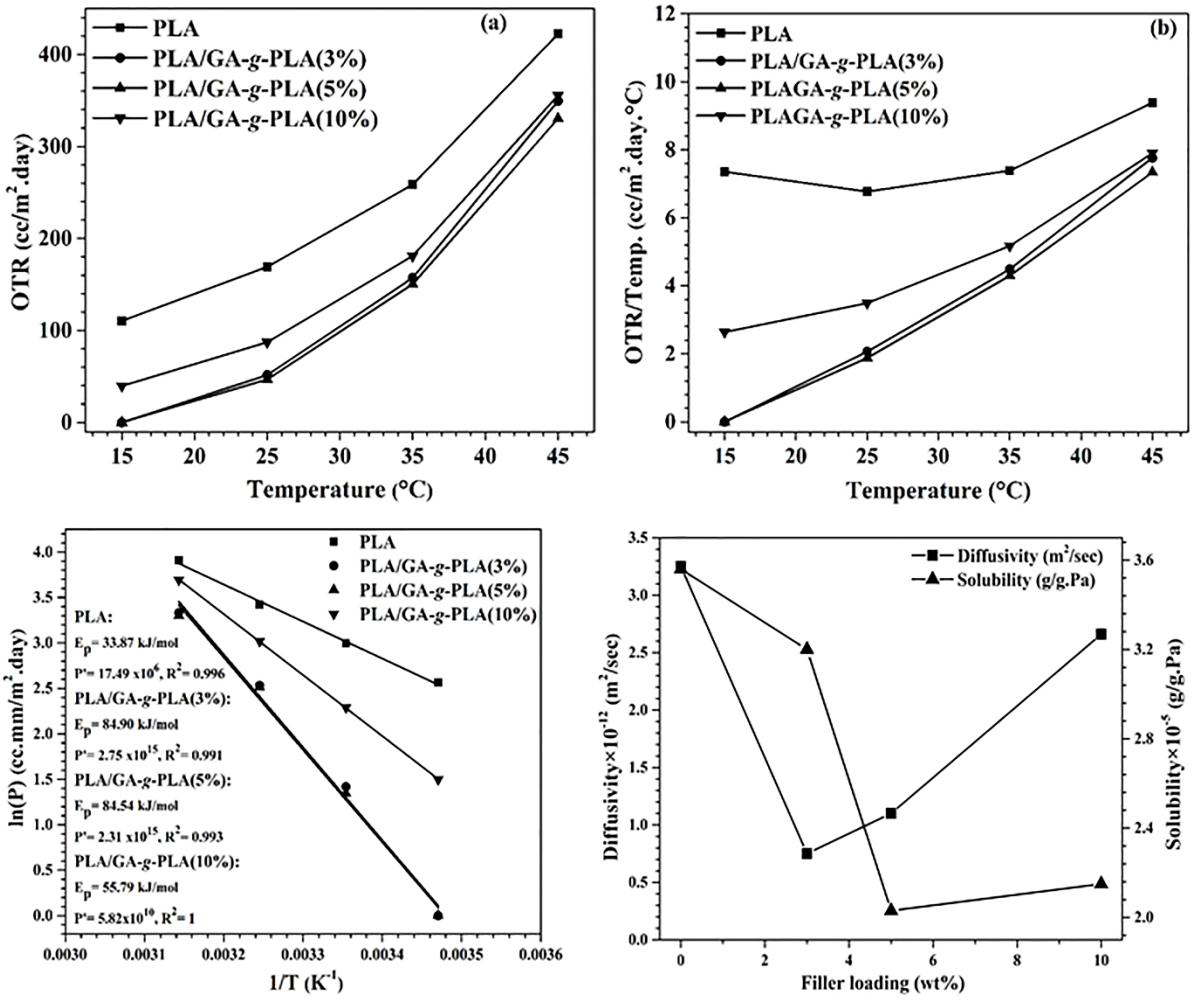

Figure 6.8. Graphs of (a) OTR vs temperature, (b) rate of change in OTR with respect to temperature, (c) ln (p) vs 1/T to check the temperature dependence of permeation rate for various GA-*g*-PLA loadings in PLA matrix and (d) diffusivity/solubility vs filler loading at 25 ± 0.1°C and 0% RH.

The activation energies increase with increase in filler loading upto 5 wt% due to the formation of stable networks that creates more tortuous path for the diffusion of gas molecules. It results the improvement in gas barrier properties. Figure 6.8(d) explains about the reduction in diffusivity and solubility values with respect to filler loading which clearly indicates that solubility is the prime factor for huge oxygen permeability reduction in bionanocomposite films.

6.2.7. Water vapour transmission rate

WVTR × e of PLA and PLA/GA-*g*-PLA films are shown in figure 6.9. The decrease in WVTR × e was observed when the filler was blended with the PLA matrix. The reduction in WVTR × e for PLA/GA-*g*-PLA(3%) films was observed around 7% and on further addition of the filler that is for PLA/GA-*g*-PLA(5%) was around 27%. This drastic decrease in the values was due to the presence of micro and nanospheres present in the matrix. Hence, the tortuous path created by these spheres helped in the sudden decrease in the WVTR × e also. On the contrary, drastic increase in WVTR × e was observed around 28% for PLA/GA-*g*-PLA(10%) films with respect to neat PLA films. This was observed due to agglomeration of micro and nanospheres which resulted in reduction in tortuosity. The decrease in intermolecular forces was also occurred in PLA/GA-*g*-PLA(10%) films due to free hydroxyl and carboxyl groups of the filler. Thus, increase in transfer of water molecules through the films was observed.

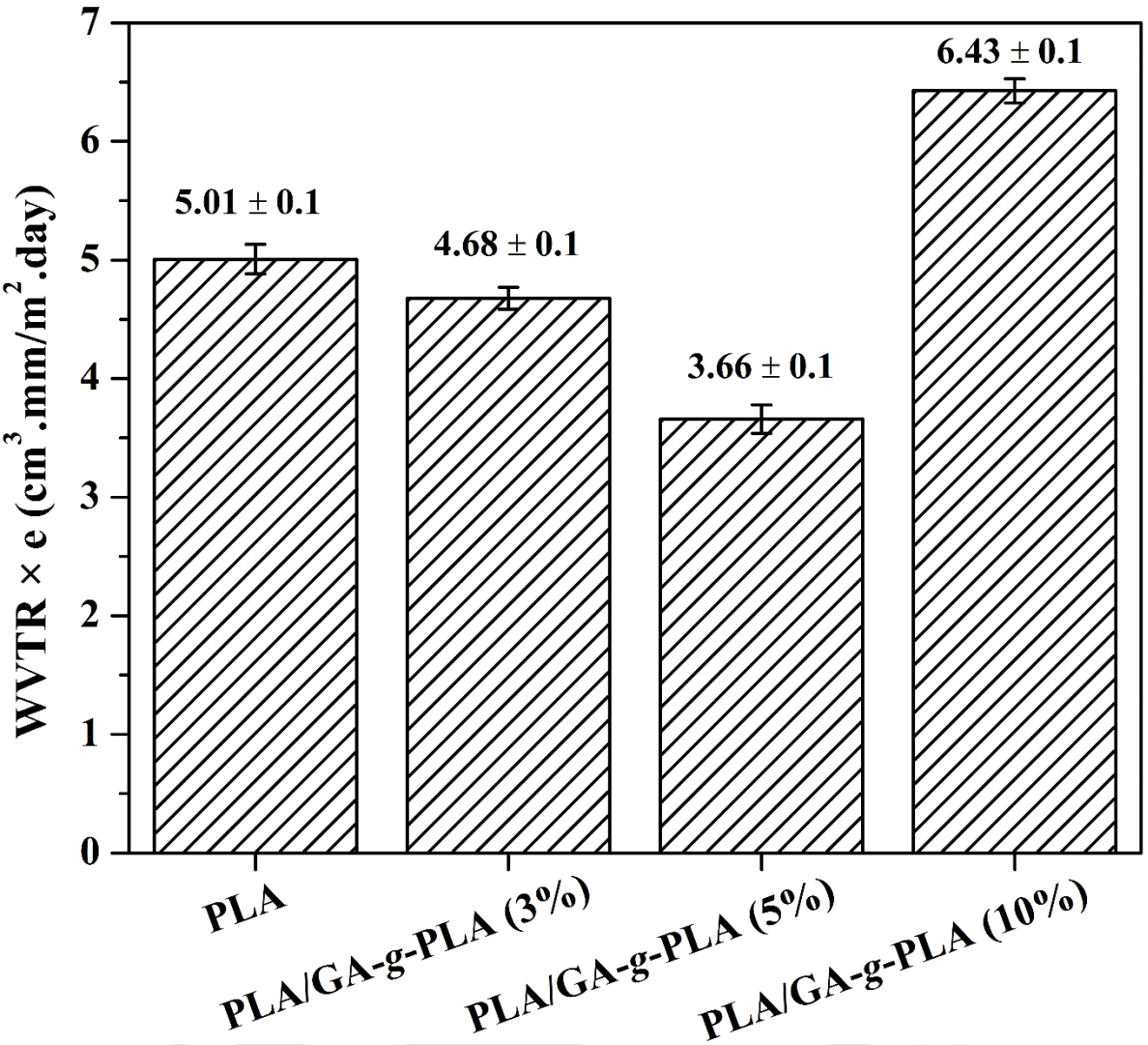

Figure 6.9. Water vapour transmission rate (WVTR × e) of neat PLA and PLA/GA-*g*-PLA bionanocomposite films.

6.3. Summary

A novel polysaccharide gum based filler was synthesized by using lactic acid and gum arabic as precursors. The synthesis was conducted by polycondensation reaction without using any catalyst or additive. The grafting occurred at $-OH$ and $-NH_2$ groups which was confirmed by NMR analysis. The PLA and PLA/GA-*g*-PLA bionanocomposite films were prepared by solution casting method. PLA was found to be compatible with the GA-*g*-PLA filler that was

confirmed by single T_g of the polymeric blends obtained by mixing the two materials in different proportions. Reduction in the glass transition temperature is indicating that these films are good for packaging applications. However, magnitude of reduction in the values of these properties was dependent on the percentage of GA-*g*-PLA. However, for 3% filler loading the film observed the highest elongation at break as ~10% which is even greater than that of neat PLA film. The presence of nanospheres is confirmed by TEM images which clearly inferred that blending of GA-*g*-PLA to PLA significantly altered the morphological characteristics of the film. The reduction in WVTR analysis for PLA/GA-*g*-PLA(3%) and PLA/GA-*g*-PLA(5%) films was observed as 7% and 27% respectively. The most important achievement of this work is the significant improvement in the oxygen transmission rate (OTR) of composite films. The OTR × e value of neat PLA films was 37.6 cm^3 mm m^{-2} day^{-1}, which is reduced to around 4 cm^3 mm m^{-2} day^{-1}. A decrease of ~10 fold in the OTR value can be regarded as very significant improvement in the barrier property of the film, especially for using them as packaging films. In addition to extremely low OTR × e values of prepared films, GA and PLA which are obtained from natural renewable resources, are possibly non-toxic, and fit well in the category of 'green' biodegradable materials for high quality packaging materials.

Chapter 7

Thermal Degradation Behaviour of High Gas Barrier Poly (lactic acid)/modified Gum Arabic based Bionanocomposite Films

The chapter demonstrates the thermal degradation behaviour of poly lactic acid (PLA) and gum arabic grafted poly l-lactic acid (GA-g-PLA) based bionanocomposite films. The GA-g-PLA has been prepared by polycondensation of lactic acid in presence of gum arabic, and proved to be a unique bio-based filler. The thermal degradation of PLA has been found to be a single-step process. Thermogravimetric Analysis hyphenated with Fourier Transform Infrared Spectroscopy (TGA-FTIR) has been conducted to study the evolved gaseous products from PLA and PLA/GA-g-PLA samples, for interpreting the degradation pathways. Activation energies obtained by Flynn-Wall-Ozawa (F-W-O) and Kissinger-Akahira-Sunose (K-A-S) models have been found to be in good agreement with Kissinger model as compared to Augis & Bennett model. The activation energies of neat PLA films have been determined from Kissinger, Augis & Bennett, F-W-O and K-A-S models, and have been found to be 254, 259, 257 and 260 kJ mol^{-1}, respectively. For the composite films, it has been observed that the activation energy of degradation dependents on its conversion.

7.1. Introduction

Nowadays, bio-based polymers have attracted much attention because of their environment friendliness and biodegradability. PLA has proved to be the most promising biodegradable

polymer which has wide variety of applications. Due to its desirable properties such as transparency, bio-safety and compostability; it has promising applications in consumer goods, fibers, biomedicines and packaging. This will result in exorbitant use of it in near future. Hence, systematic and rigorous study of degradation for PLA is of great concern towards its recyclability and nontoxic incineration process.

The thermal degradation study of PLA with novel biofillers will provide insight into determination of decomposition temperature, decomposition reaction pathway and byproducts **(Yoshikawa et al., 2014)**. For the determination of decomposition temperature and decomposition steps, thermogravimetric analysis/differential thermal analysis (TGA/DTG) technique is very useful, and hence is widely used **(Ahmad et al., 2014)**. It is noteworthy to mention that thermal degradation of PLA can propagate through oxidative, random main-chain scission, zipper-like depolymerization, hydrolysis by trace amounts of water, intermolecular transesterification to monomer & oligomeric esters, and intramolecular transesterification resulting in formation of monomeric and oligomeric lactides **(Carrasco et al., 2011)**. Residual water and moisture trapped inside the polymer matrix can initiate hydrolysis reactions. During these reactions the ester linkage split-up into alcohol and acid groups **(Carrasco et al., 2014)**. According to **Kopinke et al., (1996)**, the byproducts obtained after thermal degradation of PLA are CO, CO_2, acetaldehyde and methylketene.

Thermal degradation kinetics of the polymeric blends has been effectively studied by TGA **(Huang et al., 2015)**. Thermal degradation of polymers has been studied by thermoanalytical kinetics to reveal the information about chemical reaction mechanism and to establish relationships between temperature, extent of conversion and process rate than that of thermally stimulated processes **(Yoshikawa et al., 2014; Jakic et al., 2013)**. The kinetic modeling of

decomposition is done by crucial, reliable and accurate prediction of material behaviour under high-temperature applications or working conditions such as processing, storage of materials and service life time over a particular period of time and temperature. The mechanism of thermal degradation and thermal stability of macromolecules can also be speculated by the kinetic analysis **(Carrasco et al., 2014)**. The degradation processes of polymer blends and polymer nanocomposites are much more complex as comparison to that of neat polymers. Therefore, understanding of the complex degradation mechanism is essential and can be understood by the kinetics **(Corres et al., 2011)**. The analysis has to be conducted at multiple heating rates for calculating kinetic parameters as per International Confederation of Thermal Analysis and Calorimetry (ICTAC) **(Manafi et al., 2015)**. The important terms to understand the kinetic model are activation energy, pre-exponential factor and reaction model. These three forms put together are termed as kinetic triple **(Carrasco et al., 2014)**. Activation energy (E_a) can be viewed to be related with the energy barrier for the chemical system, and can be used to investigate the complexity of the process. E_a can be termed as 'apparent', 'effective', 'empirical' or 'global' activation energy. It is considered that if E_a is independent of α, process is considered as simple or overall single-stage degradation which can be described by kinetic triplet. On the contrary, if E_a is dependent on α, the process is considered to follow complex mechanism **(Jakic et al., 2013)**. It has also been noted that $E_a$values depend on many factors such as sample thickness, polymerization conditions, molecular weight, morphology and sample weight used for the analysis **(Majoni et al., 2010)**.

These methods of kinetic study can be divided mainly into two categories, (a) model-fitting method and (b) isoconversional / model-free method. The model-fitting methods can directly determine the kinetic parameters for solid-state reaction from single TGA measurement. These

methods are used to fit the data and that model is chosen which gives the best statistical fit. Hence, limitations of these models are the inability to specifically determine the reaction model, to determine average activation energies for complete degradation process and difficulty of selecting an appropriate model because several models can be statistically equivalent. However, the fitted kinetic parameters may vary by an order of magnitude **(Majoni et al., 2010; Vyazovkin et al., 2006; Chrissafis et al., 2009)**.

However, in isoconversional method, the limitations of model-fitting method is nullified. In this method (commonly known as model-free methods), the activation energy is calculated from the experimentally obtained temperatures from different heating rates at each conversion point. These methods are used to infer about the mechanism of processes and for predicting kinetics **(Vyazovkin et al., 2006)**. These methods are also able to detect the complex or multi-step processes, by varying E_a with α **(Achilias et al., 2011)**. Thus, due to minimization of errors, it is assumed that these methods can give accurate values of activation energy. Augis & Bennett, Flynn-Wall-Ozawa (F-W-O) and Kissinger-Akahira-Sunose (K-A-S) methods are the examples of the isoconversional methods **(Chrissafis et al., 2009; Slopiecka et al., 2011)**. It should be noted that, Kissinger method is considered to be a model-free method, and not an isoconversional method as it assumes a constant activation energy, and does not calculate activation energy corresponding to each conversion **(Slopiecka et al., 2011)**.

Hence, in the present investigation, the chemically modified hydrophobic GA-*g*-PLA was used as a filler to obtain the compatible filler-matrix blend films. Scanning electron microscopy (SEM) and thermogravimetric analysis (TGA) were conducted to understand the characteristic properties of the films. Thermogravimetric analysis hyphenated with Fourier transform infrared spectroscopy (TGA-FTIR) has been conducted for the continuous monitoring and

identification of evolved gaseous products for PLA and PLA/GA-*g*-PLA films. Literature survey reveals that no information is available on the thermal degradation kinetic study on the effect of this novel filler in the PLA matrix. In the present work, Kissinger, Augis & Bennett, Flynn-Wall-Ozawa and Kissinger-Akahira-Sunose models have been used to study the degradation kinetics of the blend films.

7.2. Theoretical Approach to Kinetics

In general, the thermal degradation reaction of a solid polymer is considered to be as follows:

$$A_{solid} \rightarrow B_{solid} + C_{gas}$$

where, A is the initial material, B and C are the residues in the solid and gas form respectively **(Cekingen et al., 2012)**. In a heterogeneous reaction, decomposition rate for a reactant can be defined as equation (7.1):

$$\frac{d\alpha}{dt} = k(T)\, f(\alpha) \qquad (7.1)$$

where, $\frac{d\alpha}{dt}$ is the rate of weight loss; α is the degree of conversion of the reactant at time 't' $\left(\alpha = \frac{\text{initial mass of sample –sample mass at time t}}{\text{initial mass of sample –final mass of sample}}\right)$; f(α) is the conversion which is a temperature-independent function; and k(T) is the temperature-dependent rate constant which can be defined from Arrhenius equation, as equation (7.2):

$$k(T) = A \exp\left(\frac{-E_a}{R\,T}\right) \qquad (7.2)$$

where, A is the pre-exponential factor or frequency factor (s^{-1}); E_a is activation energy (kJ mol^{-1}); R is universal gas constant (8.3145 J mol^{-1} K^{-1}); T is absolute temperature (K) **(Byczynski et al., 2014; Badia et al., 2008)**.

The idealized kinetic equation for a single step reaction as given in equation (7.3), has been applied to thermo-analytical curves for a range of chemical and physical processes of materials:

$$\frac{d\alpha}{dt} = A \exp\left(-\frac{E_a}{R\,T}\right) f(\alpha) \qquad (7.3)$$

where, α, A, E_a, and f(α) are the fractional conversion, the Arrhenius pre-exponential factor, the apparent activation energy, and the kinetic model function that describe the physicochemical or physico-geometrical mechanism of the reaction, respectively **(Yoshikawa et al., 2014; Achilias et al., 2011)**.

In non-isothermal condition, heating rate β = dT/dt can be substituted in equation (7.3). Thus, equation (7.3) is modified as equation (7.4):

$$\frac{d\alpha}{dT} = \left(\frac{1}{\beta}\right) A \exp\left(-\frac{E_a}{R\,T}\right) f(\alpha) \qquad (7.4)$$

Equation (7.3) and (7.4) form the basis to derive many equations to evaluate thermal analysis data **(Cekingen et al., 2012; Byczynski et al., 2014; Papageorgiou et al., 2012)**.

7.2.1. Kissinger method

Kissinger method is applicable where the maximum degradation temperature of the process is known **(Lizundia et al., 2015)**. It is used to determine the activation energy of the solid-state reactions from the equation (7.5):

$$\ln\left(\frac{\beta}{T_m^2}\right) = \left\{\ln\left(\frac{AR}{E_a}\right) + \ln[f(\alpha)]\right\} - \left(\frac{E_a}{R}\right)\frac{1}{T_m} \qquad (7.5)$$

where, T_m is the maximum decomposition temperature or the point of inflection where the rate of mass loss is highest in the thermo-degradation curve which also corresponds to the maximum reaction rate **(Achilias et al., 2011)**, β is the heating rate, A is the pre-exponential

factor **(Lizundia et al., 2015)**, f(α) is the function of conversion rate (α) **(Kissinger, 1957; Dai et al., 2014; Blaine et al., 2012)**.

7.2.2. Augis and Bennett method

According to Augis & Bennett method, the activation energy can be determined by the equation (7.6):

$$\ln\left[\frac{\beta}{(T_m - T_o)}\right] = \ln A - \left(\frac{E_a}{R}\right)\frac{1}{T_m} \quad (7.6)$$

where, T_m and T_o are peak or maximum temperature and onset temperature of the DTG peak respectively. The activation energy E_a can be obtained from the slope of the straight line in $\ln\left(\frac{\beta}{(T_m - T_o)}\right)$ versus $-\frac{1}{T_m}$ plot **(Chrissafis et al., 2009)**.

7.2.3. Flynn-Wall-Ozawa method

The Flynn-Wall-Ozawa (F-W-O) method was used to analyze data from TG curves of the sample at different heating rates. In this method, Doyle's approximation of integration was used **(Doyle, 1962)** which can be expressed as in equation (7.7):

$$\log\beta = \log\left[\frac{A\,E_a}{R\,g(\alpha)}\right] - 2.315 - 0.4567\left(\frac{E_a}{R}\right)\frac{1}{T} \quad (7.7)$$

where, E_a is the activation energy of decomposition, A is the pre-exponential factor, T is the temperature and β is the heating rate **(Zhang et al., 2014)**. According to this method, E_a can be obtained from the slope of the straight line in the plot $\log\beta$ versus $-\frac{1}{T}$ **(Dai et al., 2014; Ozawa et al., 1965; Flynn, 1983)**. In this method, E_a can be estimated without knowledge of specific reaction function **(Achilias et al., 2011)**. The 'model-free' method assumes that no change in the conversion function f(α) occurs by changing the heating rate for all values of the degree of conversion (α) **(Zou et al., 2009)**. This method finds many advantages over other

models, such as determining the activation energy without the prior knowledge of reaction mechanism or without knowing reaction order and capability to provide reasonably reliable data as all the points are applicable on the TGA curves **(Liu et al., 2010)**. In this method, fixed value of α, from experiments at different heating rates helps in determining the temperatures corresponding to these values. The single-step reaction mechanism can be confirmed if the obtained activation energy is same for all the different values of α. On the other hand, complex reaction mechanism can be confirmed if activation energy changes with increasing degree of conversion. Thus, for studying the complex reactions, this method is extremely useful for interpreting kinetics of thermogravimetric data and determining the activation energy without the knowledge of reaction order **(Zou et al., 2009)**.

7.2.4. Kissinger-Akhira-Sunose method

Kissinger-Akhira-Sunose (K-A-S) model uses another asymptotic approximation for integral, which can be expressed in the form of an equation (7.8):

$$\ln\frac{\beta}{T^2} = \ln\left[\frac{A\,R}{E_a}\right] - \left[\frac{E_a}{R}\right]\frac{1}{T} \qquad (7.8)$$

Here again, E_a can be obtained from slope of the plots of $\ln\frac{\beta}{T^2}$ versus $-\frac{1}{T}$ at constant heating rate and degree of conversion **(Achilias et al., 2011; Byczynski et al., 2014; Diaz-Celorio et al., 2012)**. Thus, E_a can be determined using different models which are summarized in Table 7.1.

Table 7.1. Kinetic methods used in evaluating various kinetic parameters.

Method	Expression	Plot
Kissinger	$\ln\left(\frac{\beta}{T_m^2}\right) = \ln\left(\frac{AR}{E_a}\right) + \ln[f(\alpha)] - \left(\frac{E_a}{R}\right)\frac{1}{T_m}$	$\ln\left(\frac{\beta}{T_m^2}\right)\ vs\ \left(-\frac{1}{T_m}\right)$
Augis & Bennett	$\ln\left[\frac{\beta}{(T_m - T_o)}\right] = \ln A - \left(\frac{E_a}{R}\right)\frac{1}{T_m}$	$\ln\left[\frac{\beta}{(T_m - T_o)}\right]\ vs\ \left(-\frac{1}{T_m}\right)$
Flynn-Wall-Ozawa	$\log\beta = \log\left[\frac{A\,E_a}{g(\alpha)\,R}\right] - 2.315 - 0.4567\left[\frac{E_a}{R}\right]\frac{1}{T}$	$\log\beta\ vs\ \left(-\frac{1}{T}\right)$
Kissinger-Akahira-Sunose	$\ln\frac{\beta}{T^2} = \ln\left[\frac{A\,R}{E_a}\right] - \left[\frac{E_a}{R}\right]\frac{1}{T}$	$\ln\frac{\beta}{T^2} vs\ \left(-\frac{1}{T}\right)$

7.3. Results and Discussion

7.3.1. Fourier transform infrared spectroscopy (FTIR)

The different functional groups of GA, OLLA and GA-*g*-PLA bionanocomposite were detected by FTIR analysis as shown in figure 7.1. In the spectrum of OLLA and GA-*g*-PLA, the peaks at 1750 cm^{-1} and 1454 cm^{-1} assigned to $-C=O$ carbonyl stretching and $-CH_3$ bending respectively. The peaks at 1204 cm^{-1}, 1133 cm^{-1}, 1094 cm^{-1} and 1045 cm^{-1} were attributed to $-C-O-$ bond stretching in the spectrum of OLLA and GA-*g*-PLA. In the spectrum of GA, the peaks at 1600 cm^{-1} was assigned to $-C=O$ stretch and $-N-H$ bending whereas the peak at 1016 cm^{-1} was attributed to $-C-O-$ stretch of alcohols and carboxylic acids. As GA has less glycoprotein, no significant absorption bands due to $N-H$ stretch were observed in FTIR spectra. All above peaks confirmed the structure of GA and OLLA. The presence of GA and LA was also confirmed by the presence of common peaks in GA-*g*-PLA. It was observed that the peak at 3635 cm^{-1} was shifted to 3641 cm^{-1} and the reduction in intensity was also detected which suggested that an appreciable quantity of $O-H$ and $N-H$ groups in GA were grafted with OLLA chains.

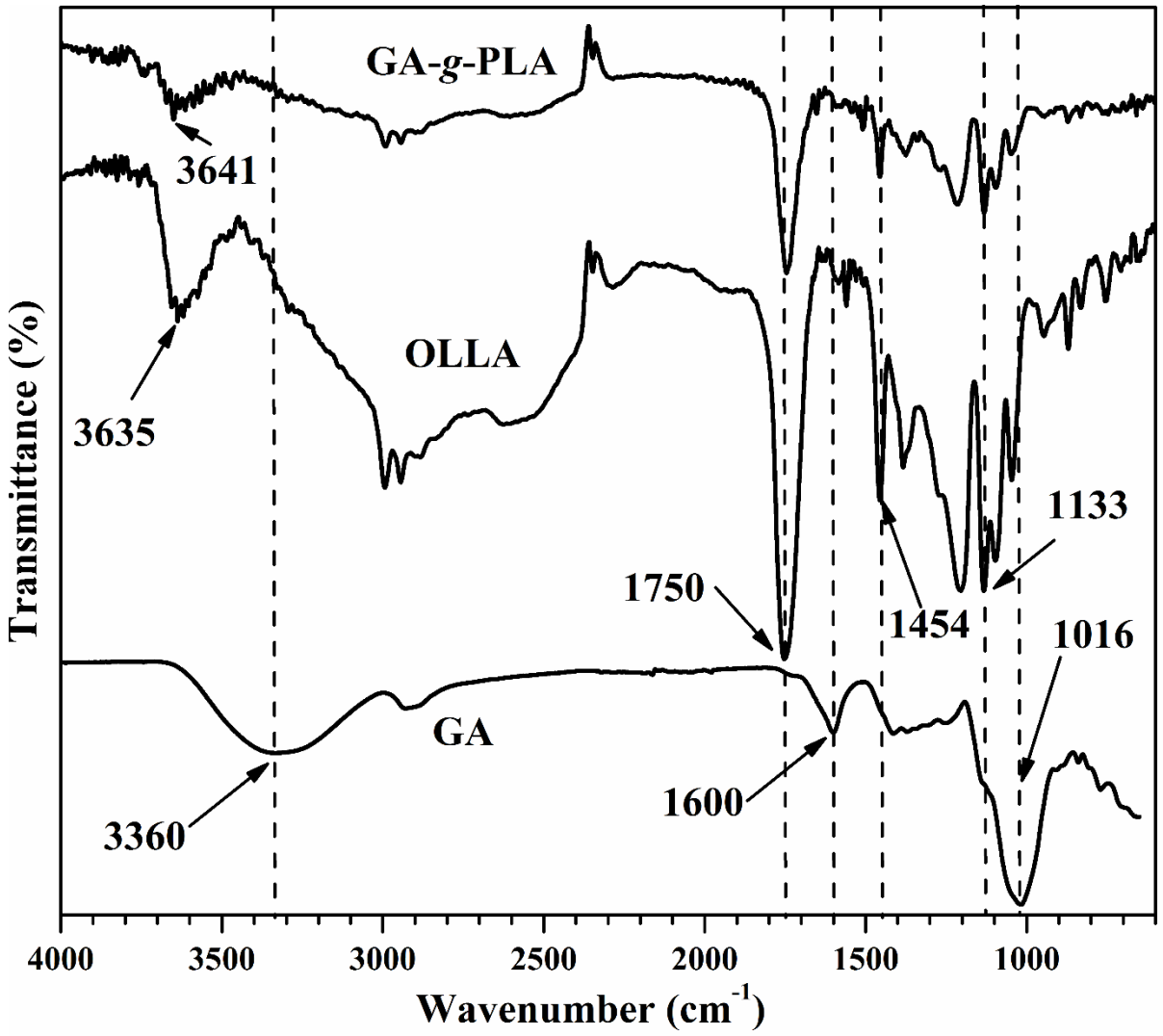

Figure 7.1. FTIR spectra of GA, OLLA and GA-*g*-PLA bionanocomposite.

7.3.2. Scanning electron microscopy (SEM)

Scanning electron microscopy (SEM) of all the film samples was conducted to investigate the effect of GA-*g*-PLA loading in surface morphology, and the results of analysis have been shown in figure 7.2(a) which shows a homogeneous surface for neat PLA film. In PLA/GA-*g*-PLA films, uniformly dispersed spheres appeared throughout the films (figure 7.2 (b)-(d)). As the loading was further increased to 10%, spheres became much larger and more agglomeration

was observed as shown in figure 7.2(d). Surface erosion and phase separation had also occurred which made the surface rough, and reduction in compatibility between PLA matrix and filler was also observed.

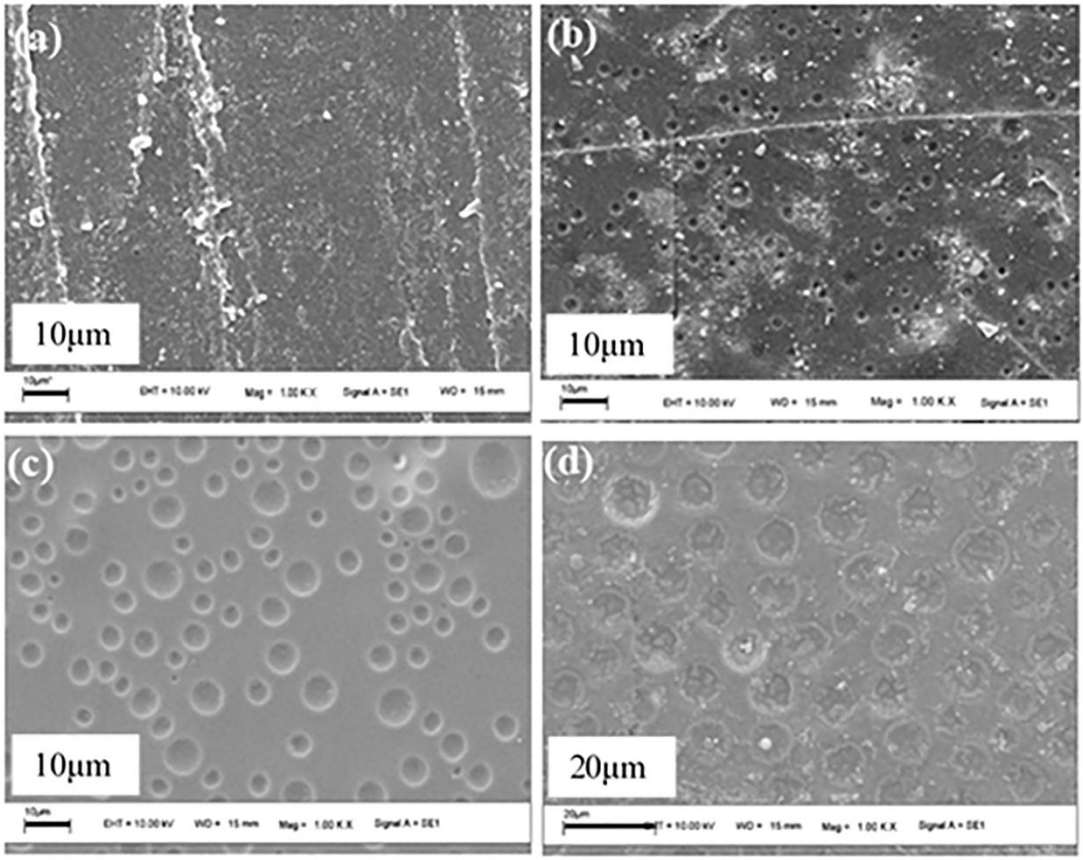

Figure 7.2. SEM micrograms at 1.00 KX of film samples of (a) PLA, (b) PLA/GA-*g*-PLA (3%), (c) PLA/GA-*g*-PLA(5%) and (d) PLA/GA-*g*-PLA(10%).

7.3.3. Thermogravimetric analysis (TGA)

Table 7.2 illustrates TGA data of the film samples analyzed in the presence of nitrogen at 10 °C min^{-1} heating rate. The temperatures at which 10% weight loss, 90% weight loss and maximum rate of degradation were observed have been presented in the table 7.2 as

$T_{10\% \text{ weight loss}}$, $T_{90\% \text{ weight loss}}$ and $T_{\text{max rate of degradation}}$ respectively. The degradation temperature of PLA at 10% weight loss was observed to be 336.9 °C. As the loading of the filler was increased to 3%, 5% and 10%, the onset degradation temperature reduced to 289.9 °C, 270.3 °C and 218.6 °C respectively. The possible reason for decrease in temperature could be attributed to small irregular branching of the filler which increased 'free volume' between the polymer chains resulting in lowering of degradation temperature. The maximum degradation temperature ($T_{\text{max rate of degradation}}$) of the PLA was found as 370.3 °C. On increasing the loading to 3%, 5% and 10%, reduction in the temperature was also observed to 344.9 °C, 338.9 °C and 323.2 °C respectively. Similar trend was observed at 90% weight loss. Hence, it can be concluded that, with increase in filler loading in PLA matrix, the degradation of the PLA/GA-*g*-PLA bionanocomposite films also increased.

Table 7.2. TGA of PLA, PLA/GA-*g*-PLA(3%), PLA/GA-*g*-PLA(5%) and PLA/GA-*g*-PLA(10%) bionanocomposite films.

Sample code	$T_{10\% \text{ weight loss}}$ (°C)	$T_{50\% \text{ weight loss}}$ (°C)	$T_{\text{max rate of degradation}}$ (°C)	$T_{90\% \text{ weight loss}}$ (°C)
PLA	336.9	364.1	370.3	380.2
PLA/GA-*g*-PLA(3%)	289.9	331.8	344.9	351.9
PLA/GA-*g*-PLA(5%)	270.3	321.9	338.9	347.7
PLA/GA-*g*-PLA(10%)	224.6	299.1	323.2	332.6

Figure 7.3 shows DTG and TGA curves of PLA, PLA/GA-*g*-PLA(3%), PLA/GA-*g*-PLA(5%) and PLA/GA-*g*-PLA(10%) bionanocomposite films at the heating rates of 2, 5 and 10 °C min^{-1}. The peak temperature in the DTG curves determines the maximum rate of weight

loss and maximum degradation temperature of the film samples. For the film samples, a broad peak or hump at a temperature around 100 °C was observed which signifies bound and unbound moisture removal entrapped in the films. At 10% filler loading, maximum moisture removal was observed. This can be attributed to increase in molecular segmental mobility with increase in the loading of filler which has the tendency to absorb more moisture. With increase in heating rate, a shift or change in the thermal degradation temperature was noted. This could be because of less time provided to the samples for phase change at higher heating rates or due to time lag for thermal conduction **(Valapa et al., 2014; Chen et al., 2013)**. Single stage degradation peak was observed in PLA and PLA/GA-*g*-PLA film samples which suggested good compatibility of PLA with GA-*g*-PLA in PLA/GA-*g*-PLA bionanocomposite films. Decrease in thermal stability was observed with increase in concentration of the filler due to the plasticizing effect caused by the smaller molecular chains of the filler. Moreover, all the films observed sharp peak except PLA/GA-*g*-PLA(10%) bionanocomposite film samples which exhibited broader peak. This can be caused due to the inefficient heat diffusion or due to the entrapment of the molecular chains of the filler within the matrix which finally resulted in time lapse caused by volatiles to escape from the sample.

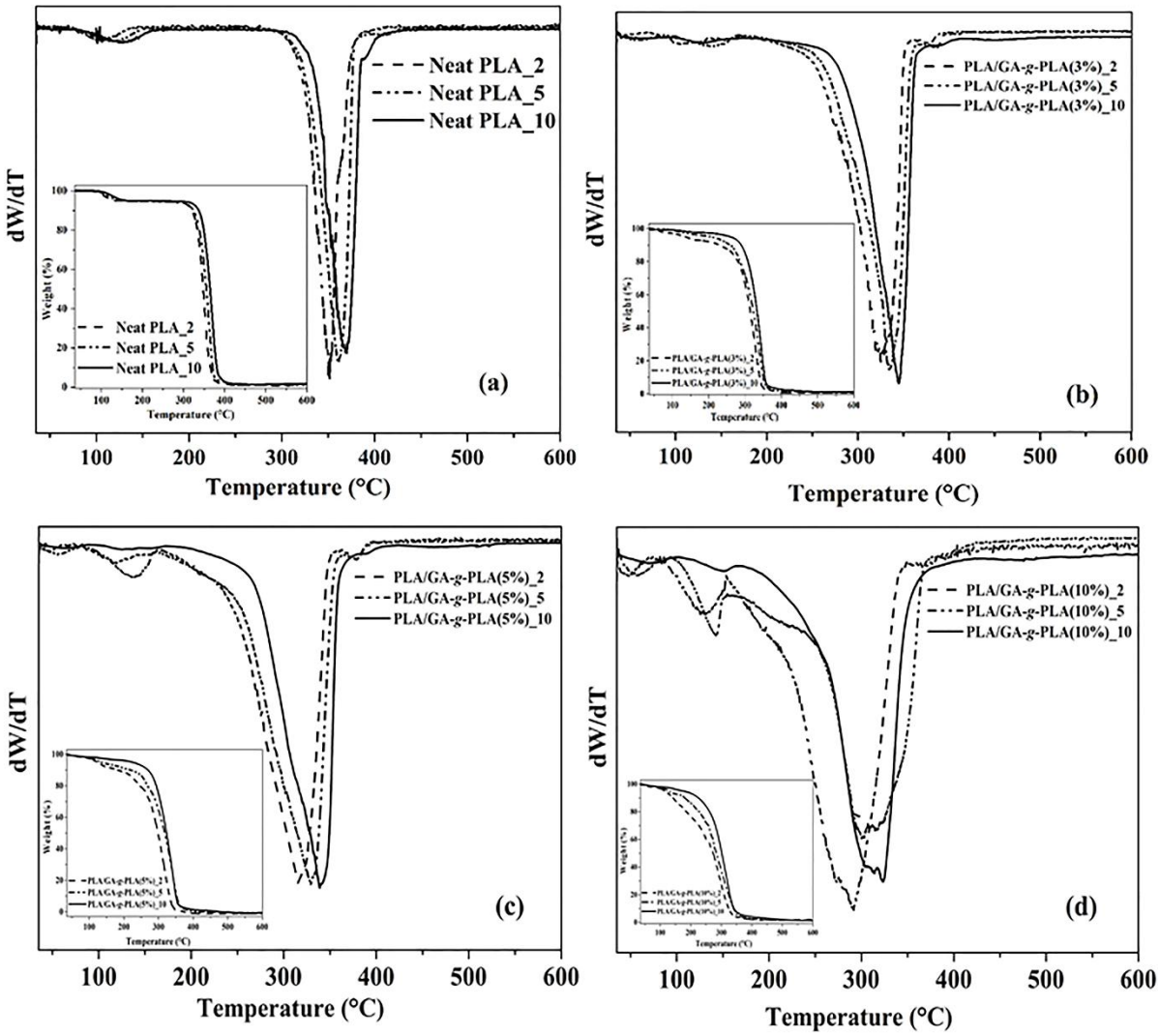

Figure 7.3. DTG and TGA curves of (a) Neat PLA, (b) PLA/GA-*g*-PLA(3%), (c) PLA/GA-*g*-PLA(5%) and (d) PLA/GA-*g*-PLA(10%) bionanocomposite films at the heating rates of 2, 5, 10 °C min^{-1}.

Figure 7.4 shows the relationship between heating rates with peak temperature obtained for the samples. It was observed that with increase in the heating rate of samples the degradation peak temperature also increased. The correlation coefficient obtained for PLA,

PLA/GA-*g*-PLA(3%), PLA/GA-*g*-PLA(5%) and PLA/GA-*g*-PLA(10%) were 0.91, 0.93, 0.87 and 0.95 respectively.

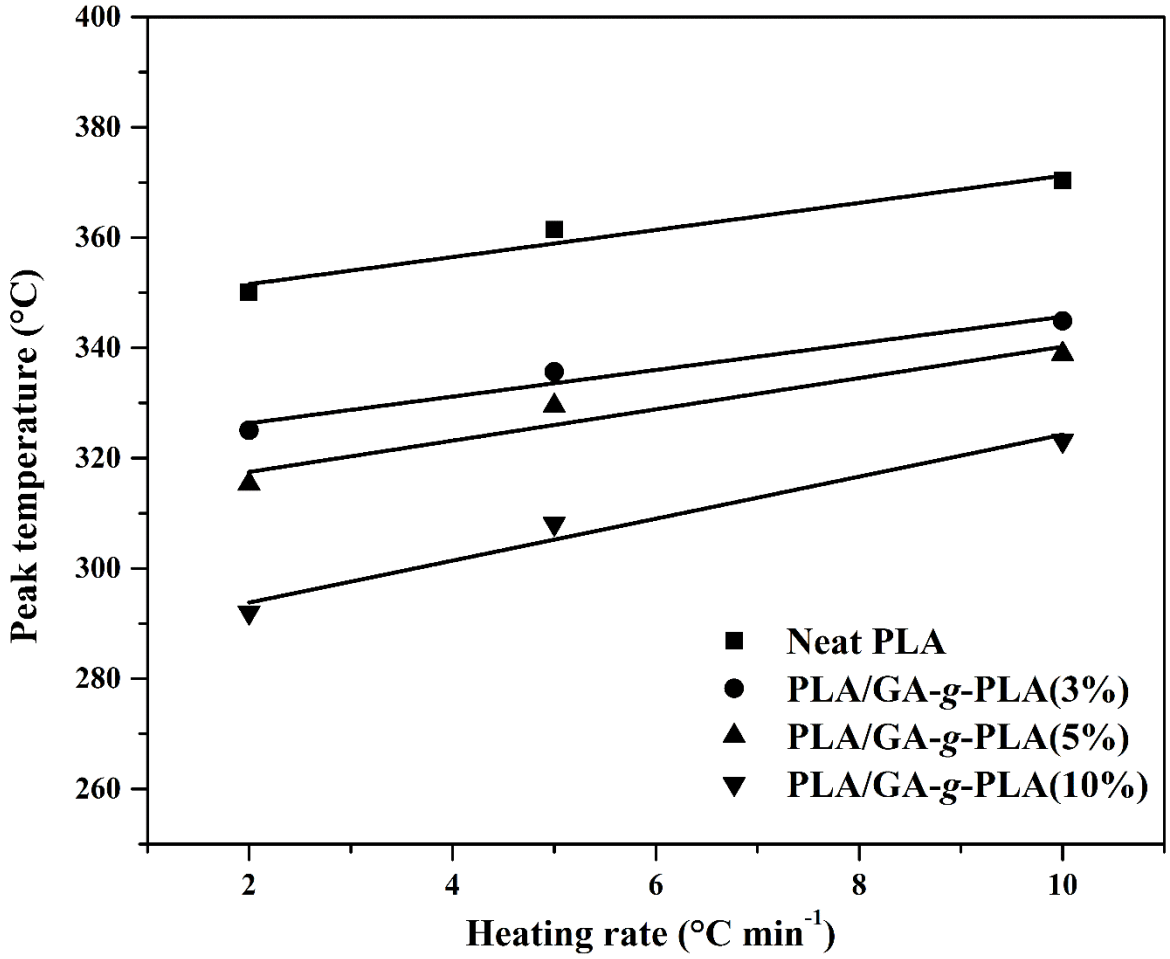

Figure 7.4. Peak temperature change at different heating rates for neat PLA and bionanocomposite films.

7.3.4. Thermal analysis-Fourier transform infrared spectroscopy (TGA-FTIR)

In order to investigate the gaseous products obtained from the TGA furnace by decomposition of PLA and PLA/GA-*g*-PLA(5%) samples, the three-dimensional (3D) stacked FTIR diagrams and FTIR curves at different temperatures were plotted and shown in figure 7.5. The three axes

represent the wavenumber (cm^{-1}), absorbance and temperature (°C). The variation in absorbance intensities were observed from the evolved gaseous at complete range of temperature in figure 7.5(a) and 7.5(c). These 3D spectra were used to select specific temperatures at which the variation in peak intensities of degradation products were observed. The obtained temperatures were then used to plot FTIR spectra of PLA and PLA/GA-*g*-PLA(5%) samples to identify the functional groups as shown in figure 7.5(b) and 7.5(d). Figure 7.5(b) and 7.5(d) represent the FTIR spectra of evolved gaseous products of PLA and PLA/GA-*g*-PLA(5%) respectively at different temperatures. The main decomposition peaks were observed in the temperature range of 200-455 °C. The common peaks at 3573 cm^{-1}, 3004 cm^{-1}, 2951 cm^{-1}, 2310 cm^{-1} and 2179 cm^{-1} were observed for PLA and PLA/GA-*g*-PLA(5%) which denote – OH group due to moisture, $-CH_3$ asymmetric stretching, $-CH_3$ symmetric stretching due to methane, $-C=O$ stretching due to CO_2 and $C-O$ bending vibration due to carbon-monoxide respectively. In the case of PLA, the peaks at 2736 cm^{-1}, 1766 cm^{-1}, 1505 cm^{-1}, 1249 cm^{-1} and 936 cm^{-1} correspond to $O=C-H$ due to aldehyde, $O=C$ stretching due to lactide, $-CH_3$ stretching, CO stretching due to lactide removal and cyclic or ring structure respectively. On the other hand, the peak intensities at 1786 cm^{-1}, 1380 cm^{-1} and 1249 cm^{-1} correspond to $O=C$ stretching, $-CH_3$ stretching and CO stretching in the case of PLA/GA-*g*-PLA(5%) films. The shift in peaks position was observed in PLA/GA-*g*-PLA(5%) film sample as compared to PLA confirmed the structural modification. A new small and sharp peak was observed at 1517 cm^{-1} in PLA/GA-*g*-PLA(5%) sample which shows the presence of $N-H$ stretching which was not present in PLA sample. Hence, the evolved gaseous products from PLA, are cyclic oligomers, lactide, acetaldehyde,

carbon-monoxide and carbon-dioxide which are attributed to the thermal degradation of PLA based upon a hydroxyl end-initiated ester interchange process. Carbonyl compound and carbon-dioxide exist in the products until the end of the experiments, whereas carbon-monoxide gradually decreases above the peak temperature. CO_2 is one of the main decomposition products which is attributed to the thermal degradation based upon chain homolysis of PLA **(Huang et al., 2015; Zou et al., 2009; Tudorachi et al., 2012)**. PLA/GA-*g*-PLA based bionanocomposite films are most likely degrade via random depolymerization which leads to the evolution of cyclic oligomers, lactide, acetaldehyde, methane, carbon-monoxide, carbon-dioxide and N – H compound.

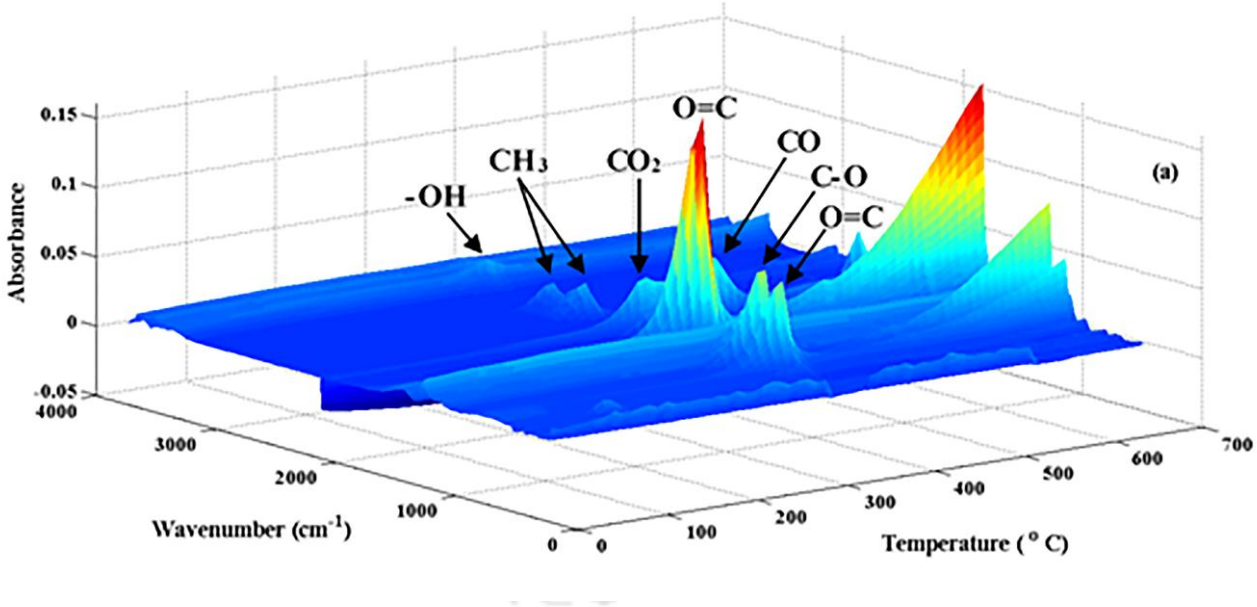

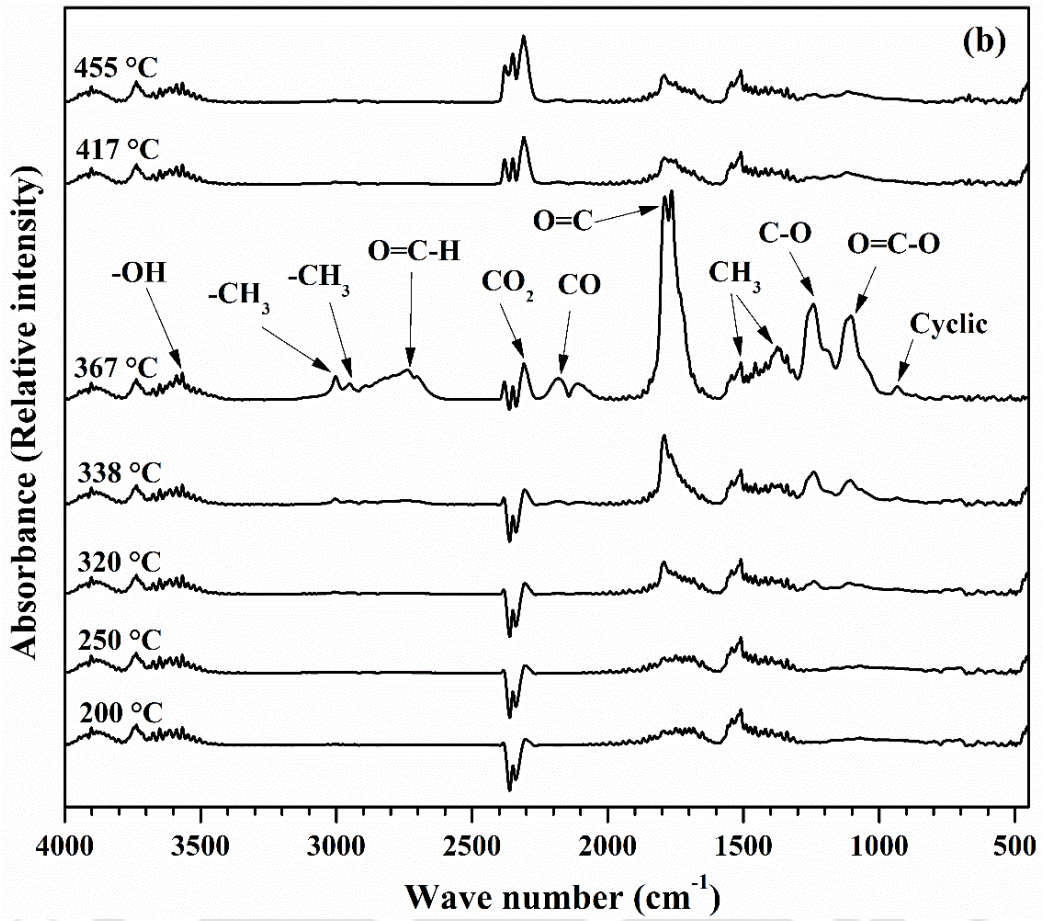

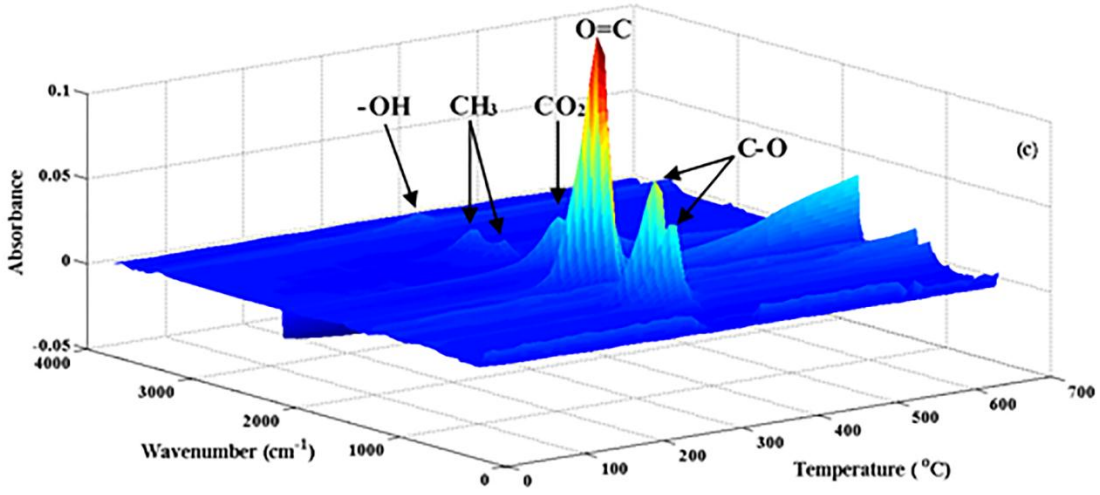

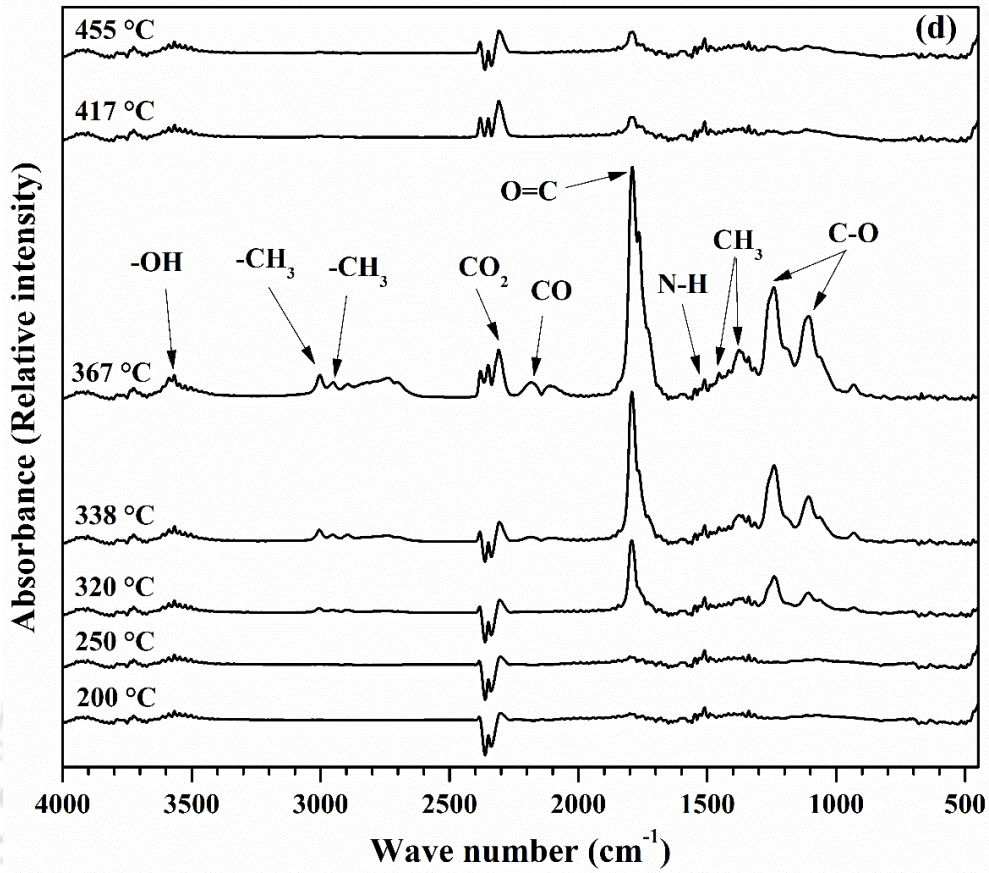

Figure 7.5. Evolved gaseous products (a) 3D-FTIR spectra of PLA, (b) FTIR spectra of PLA at different temperatures, (c) 3D-FTIR spectra of PLA/GA-*g*-PLA(5%) bionanocomposite film and (d) FTIR spectra of PLA/GA-*g*-PLA(5%) bionanocomposite film at different temperatures.

7.3.5. Degradation pathways

The probable mechanism of degradation of PLA/GA-*g*-PLA bionanocomposite films is presented in figure 7.6. Since the composite film is composed of PLA and GA molecules, better understanding to the thermal degradation mechanism of these molecules individually is needed. It was observed that the interaction of PLA and GA-*g*-PLA molecules formed the microcapsules in the PLA film. The figure 7.6 depicts the dissociation of PLA matrix into smaller fragments during thermal degradation. Simultaneously, the proposed effect of heat on

the hydrophilic part has also been shown. The core part of the microcapsule appeared to have formed due to hydrophilic linkages in GA. Here, the structure of GA has been considered according to 'Wattle blossom' model **(Randall et al., 1989)**. Accordingly, the hydrophilic polysaccharide blocks of GA have been shown to be attached to the backbone which is a hydrophobic polypeptide chain. On heat treatment, initially the unfolding of the polypeptide chain occurred, thereafter, denaturing of the protein moieties degraded the proteinaceous part **(Islam et al., 1997)**. Since, very less amount of polypeptide chain is present in GA, the degradation of polysaccharide is basically focused. On heating, GA molecules break into smaller fragments. A tentative model for GA dissociation was also proposed by **Connolly et al. (1987)** with the treatment of *pronase*. It was predicted in the model that the degradation of polysaccharide may lead to the formation of small molecules which are its building blocks. The molecules obtained on degradation of polysaccharide blocks were found to be D-galactopyranose, L-arabinofuranose, L-rhamnopyranose, and D-glucopyranosuronic acid **(Gils et al., 2010)**. It is documented in the literature that the degradation of PLA follows single step degradation process **(Yang et al., 2009)**. Thermal degradation of PLA predominantly follows random main-chain scission and unzipping depolymerization reactions. The ester linkage of PLA reduces degradation due to the two main susceptible linkages, viz. carbonyl carbon-carbon and carbonyl carbon-oxygen **(Nalbandi, 2001)**. However, in isothermal heating, carbonyl $C-O$ linkage was found to be the most susceptible because its non-bonding electrons, due to which changes in electron charge distribution occurred. In addition, breakage of $C-O$ linkage was confirmed by the presence of more $-COOH$ end groups rather than $-OH$ end groups. Furthermore, PLA oligomers resulted in autocatalysis by the terminal carboxylic acid groups which resulted in faster degradation rate of PLA **(Valapa et al., 2014)**. These

reactions include depolymerisation, thermohydrolysis, intermolecular transesterification, intramolecular transesterification and cyclic oligomerization. The molecules obtained on thermal degradation of PLA, as shown in figure 7.6, mainly are 2-((2-hydroxypropanoyl)oxy)propanoic acid, 2-hydroxypropanoic acid or lactic acid, acrylic acid, acetaldehyde and 3,6-dimethyl-1,4-dioxane-2,5-dione or lactide. Compounds associated with polymer that enhance the degradation process include polymerization catalysts, oligomers, monomers and water. Thus, it can be interpreted that the thermal stability of PLA can be achieved by blocking the hydroxyl end-groups and non-polymeric molecules **(Maharana et al., 2009)**. It was also reported that the thermal degradation of PLA produced gases such as CO_2, CO and acetaldehyde.

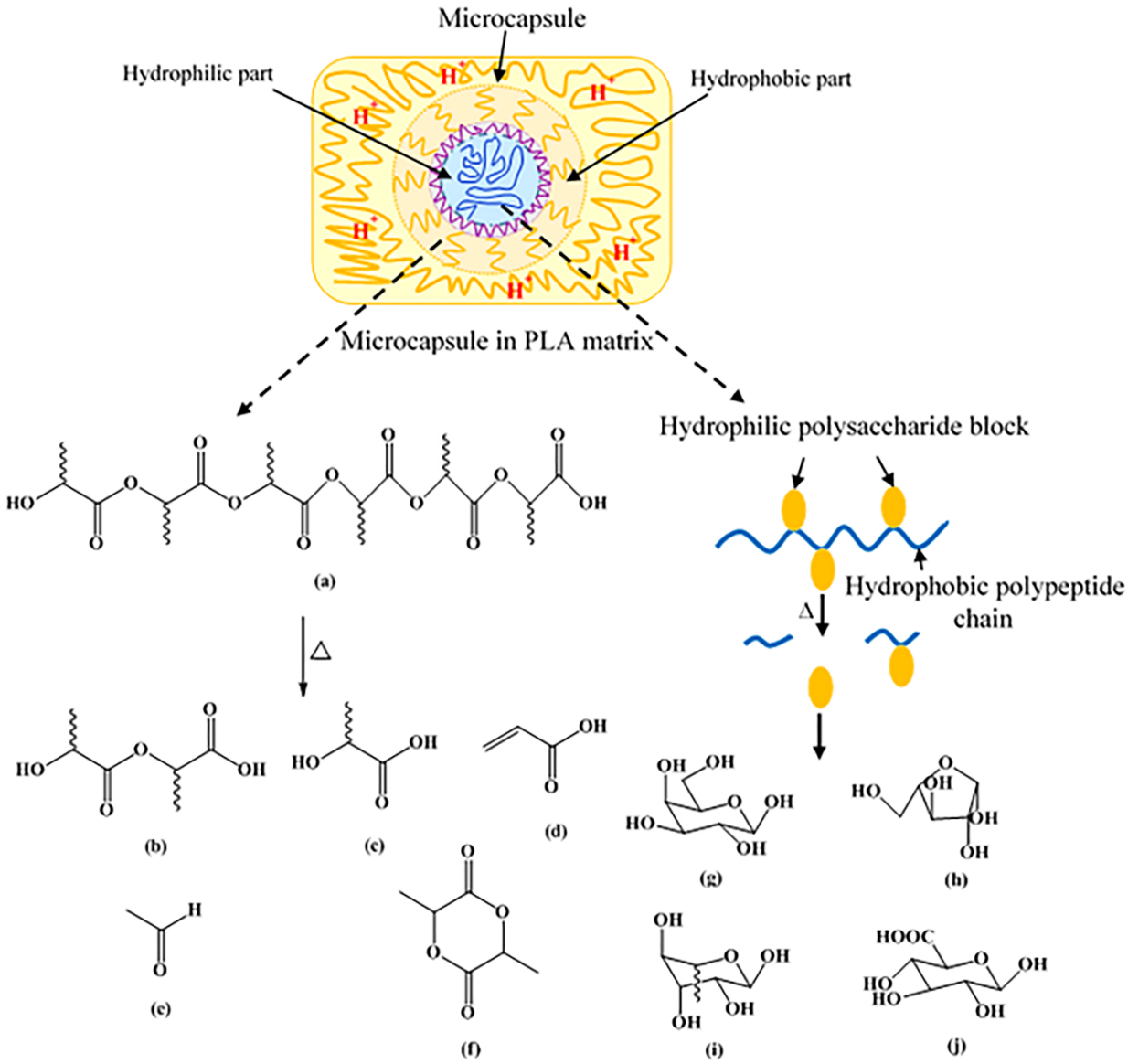

Figure 7.6. Proposed degradation pathway of bionanocomposite film and its degraded products (a) PLA, (b) oligomer, (c) lactic acid, (d) acrylic acid, (e) acetaldehyde, (f) lactide, (g) D-galactopyranose, (h) L-arabinofuranose, (i) L-rhamnopyranose and (j) D-glucopyranosuronic acid.

7.3.6. Thermal degradation kinetics

The Kissinger method was analyzed firstly because it is independent of thermal degradation mechanism. The method needs non-isothermal TGA measurement to obtain a constant degradation rate. The Kissinger plot is based on equation (7.5) and thermograms of inflection point temperatures. In this method, E_a can be obtained from the slope of the line plotted between $\ln\left(\frac{\beta}{T_m^2}\right)$ against $-\frac{1}{T_m}$ without the precise knowledge of reaction mechanism and intercept of the line can be used to determine the frequency factor **(Huang et al., 2015; Zeng et al., 2009; Yang et al., 2003; Hu et al., 2004)**. The Kissinger plot for all the samples have been presented in figure 7.7. The activation energy obtained for PLA, PLA/GA-*g*-PLA(3%), PLA/GA-*g*-PLA(5%) and PLA/GA-*g*-PLA(10%) bionanocomposite film samples were obtained to be 254.08, 239.73, 193.36 and 135.21 kJ mol^{-1} respectively with the correlation coefficient in the range of 0.9976 to 1 which suggests that the data fit in the straight line. It can be seen that all the fitted straight lines are almost parallel, which suggests that Kissinger method can be well applied in this system studied through present investigation.

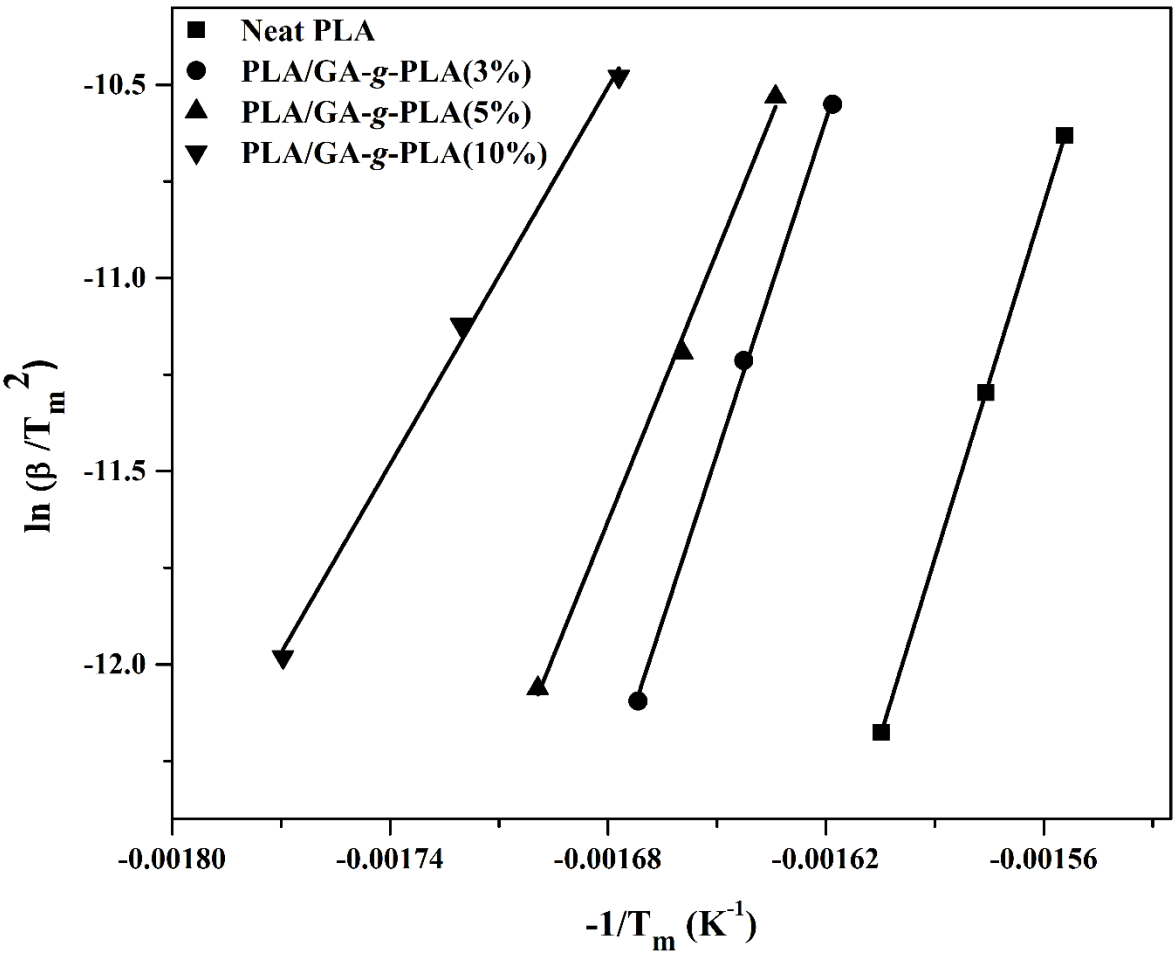

Figure 7.7. Kissinger plot for Neat PLA, PLA/GA-*g*-PLA(3%), PLA/GA-*g*-PLA(5%) and PLA/GA-*g*-PLA(10%) bionanocomposite films.

The Augis & Bennett method was also used to determine E_a as explained in equation (7.6) from the slope of the straight line in the plot of $\ln\left[\frac{\beta}{(T_m - T_o)}\right]$ versus $-\frac{1}{T_m}$. Figure 7.8 was used to determine the E_a values from the slope of the straight lines. The E_a obtained for PLA, PLA/GA-*g*-PLA(3%), PLA/GA-*g*-PLA(5%) and PLA/GA-*g*-PLA(10%) samples were 259.08, 254.09, 224.13 and 139.92 kJ mol^{-1} respectively. The correlation coefficient obtained were in the range of 0.9999 to 0.9946 which suggests that the straight line fits the data. It can be seen

that the fitted straight lines are not parallel which suggests the non-applicability of the present system with Augis & Bennett model.

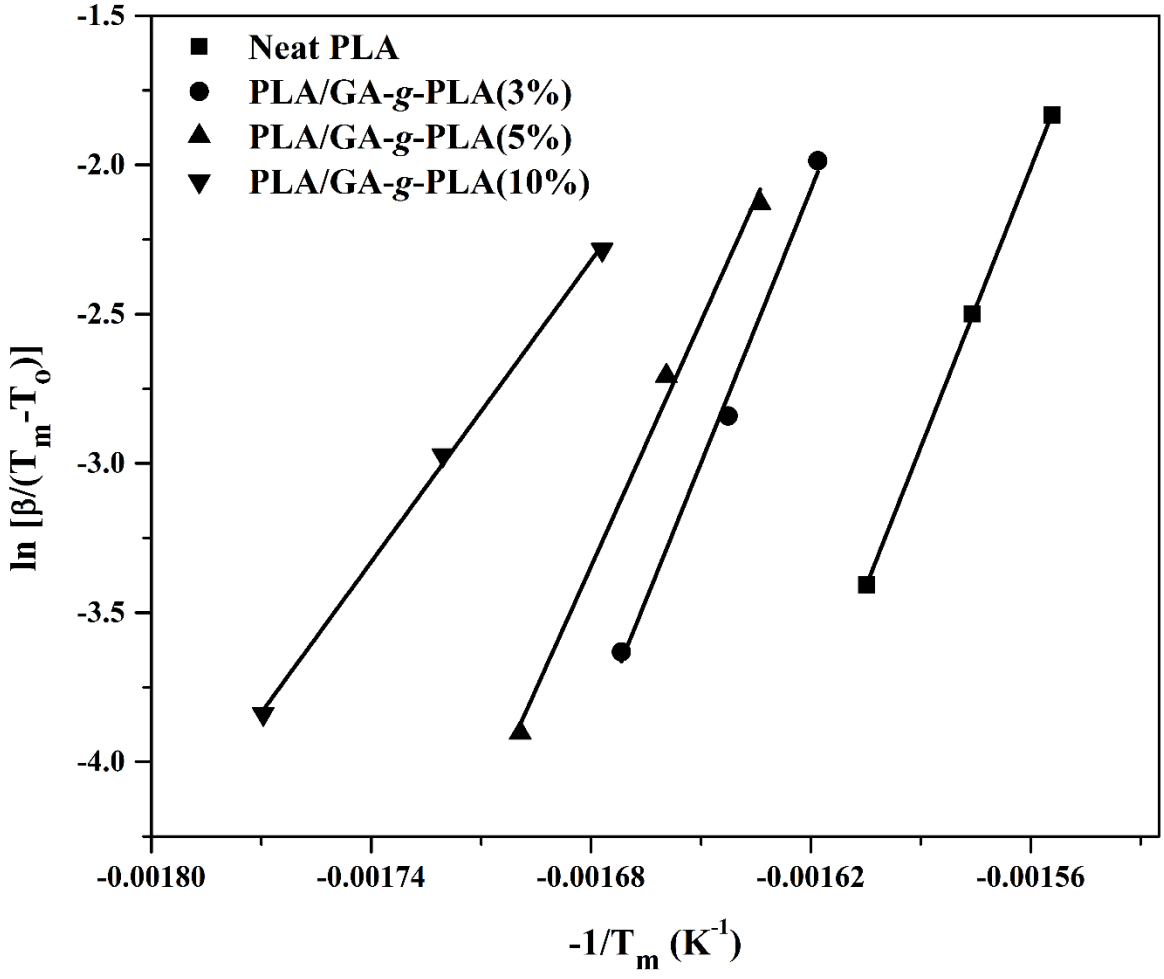

Figure 7.8. Augis & Bennett plot for PLA, PLA/GA-*g*-PLA(3%), PLA/GA-*g*-PLA(5%) and PLA/GA-*g*-PLA(10%) bionanocomposite films.

F-W-O model, an integral method, is also independent of degradation mechanism **(Zeng et al., 2009)**. In this isoconversional method, the activation energy for different conversion values were calculated from the slope of the straight lines which fits linearly in a plot of $\log \beta$ versus $\frac{1}{T}$ as explained in equation (7.7). The conversion values taken for the study were

0.1, 0.2, 0.3, 0.4, 0.5, 0.6, 0.7, 0.8 and 0.9 to determine the values of activation energy. The activation energy and correlation coefficient obtained for the different samples have been presented in table 7.3. At lower conversion values, lower E_a values were observed because of the removal of solvent, moisture and volatile groups **(Ahmad et al., 2014)**. Hence, the analysis can be focused in higher range of conversion value which predicts main mass loss decomposition process. It was also observed that the straight lines of PLA/GA-*g*-PLA bionanocomposite film samples shifted to lower $-\frac{1}{T}$ values with respect to neat PLA film which suggested that the filler is causing an increase in the degradability of PLA. Figure 7.9 displays the straight lines that fit the data, are almost parallel to each other for each samples at higher conversion values which suggests that F-W-O model is also applicable to this system. The average value of the activation energies ($\overline{E}_a$) at different conversions were calculated for all the samples, and have been given in table 7.3. Change in activation energy was observed with increase in the degree of conversion which indicates that the samples were following a complex decomposition mechanism **(Zou et al., 2009)**.

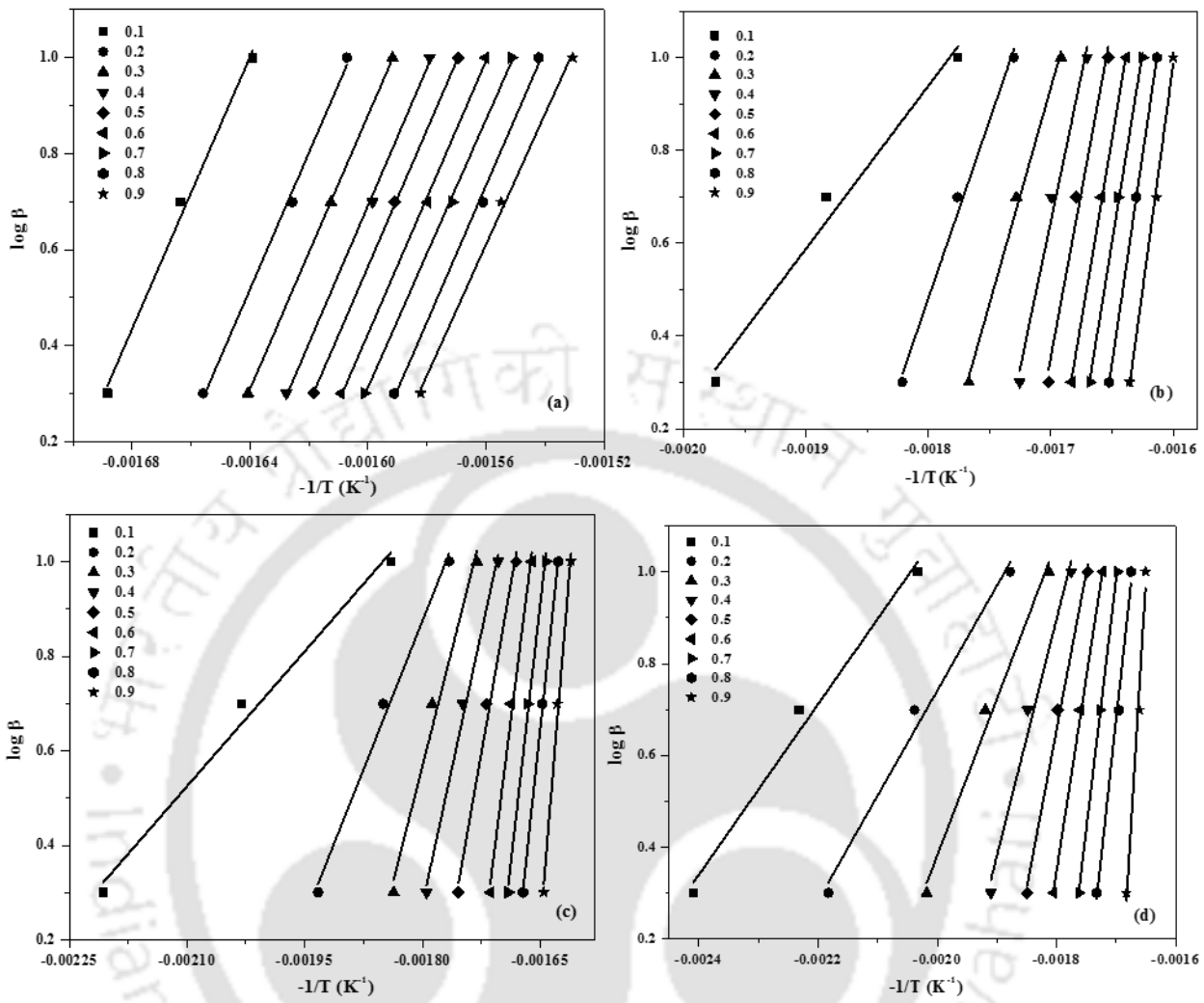

Figure 7.9. Flynn-Wall-Ozawa plots of (a) Neat PLA, (b) PLA/GA-*g*-PLA(3%), (c) PLA/GA-*g*-PLA(5%) and (d) PLA/GA-*g*-PLA(10%) bionanocomposite films.

The K-A-S model is also an integral method which can be used to calculate the activation energies of the samples. By this method, the activation energies of decomposition were calculated from TGA data at different heating rates (β = 5, 10 and 15 °C min^{-1}). In the present work, the conversion values of 10%, 20%, 30%, 40%, 50%, 60%, 70%, 80% and 90% were used. According to equation (7.8), the activation energies can be determined from the

slope of the straight lines of plots $\ln\frac{\beta}{T^2}$ versus $-\frac{1}{T}$ for each degree of conversion. Good linearity was observed for E_a data at these conversion values with correlation coefficient in the range of 0.987 to 0.998. The mean values of activation energies obtained from the figure 7.10 are listed in table 7.3. K-A-S also follows the similar trend as F-W-O model.

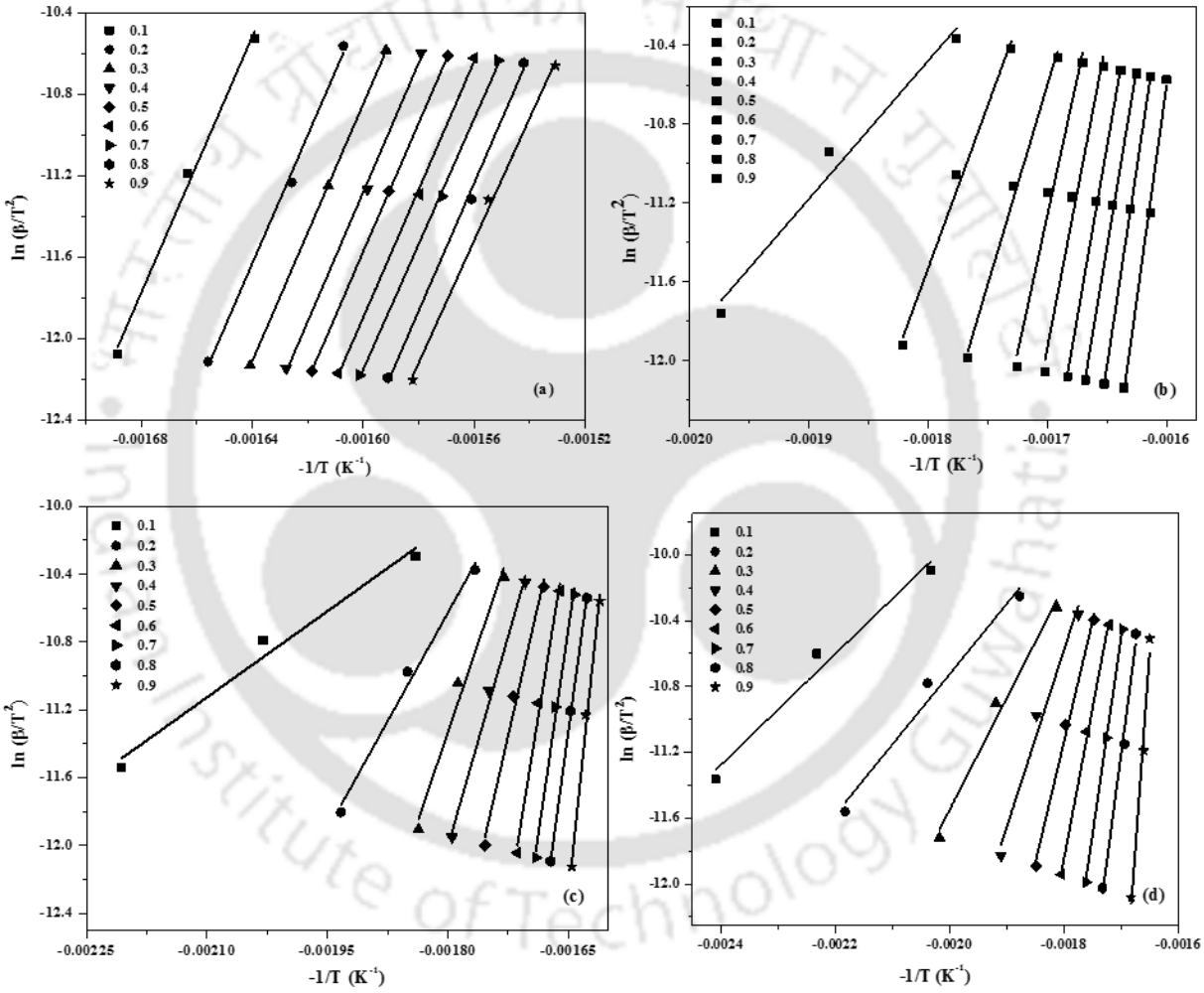

Figure 7.10. Kissinger-Akhira-Sunose plots of (a) Neat PLA, (b) PLA/GA-*g*-PLA(3%), (c) PLA/GA-*g*-PLA(5%) and (d) PLA/GA-*g*-PLA(10%) bionanocomposite films.

Figure 7.11 shows the activation energy versus conversion (α) plot. It was observed that with increase in degree of conversion, no change in E_a values occurred for neat PLA film which was also found by **Dai et al., (2014)**. This indicates that activation energy of PLA is independent of the conversion values which indicates that degradation stage of PLA followed one-dimensional diffusion or unification of multiple-reaction mechanism **(Jakic et al., 2013; Dai et al., 2014)**. However, for PLA/GA-*g*-PLA bionanocomposite films, E_a values increased as a function of conversion which shows that neat PLA film and PLA/GA-*g*-PLA bionanocomposite films are following different mechanisms. In PLA/GA-*g*-PLA bionanocomposite films, the oligomeric molecules in filler resulted in creating the weak link sites in the matrix by enhancing molecular chain mobility and generating intermolecular distance by small chain segment molecules of the filler. These weak links attributed to initiate the thermal degradation. In the range $0.1 \leq \alpha \leq 0.6$, lower E_a values for PLA/GA-g-PLA bionanocomposite films were observed because of the presence of filler. As the weak links in PLA/GA-*g*-PLA bionanocomposite films were broken, increase in E_a values occurred. For PLA/GA-*g*-PLA(3%), PLA/GA-*g*-PLA(5%)and PLA/GA-*g*-PLA(10%) bionanocomposite films, it was inferred that increase in the filler loading also resulted in decrease in E_a value. Moreover, it can also be inferred from the figure 7.10 that the blending of GA-*g*-PLA filler decreased the thermal stability of neat PLA film due to the effective heat transfer between the filler and the matrix which attributed to the non-uniformity in the neat PLA matrix. It can also be observed that increase in filler concentration increases the weak sites in the matrix which resulted in lowering the E_a values at different conversions. At later stages of degradation, i.e. at 90% conversion, the PLA/GA-*g*-PLA bionanocomposite films attain the highest E_a values which could be due to char content which resisted the samples from further degradation.

Hence, it can be concluded that in PLA and PLA/GA-*g*-PLA bionanocomposite films, complex interaction was taking place following two different mechanisms.

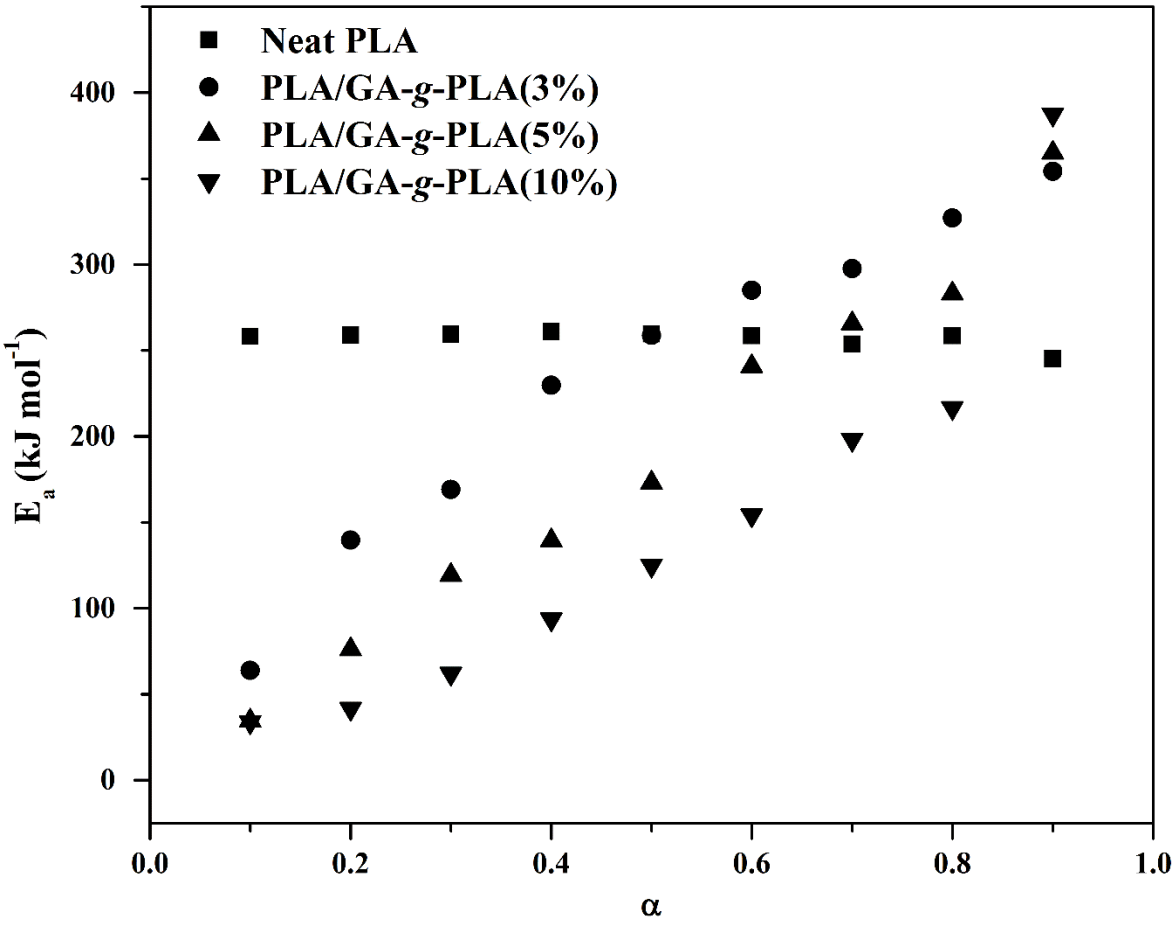

Figure 7.11. Activation energy versus conversion plot obtained from F-W-O and K-A-S model.

Activation energy and regression co-efficient for the films obtained by Kissinger, Augis & Bennett, F-W-O and K-A-S methods are summarized in table 7.3. It was observed that E_a values of PLA obtained from different methods were around 250 kJ mol^{-1} which is in good agreement with the values reported in the literature. **Carrasco et al., (2014)** found E_a value of pellets to be more than 200 kJ mol^{-1}, **Carrasco et al., (2010)**, observed E_a value in the range

of 243-255 kJ mol^{-1} for processed materials and **Tsuji et al., (2003)**, found it in the range of 205-297 kJ mol^{-1} for PLLA/PDLA. The E_a calculated from Kissinger and Augis & Bennett method may not display the overall trend because the values were obtained from the fixed conversion rate **(Dai et al., 2014)**. The average E_a value obtained by F-W-O method for PLA, PLA/GA-*g*-PLA(3%), PLA/GA-*g*-PLA(5%) and PLA/GA-*g*-PLA(10%) were 257.01, 236.14, 188.55 and 145.76 kJ mol^{-1} respectively. The average E_a value ($\overline{E}_a$) obtained by K-A-S method for PLA, PLA/GA-*g*-PLA(3%), PLA/GA-*g*-PLA(5%) and PLA/GA-*g*-PLA(10%) were 260.17, 238.52, 188.74 and 144.23 kJ mol^{-1} respectively. Hence, the same trend was followed by both the methods that is $\overline{E}_a$ of PLA > PLA/GA-*g*-PLA(3%) > PLA/GA-*g*-PLA(5%) > PLA/GA-*g*-PLA(10%). The decrease in these values with increase in filler loading could be explained by increase in chain mobility and intermolecular distance caused by the small molecular chains of oligomer **(Dai et al., 2014)**. Table 7.3 shows that the obtained values are close to the values obtained from the other models. It can also be observed that E_a and $\overline{E}_a$ values obtained from all the methods are very close and consistent, which suggests that these values are reasonable and are in good agreement with each other.

Table 7.3. Activation energy and regression co-efficient for PLA and PLA/GA-*g*-PLA bionanocomposite films obtained by Kissinger, Augis & Bennett, F-W-O and K-A-S methods.

Sample name	Kissinger method		Augis & Bennett method		Flynn-Wall-Ozawa method		Kissinger-Akahira-Sunose method	
	E_a (kJ mol^{-1})	R^2	E_a (kJ mol^{-1})	R^2	$\bar{E}_a$ (kJ mol^{-1})	$\bar{R}^2$	$\bar{E}_a$ (kJ mol^{-1})	$\bar{R}^2$
PLA	254.08	1	259.08	0.999	257.01	0.998	260.17	0.998
PLA/GA-*g*-PLA(3%)	239.73	0.999	254.09	0.995	236.14	0.993	238.52	0.992
PLA/GA-*g*-PLA(5%)	193.36	0.997	224.13	0.995	188.55	0.992	188.74	0.990
PLA/GA-*g*-PLA(10%)	135.21	0.997	139.92	0.999	145.76	0.990	144.23	0.987

7.4. Summary

In this research work, the effects of fabricated GA-*g*-PLA on the thermal behavior of PLA films were investigated using thermal characterization followed by its degradation kinetics. The good dispersion of micro and nanospheres throughout the PLA matrix was observed in SEM analysis which resulted in increase in the tortuosity of PLA/GA-*g*-PLA bionanocomposite films with respect to neat PLA films. The TGA results indicated that thermal stability of PLA decreased with increase in loading of the filler due to the plasticizing effect caused by oligomeric molecules of the filler. Thermogravimetric analysis hyphenated to Fourier transform infrared spectroscopy (TGA-FTIR) was used to investigate the gaseous products of the decomposition process of PLA and PLA/GA-*g*-PLA(5%). The maximum degradation temperature and activation energies from Kissinger, Augis & Bennett, F-W-O and K-A-S models were determined. Furthermore, different degradation pathways and subsequent byproducts formation were proposed for PLA and PLA/GA-*g*-PLA bionanocomposite films. E_a versus conversion plot indicated that the degradation stage of PLA followed one-dimensional diffusion mechanism or unification of multiple-reaction mechanism. The increase in activation energy with increase in conversion indicates complex reaction in PLA/GA-g-PLA bionanocomposite films. The results also proved that the kinetic models are in good agreement, and the models are complementary to each other. Hence, the results can provide valuable information for researchers in order to predict kinetic model and optimization of the process conditions for the system.

Chapter 8

Conclusions and Future Scope

The chapter summarizes the major inferences drawn from the work, and presents an outlook for future studies.

8.1. Conclusions

Major conclusions drawn on the basis of overall observation, and major findings of the research work are as follows:

- Synthesis of GA-*g*-PLA samples resulted in the conversion of hydrophilic GA to hydrophobic bionanocomposite. The FTIR and NMR analyses confirmed that the grafting of *oligo*-(lactic acid) on GA backbone occurred at −OH and −NH groups. The number average molecular weights of the bionanocomposites determined by GPC were in the range of 1060 to 1140 g mol^{-1}. Significant change in the surface morphology was observed by SEM analysis which also supports grafting. The improvement in hydrophobicity occurred with increase in GA concentration confirmed the reduction in polar groups due to grafting.
- Shear test parameters were optimized to check the adhesive strength of the synthesized bionanocomposites for glass as well as granite substrates. The single lap shear test for the adhesive resulted in substrate failure. The prepared bionanocomposite was proved to be remarkable adhesive with respect to the existing bio-based adhesives.

- PLA and PLA/GA-*g*-PLA bionanocomposite films were prepared by solution casting method. PLA was found to be compatible with the GA-*g*-PLA filler that was confirmed by single T_g of the polymeric blends obtained by mixing the two materials in different proportions. However, for 3% filler loading, the film observed the highest elongation at break as ~10% which is even greater than that of neat PLA film. The presence of nanospheres is confirmed by TEM images which clearly inferred that blending of GA-*g*-PLA with PLA significantly altered the morphological characteristics of the film.
- The reduction in WVTR of PLA/GA-*g*-PLA(3%) and PLA/GA-*g*-PLA(5%) films was observed as 7% and 27% respectively. The most important achievement of this work is the significant decrease in the oxygen transmission rate (OTR) of composite films. The OTR × e value of neat PLA films was 37.6 cm^3 mm m^{-2} day^{-1}, which is reduced to around 4 cm^3 mm m^{-2} day^{-1}. A decrease of ~10 fold in the OTR value can be regarded as a very significant improvement in the gas (oxygen) barrier property of the film, especially for using them as packaging films.
- E_a versus conversion plot indicated that the degradation stage of PLA followed one-dimensional diffusion mechanism or unification of multiple-reaction mechanism. The increase in activation energy with increase in conversion indicates complex reaction in PLA/GA-*g*-PLA bionanocomposite films. The results also proved that the kinetic models such as Kissinger, Augis & Bennett, F-W-O and K-A-S are in good agreement, and the models have been found to be complementary to each other.

8.2. Scope for Future Work

A few recommendations for carrying out future research in this field are as follows:

- Detailed study can be done on insight of structural modification in gum arabic grafted lactic acid and its computational validation.
- Mechanism of adhesive bonding, of gum arabic grafted lactic acid can be thoroughly investigated.
- PLA-gum bionanocomposite films can be fabricated by using melt extrusion technique at pilot scale, to evaluate their commercial adaptability.
- Detailed studies on toxicity, migration, biodegradation and recycling of PLA-gum bionanocomposite films can be undertaken.
- Anti-microbial properties of the bionanocomposite films can be tested for their applications as food packaging materials.
- OTR at different relative humidity can be tested for packaging applications.

References

Abdel-Halim, E. S.; Al-Deyab, S. S. Hydrogel from crosslinked polyacrylamide/guar gum graft copolymer for sorption of hexavalent chromium ion, *Carbohydrate Polymers* **2011**, 86, 1306-1312.

Abdel-Razik, E. A.; Ayaad, D. M.; Elbedwehy, A. M. Graft copolymerization of acrylonitrile onto acacia gum by manganese (IV)–nitric acid as a redox initiator in aqueous media under visible light, *International Journal of Modern Organic Chemistry* **2013**, 2, 191-206.

Achilias, D. S.; Panayotidou, E.; Zuburtikudis, I. Thermal degradation kinetics and isoconversional analysis of biodegradable poly(3-hydroxybutyrate)/organomodified montmorillonite nanocomposites, *Thermochimica Acta* **2011**, 514, 58-66.

Ahmad, N.; Alam, M.; Alotaibi, M. A. N. Synthesis, characterization and thermal degradation kinetics of biuret–formaldehyde polymeric ligand and its polymer metal complexes, *Journal of Thermal Analysis and Calorimetry* **2015**, 119, 1381-1391.

Ahmad, S. I.; Mazumdar, N.; Kumar, S. Functionalization of natural gum: an effective method to prepare iodine complex, *Carbohydrate Polymers* **2013**, 92, 497-502.

Ajioka, M.; Enomoto, K.; Suzuki, K.; Yamaguchi, A. The basic properties of poly(lactic acid) produced by the direct condensation polymerization of lactic acid, *Journal of Environmental Polymer Degradation* **1995**, 68, 225-234.

Alfaifi, A. Y. A.; El-Newehy, M. H.; Abdel-Halim, E. S.; Al-Deyab, S. S. Microwave-assisted graft copolymerization of amino acid based monomers onto starch and their use as drug carriers, *Carbohydrate Polymers* **2014**, 106, 440-452.

Ali, A.; Maqbool, M.; Ramachandran, S.; Alderson, P. G. Gum arabic as a novel edible coating for enhancing shelf-life and improving postharvest quality of tomato (*Solanum lycopersicum L.*) fruit, *Postharvest Biology and Technology* **2010**, 58, 42-47.

Ali, B. H.; Ziada, A.; Blunden, G. Biological effects of gum arabic: A review of some recent research, *Food and Chemical Toxicology* **2009**, 47, 1-8.

Almuslet, N. A.; Hassan, E. A.; Al-Sherbani, A. S. A.; Muhgoub, M. G. A. diode laser (532 nm) induced grafting of polyacrylamide onto gum arabic, *Journal of Physical Science* **2012**, 23, 43-53.

Arrieta, M. P.; Fortunati, E.; Dominicib, F.; Lopez, J.; Kenny, J. M. Bionanocomposite films based on plasticized PLA-PHB/cellulose nanocrystal blends, *Carbohydrate Polymers* **2015**, 121, 265-275.

Auras, R.; Harte, B.; Selke, S. An overview of polylactides as packaging materials, *Macromolecular Bioscience* **2004**, 4, 835-864.

Badia, J. D.; Moriana, R.; Santonja-Blasco, L.; Ribes-Greus, A. A thermogravimetric approach to study the influence of a biodegradation in soil test to a poly(lactic acid), *Macromolecular Symposia* **2008**, 272, 93-99.

Bilanovic, D.; Chang, F. H.; Isobaev, P.; Welle, P. Lactic acid and xanthan fermentations on an alternative potato residues media-Carbon source costs, *Biomass and bioenergy* **2011**, 35, 2683-2689.

Blaine, R. L.; Kissinger, H. E. Homer Kissinger and the Kissinger equation, *Thermochimica Acta* **2012**, 540, 1-6.

Bonilla, J.; Fortunati, E.; Vargas, M.; Chiralt, A.; Kenny, J. M. Effects of chitosan on the physicochemical and antimicrobial properties of PLA films, *Journal of Food Engineering* **2013**, 119, 236-243.

Bueno, V. B.; Petri, D.F. S. Xanthan hydrogel films: Molecular conformation, charge density and protein carriers, *Carbohydrate Polymers* **2014**, 101, 897- 904.

Burgos, N.; Martino, V. P.; Jimenez, A. Characterization and ageing study of poly (lactic acid) films plasticized with oligomeric lactic acid, *Polymer Degradation and Stability* **2013**, 98, 651-658.

Byczynski, L.; Dutkiewicz, M.; Maciejewski, H. Thermal degradation studies of poly(urethane–siloxane) thermosets based on co-poly(dimethyl) (methyl,hydroxypolyoxyethylenepropyl) siloxane, *Thermochimica Acta* **2014**, 589, 252-261.

Carrasco, F.; Gamez-Perez, J.; Santana, O. O.; Maspoch, M. Ll. Processing of poly(lactic acid)/organomontmorillonite nanocomposites: microstructure, thermal stability and kinetics of the thermal decomposition, *Chemical Engineering Journal* **2011**, 178, 451-460.

Carrasco, F.; Pages, P.; Gamez-Perez, J.; Santana, O. O.; Maspoch, M. L. Kinetics of the thermal decomposition of processed poly(lactic acid), *Polymer Degradation and Stability* **2010**, 95, 2508-2514.

Carrasco, F.; Perez-Maqueda, L. A.; Santana, O. O.;Maspoch, M. Ll. Enhanced general analytical equation for the kinetics of the thermal degradation of poly(lactic acid)/montmorillonite nanocomposites driven by random scission, *Polymer Degradation and Stability* **2014**, 101, 52-59.

Catia Bastioli, Handbook of biodegradable polymers **2005**, Rapra Technology Limited, Chapter 6, 183.

Cekingen, S. K.; Saltan, F.; Yildirim, Y.; Akat, H. A novel HEMA-derived monomer and copolymers containing side-chain thiophene units: synthesis, characterization and thermal degradation kinetics, *Thermochimica Acta* **2012**, 546, 87-93.

Chang, J. H.; An, Y. U.; Cho, D.; Giannelis, E. P. Poly(lactic acid) nanocomposites: comparison of their properties with montmorillonite and synthetic mica (II), *Polymer* **2003**, 44, 3715.

Chataigner, S.; Caron, J. F.; Benzarti, K.; Quiertant, M.; Aubagnac, C. Use of a single lap shear test to characterize composite-to-concrete or composite-to-steel bonded interfaces, *Construction and Building Materials* **2011,** 25, 468-478.

Chen, H. B.; Donga, X.; Schiraldi, D. A.; Chen, L.; Wang, D. Y.; Wang, Y. Z. Phosphorus-containing poly(trimethylene terephthalate) derived from 2-(6-oxido-6H-dibenz <c,e> <1,2> oxaphosphorin-6-yl)-1,4-hydroxyethoxyphenylene: synthesis, thermal, degradation, combustion and pyrolysis behavior, *Journal of Analytical and Applied Pyrolysis* **2013**, 99, 40-48.

Chou, P.M.; Mariatti, M.; Zulkifli, A.; Sreekantan, S. Evaluation of the flexural properties and bioactivity of bioresorbable PLLA/PBSL/CNT and PLLA/PBSL/TiO_2 nanocomposites, *Composites: Part B.* **2012**, 43, 1374-1381.

Chrissafis, K. Kinetics of thermal degradation of polymers: complementary use of isoconversional and model-fitting methods, *Journal of Thermal Analysis and Calorimetry* **2009**, 95, 273-283.

Connolly, S.; Fenyo, J. C.; Vandevelde, M. C. Heterogeneity and homogeneity of anarabinogalactan protein: *Acacia Senegal* gum, *Food Hydrocolloids* **1987**, 5/6, 477-480.

Corres, M. A.; Zubitur, M.; Cortazar, M.; Mugica, A. Thermal and thermo-oxidative degradation of poly(hydroxy ether of bisphenol-A) studied by TGA/FTIR and TGA/MS, *Journal of Analytical and Applied Pyrolysis* **2011**, 92, 407-416.

Cutter, C. N. Opportunities for bio-based packaging technologies to improve the quality and safety of fresh and further processed muscle foods, *Meat Science* **2006**, 74, 131-142.

Dai, L.; Wang, L. Y.; Yuan, T. Q.; He, J. Study on thermal degradation kinetics of cellulose-*graft*-poly(l-lactic acid) by thermogravimetric analysis, *Polymer Degradation and Stability* **2014**, 99, 233-239.

Das, D.; Ara, T.; Dutta, S.; Mukherjee, A. New water resistant biomaterial biocide film based on guar gum, *Bioresource Technology* **2011**, 102, 5878-5883.

Datta, R.; Tsai, S.; Bonsignore, P.; Moon, S.; Frank, J.; Technological and economic potential of poly(lactic acid) and lactic acid derivatives, *FEMS Micro-biology Reviews*, **1995**,16, 221-231.

David K. Platt, Biodegradable polymers: market report **2006**, Rapra Technology Limited, Chapter 1, 1.

Diaz-Celorio, E.; Franco, L.; Marquez, Y.; Rodriguez-Galan, A.; Puiggali, J. Thermal degradation studies on homopolymers and copolymers based on trimethylene carbonate and glycolide units, *Thermochimica Acta* **2012**, 528, 23-31.

Doyle, C. D. Estimating isothermal life from thermogravimetric data, *Journal of Applied Polymer Science* **1962**, 6, 639-642.

Duncan, T. V. Applications of nanotechnology in food packaging and food safety: barrier materials, antimicrobials and sensors, *Journal of Colloid and Interface Science* **2011**, 363, 1-24.

Dunn, D. J., Adhesives and sealants-technology, applications and markets, *Rapra Technology Limited: UK*, **2003**; pp 3-14.

Enomoto, K.; Ajioka, M.; Yamaguchi, A. Polyhydroxycarboxylic acid and preparation process thereof. US Patent 5310865A, May 10, **1994**.

Flynn, J. H. The isoconversional method for determination of energy of activation at constant heating rates: corrections for the Doyle approximation, *Journal of Thermal Analysis* **1983**, 27, 95-102.

Fortunati, E.; Armentano, I.; Zhou, Q.; Puglia, D.; Terenzi, A.; Berglund, L. A.; Kenny, J. M. Microstructure and nonisothermal cold crystallization of PLA composites based on silver nanoparticles and nanocrystalline cellulose, *Polymer Degradation and Stability* **2012**, 97, 2027-2036.

Ganie, S. A.; Ali, A.; Mazumdar, N. Iodine derivatives of chemically modified gum arabic microspheres, *Carbohydrate Polymers* **2015**, 129, 224-231.

Garcia-Ochoa, F.; Santos, V.E.; Casas, J. A.; Gomez, E. Xanthan gum: production, recovery, and properties, *Biotechnology Advances* **2000**, 18, 549-579.

Garlotta, D. A literature review of poly(Lactic Acid), *Journal of Polymers and the Environment* **2002**, 9, 63. 63-84.

Ge, L.; Li, X.; Zhang, R.; Yang, T.; Ye, X.; Li, D.; Mu, C. Development and characterization of dialdehyde xanthan gum crosslinked gelatin based edible films incorporated with amino functionalized montmorillonite, *Food Hydrocolloids* **2015**, 51, 129-135.

Gils, P. S.; Ray, D.; Sahoo, P. K. Designing of silver nanoparticles in gum arabic based semi-IPN hydrogel, *International Journal of Biological Macromolecules* **2010**, 46, 237-244.

Goncalves, C. M. B.; Tome, L. C.; Garcia, H.; Brandao, L.; Mendes, A. M.; Marrucho, I. M. Effect of natural and synthetic antioxidants incorporation on the gas permeation properties of poly(lactic acid) films, *Journal of Food Engineering* **2013**, 116, 562-571.

Gonzalez, A.; Igarzabal, C. I. A. Soy protein - Poly (lactic acid) bilayer films as biodegradable material for active food packaging, *Food Hydrocolloids* **2013**, 33, 289-296.

Guan, J. J.; Qiu, A. Y.; Liu, X. Y.; Hua, Y. F.; Ma, Y. H. Microwave improvement of soy protein isolate-saccharide graft reactions, *Food Chemistry* **2006**, 97, 577-585.

Guan, J. J.; Zhang, T. B.; Hui, M.; Yin, H. C.; Qiu, A. Y.; Liu, X. Y. Mechanism of microwave-accelerated soy protein isolate-saccharide graft reactions, *Food Research International* **2011**, 44, 2647-2654.

Guo, J.; Ge, L.; Li, X.; Mu, C.; Li, D. Periodate oxidation of xanthan gum and its crosslinking effects on gelatin-based edible films, *Food Hydrocolloids* **2014**, 39, 243-250.

Gupta, A. P.; Arora, G. Preparation and characterization of cross-linked guar-gum poly(vinylalcohol) green films, *Der Chemica Sinica* **2012**, 3, 1191-1197.

Gupta, N. R.; Ghute, P. P.; Badiger, M. V. Synthesis and characterization of thermo-sensitive graft copolymer of carboxymethyl guar and poly(N-isopropylacrylamide), *Carbohydrate Polymers* **2011**, 83, 74-80.

Gutierrez, J.; Tercjak, A. Natural gum rosin thin films nanopatterned by poly(styrene)-block-poly(4-vinylpiridine) block copolymer, *Royal Society of Chemistry* **2014**, 4, 32024-32030.

Haafiz, M. K. M.; Hassan, A.; Zakaria, Z.; Inuwa, I. M.; Islam, M. S.; Jawaid, M. Properties of polylactic acid composites reinforced with oil palm biomass microcrystalline cellulose, *Carbohydrate Polymers* **2013**, 98, 139-145.

Hartmann, M. H. Biopolymers from renewable resources **1998**, Springer, Berlin, Germany, Chapter 15, 367.

Huang, G.; Zou, Y.; Xiao, M.; Wang, S.; Luo, W.; Han, D.; Meng, Y. Thermal degradation of poly(lactide-co-propylene carbonate) measured by TG/FTIR and Py-GC/MS, *Polymer Degradation and Stability* **2015**, 117, 16-21.

Hu, Y. H.; Chen, C. Y.; Wang, C. C. Thermal degradation kinetics of poly(N-butyl acrylate) initiated by lactams and thiols, *Polymer Degradation and Stability* **2004**, 84, 505-514.

Illing, H.P.A.; Malmfors, T.; Rodenburg, L. Skin sensitization and possible groupings for 'read across' for rosin based substances, *Regulatory Toxicology and Pharmacology* **2009**, 54, 234-241.

Imam, S. H.; Bilbao-Sainz, C.; Chiou, B. S.; Glenn, G. M.; Orts, W. J. Biobased adhesives, gums, emulsions, and binders: current trends and future prospects, *Journal of Adhesion Science and Technology* **2013**, 27, 1972-1997.

Imre, B.; Pukanszky, B. Compatibilization in bio-based and biodegradable polymer blends, E*uropean Polymer Journal* **2013**, 49, 1215-1233.

Islam, A. M.; Phillips, G. O.; Sljivo, A.; Snowden, M. J.; Williams, P. A. A review of recent development on the regulatory, structural and functional aspects of gum arabic, *Food Hydrocolloids* **1997**, 11, 493-505.

Jakic, M.; Vrandecic, N. S.; Klaric, I. Thermal degradation of poly(vinyl chloride)/poly(ethylene oxide) blends: thermogravimetric analysis, *Polymer Degradation and Stability* **2013**, 98, 1738-1743.

Jina, W.; Song, R.; Xu, W.; Wang, Y.; Li, J.; Shah, B. R.; Li, Y.; Li, B. Analysis of deacetylated konjac glucomannan and xanthan gum phase separation by film forming, *Food Hydrocolloids* **2015**, 48, 320-326.

Khshain, N. T.; Al-Mahaidi, R., Abdouka, K. Bond behaviour between NSM CFRP strips and concrete substrate using single-lap shear testing with epoxy adhesive, *Composite Structures* **2015**, 132, 205-214.

Kimura, Y. Bio-based polymers **2013**, CMC Publishing Co., Ltd. Chapter 1, 1-23.

Kissinger, H. E. Reaction kinetics in differential thermal analysis, *Analytical Chemistry* **1957**, 29, 1702-1706.

Kopinke, F. D.; Remmler, M.; Mackenzie, K.; Milder, M.; Wachsen, O. Thermal decomposition of biodegradable polyesters-II. poly(lactic acid), *Polymer Degradation and Stability* **1996**, 43, 329-342.

Kumar, A.; Singh, K.; Ahuja, M. Xanthan-*g*-poly(acrylamide): Microwave-assisted synthesis, characterization and *in vitro* release behavior, *Carbohydrate Polymers* **2009**, 76, 261-267.

Li, C.; Zhu, W.; Xue, H.; Chen, Z.; Chen, Y.; Wang, X. Physical and structural properties of peanut protein isolate-gum Arabic films prepared by various glycation time, *Food Hydrocolloids* **2015**, 43, 322-328.

Likhitha, M.; Sailaja, R. R. N., Priyambika, V. S.; Ravibabu, M. V. Microwave assisted synthesis of guar gum grafted sodium acrylate/cloisite superabsorbent

nanocomposites: reaction parameters and swelling characteristics, *International Journal of Biological Macromolecules* **2014**, 65, 500-508.

Liu, Y.; Peng, D.; Huang, K.; Liu, S.; Liu, Z. Preparation and thermal degradation kinetics of terpolymer poly(ε-caprolactone-co-1,2-butylene carbonate), *Polymer Degradation and Stability* **2010**, 95, 2453-2460.

Lizundia, E.; Vilas, J. L.; Leon, L. M. Crystallization, structural relaxation and thermal degradation in poly(l-lactide)/cellulose nanocrystal renewable nanocomposites, *Carbohydrate Polymers* **2015**, 123, 256-265.

Lo, Y. M.; Yang, S. T.; Min, D. B. Kinetic and feasibility studies of ultrafiltration of viscous xanthan gum fermentation broth, *Journal of Membrane Science* **1996**, 117, 237-249.

Lunt, J. Large-scale production, properties and commercial applications of polylactic acid polymers, *Polymer Degradation and Stability* **1998**, 59, 145-152.

Maharana, T.; Mohanty, B.; Negi, Y. S. Melt-solid polycondensation of lactic acid and its biodegradability, *Progress in Polymer Science* **2009**, 34, 99-124.

Mahto, D.; Rani, P.; Mishra, S.; Sen, G. Microwave assisted synthesis of polyacrylamide grafted soya peptone and its application as water soluble adhesive, *Industrial Crops and Products* **2014**, 58, 251-258.

Maiti, S.; Ray, S. S.; Kundu, A. K. Rosin: A renewable resource for polymers and polymer chemical, *Progress in Polymer Science* **1989**, 14, 297-338.

Majoni, S.; Su, S.; Hossenlopp, J. M. The effect of boron-containing layered hydroxy salt (LHS) on the thermal stability and degradation kinetics of poly (methyl methacrylate), *Polymer Degradation and Stability* **2010**, 95, 1593-1604.

Manafi, P.; Ghasemi, I.; Karrabi, M.; Azizi, H.; Manafi, M. R.; Ehsaninamin, P. Thermal stability and thermal degradation kinetics (model-free kinetics) of nanocomposites based on poly (lactic acid)/graphene: the influence of functionalization, *Polymer Bulletin* **2015**, 72, 1095-1112.

Manna, P. J.; Mitra, T.; Pramanik, N.; Kavitha, V.; Gnanamani, A.; Kundu, P. P. Potential use of curcumin loaded carboxymethylated guar gum grafted gelatin film for biomedical applications, *International Journal of Biological Macromolecules* **2015**, 75, 437-446.

Mirhosseini, H.; Amid, B. T. A review study on chemical composition and molecular structure of newly plant gum exudates and seed gums, *Food Research International* **2012**, 46, 387-398.

Mishra, M. M.; Mishra, D. K.; Mishra, P.; Behari, K. Synthesis and characterization of a novel graft copolymer of partially carboxymethylated guar gum and N-vinylformamide, *Carbohydrate Polymers* **2015**, 115, 776-784.

Mishra, S.; Sen, G. Microwave initiated synthesis of polymethylmethacrylate grafted guar (GG-g-PMMA), characterizations and applications, *International Journal of Biological Macromolecules* **2011**; 48, 688-694.

Miyata, T.; Masuko, T. Crystallization behaviour of poly(L-lactide), *Polymer* **1998**, 39, 5515-5521.

Moon, S. I.; Lee, C. W.; Kimura, Y. Melt/solid polycondensation of l-lactic acid: an alternative route to poly(l-lactic acid) with high molecular weight, *Polymer* **2001**, 42, 5059.

Mu, L.; Zhao, M.; Yang, B.; Zhao, H.; Cui, C.; Zhao, Q. Effect of ultrasonic treatment on the graft reaction between soy protein isolate and gum acacia and on the physicochemical

properties of conjugates, *Journal of Agricultural and Food Chemistry* **2010**, 58, 4494-4499.

Mundargi, R. C.; Patil, S. A.; Aminabhavi, T. M. Evaluation of acrylamide-grafted-xanthan gum copolymer matrix tablets for oral controlled delivery of antihypertensive drugs, *Carbohydrate Polymers* **2007**, 69, 130-141.

Nalbandi, A.; Kinetics of thermal degradation of polylactic acid under N_2 atmosphere, *Iranian Polymer Journal* **2001**, 10, 371-376.

Nayak, A. K.; Das, B.; Maji, R. Calcium alginate/gum arabic beads containing glibenclamide: development and *in vitro* characterization, *International Journal of Biological Macromolecules* **2012**, 51, 1070-1078.

Norströma, E.; Fogelström, L.; Nordqvist, P.; Khabbaz, F.; Malmström, E. Gum dispersions as environmentally friendly wood adhesives, *Industrial Crops and Products* **2014**, 52, 736-744.

Oprea, S. Effects of guar gum content on structure and properties of multi-cross-linked polyurethane composite films, *Composites: Part B* **2013**, 44, 76-83.

Ozawa, T. A new method of analyzing thermogravimetric data, *Bulletin of the Chemical Society of Japan* **1965**, 38, 1881-1886.

Pandey, P. K.; Srivastava, A.; Tripathy, J.; Behari, K. Graft copolymerization of acrylic acid onto guar gum initiated by vanadium (V)-mercaptosuccinic acid redox pair, *Carbohydrate Polymers* **2006**, 65, 414-420.

Pandey, S.; Mishra, S. B. Graft copolymerization of ethylacrylate onto xanthan gum, using potassium peroxydisulfate as an initiator, *International Journal of Biological Macromolecules* **2011**, 49, 527-535.

Pandey, S.; Mishra, S. B. Microwave synthesized xanthan gum-g-poly(ethylacrylate): An efficient Pb^{2+} ion binder, *Carbohydrate Polymers* **2012**, 90, 370-379.

Pandey, V. S.; Verma, S. K.; Yadav, M.; Behari, K. Guar gum-g-N,N´-*dimethylacrylamide*: Synthesis, characterization and applications, *Carbohydrate Polymers* **2014**, 99, 284-290.

Papageorgiou, D. G.; Bikiaris, D. N.; Chrissafis, K. Effect of crystalline structure of polypropylene random copolymers on mechanical properties and thermal degradation kinetics, *Thermochimica Acta* **2012**, 543. 288-294.

Parija, S.; Misra, M.; Mohanty, A. K. Studies of natural gum adhesive extracts: an overview. *J. Macromol. Sci. – Polymer Reviews* **2001**, 175-197.

Park, S.; Baker, J. O.; Himmel, M. E.; Parilla, P. A.; Johnson, D. K. Cellulose crystallinity index: measurement techniques and their impact on interpreting cellulase performance, *Biotechnology for Biofuels* **2010**, 3, 1-10.

Ramos, M.; Jimenez, A.; Peltzer, M.; Garrigos, M. C. Development of novel nano-biocomposite antioxidant films based on poly (lactic acid) and thymol for active packaging, *Food Chemistry* **2014**, 162,149-155.

Randall, R. C.; Phillips, G. O.; Williams, P. A. Fractionation and characterization of gum form *Acacia senegal*, *Food Hydrocolloids* **1989**, 3, 65-75.

Rani, G. U.; Mishra, S.; Pathak, G.; Jha, U.; Sen, G. Synthesis and applications of poly(2-hydroxyethylmethacrylate) grafted agar: A microwave based approach, *International Journal of Biological Macromolecules* **2013**, 61, 276-84.

Rani, P.; Mishra, S.; Sen, G. Microwave based synthesis of polymethyl methacrylate grafted sodium alginate: Its application as flocculant, *Carbohydrate Polymers* **2013**, 91, 686-692.

Rao, M. S.; Kanatt, S. R.; Chawla, S. P.; Sharma, A. Chitosan and guar gum composite films: Preparation, physical, mechanical and antimicrobial properties, *Carbohydrate Polymers* **2010**, 82, 1243-1247.

Raquez, J. M.; Habibi, Y.; Murariu, M.; Dubois, P. Poly lactide (PLA)-based nanocomposites, *Progress in Polymer Science* **2013**, 38, 1504-1542.

Reddy, M. M.; Vivekanandhan, S.; Misra, M.; Bhatia, S. K.; Mohanty, A. K. Biobased plastics and bionanocomposites: current status and future opportunities, *Progress in Polymer Science* **2013**, 38, 1653-1689.

Rhim, J. W.; Park, H. M.; Ha, C. S. Bio-nanocomposites for food packaging applications, *Progress in Polymer Science* **2013**, 38, 1629-1652.

Rudnik, E.; Briassoulis, D. Degradation behaviour of poly(lactic acid) films and fibres in soil under Mediterranean field conditions and laboratory simulations testing, *Industrial Crops and Products* **2011**, 33, 648-658.

Sakloetsakun, D; Preechagoon, D.; Bernkop-Schnürch, A.; Pongjanyakul, T. Chitosan–gum arabic polyelectrolyte complex films: physicochemical, mechanical and mucoadhesive properties, *Pharmaceutical development and technology* **2015**, 1-10.

Saurabh, C. K.; Sumit Gupta, S.; Bahadur, J.; Mazumderb, S.; Variyar, P. S.; Sharma, A. Radiation dose dependent change in physiochemical, mechanical and barrier properties of guar gum based films, *Carbohydrate Polymers* **2013**, 98, 1610-1617.

Segal, L.; Creely, J. J.; Martin, Jr. A. E.; Conrad, C. M. An empirical method for estimating the degree of crystallinity of native cellulose using the x-ray diffractometer, *Textile research journal* **1959**, 786-794.

Sen, G.; Mishra, S.; Jha, U.; Pal, S. Microwave initiated synthesis of polyacrylamide grafted guar gum (GG-g-PAM)—Characterizations and application as matrix for controlled release of 5-amino salicylic acid, *International Journal of Biological Macromolecules* **2010** , 47, 164-170.

Setia, A.; Kumar, R. Microwave assisted synthesis and optimization of *Aegle marmelos*-g-poly(acrylamide): release kinetics studies, *International Journal of Biological Macromolecules* **2014**, 65, 462-470.

Sevigne-Itoiz, E.; Gasol, C. M.; Rieradevall, J.; Gabarrell, X. Contribution of plastic waste recovery to greenhouse gas (GHG) savings in Spain, *Waste Management* **2015**, 46, 557-567.

Shahid, M.; Bukhari, S. A.; Gul, Y.; Munir, H.; Anjum, F.; Zuber, M.; Jamil, T.; Zia, K. M. Graft polymerization of guar gum with acryl amide irradiated by microwaves for colonic drug delivery, *International Journal of Biological Macromolecules* **2013**, 62, 172-179.

Silverajah, V. S. G.; Ibrahim, N. A.; Zainuddin,N.; Yunus, W. M. Z. W.; Hassan, H. A. Mechanical, thermal and morphological properties of poly(lactic acid)/epoxidized palm olein blend, *Molecules* **2012**, *17*, 11729-11747.

Singh, V.; Kumar, P.; Sanghi, R. Use of microwave irradiation in the grafting modification of the polysaccharides-A review, *Progress in Polymer Science* **2012**, 37, 340-364.

Singh, V.; Tiwari, A.; Tripathi, D. N.; Sanghi, R. Microwave enhanced synthesis of chitosan-*graft*-polyacrylamide, *Polymer* **2006**, 47, 254-260.

Sinha, S.; Mishra, S.; Sen, G. Microwave initiated synthesis of polyacrylamide grafted casein (CAS-g-PAM)–Its application as a flocculent, *International Journal of Biological Macromolecules* **2013**, 60, 141-147.

Slopiecka, K.; Bartocci, P.; Fantozzi, F. Thermogravimetric analysis and kinetic study of popular wood pyrolysis, *Third International Conference on Applied Energy* **2011**, 1687-1698.

Sodergard, A.; Stolt, M. Properties of lactic acid based polymers and their correlation with composition, *Progress in Polymer Science* **2002**, 27, 1123-1163.

Soppirnath, K. S.; Aminabhavi, T. M. Water transport and drug release study from cross-linked polyacrylamide grafted guar gum hydrogel microspheres for the controlled release application, *European Journal of Pharmaceutics and Biopharmaceutics* **2002**, 53, 87-98.

Talukdar, M.M.; Kinget, R. Swelling and drug release behaviour of xanthan gum matrix tablets, *International Journal of Pharmaceutics* **1995**, 120, 63-72.

Thota, G.; Srinivas, P. Ag(I) Catalyzed grafting of acrylonitrile onto gum arabic by Ce(IV) in H_2SO_4 medium: A kinetic study, *International Scholarly Research Network Physical Chemistry* **2012**, 2012, 1-7.

Tiwari, A. Gum Arabic-Graft-Polyaniline: An electrically active redox biomaterial for sensor applications, *Journal of Macromolecular Science, Part A: Pure and Applied Chemistry* **2007**, 44, 735-745.

Tiwari, A.; Singh, V. Microwave-induced synthesis of electrical conducting gum acacia-*graft*-polyaniline, *Carbohydrate Polymers* **2008**, 74, 427-434.

Tripathi, N.; Katiyar, V. PLA/functionalized-gum arabic based bionanocomposite films for high gas barrier applications, *Journal of Applied Polymer Science* **2016**, 133, 43458; DOI: 10.1002/app.43458 in press.

Tsai, R. Y.; Chen, P. W.; Kuo, T. Y.; Lin, C. M.; Wang, D. M.; Hsien, T. Y.; Hsieh, H. J. Chitosan/pectin/gum Arabic polyelectrolyte complex: Process-dependent appearance, microstructure analysis and its application, *Carbohydrate Polymers* **2014**, 101, 752-759.

Tsuji, H.; Fukui, I. Enhanced thermal stability of poly(lactide)s in the melt by enantiomeric polymer blending, *Polymer* **2003**, 44, 2891-2896.

Tudorachi, N.; Lipsa, R.; Mustata, F. R. Thermal degradation of carboxymethyl starch-g-poly(lactic acid) copolymer by TG-FTIR-MS analysis, *Industrial and Engineering Chemistry Research* **2012**, 51, 15537-15545.

Valapa, R.; Pugazhenthi, G.; Katiyar, V. Thermal degradation kinetics of sucrose palmitate reinforced poly(lactic acid) biocomposites, *International Journal of Biological Macromolecules*. **2014**, 65, 275-283.

Veiga-Santos, P.; Oliveira, L. M.; Cereda, M. P.; Alves, A. J.; Scamparini, A.R.P. Mechanical properties, hydrophilicity and water activity of starch-gum films: effect of additives and deacetylated xanthan gum, *Food Hydrocolloids* **2005**, 19, 341-349.

Verbeken, D.; Dierckx, S.; Dewettinck, K. Exudate gums: occurrence, production, and applications, *Applied Microbiology and Biotechnology* **2003,** 63, 10-21.

Vijan, V.; Kaity, S.; Biswas, S.; Isaac, J.; Ghosh, A. Microwave assisted synthesis and characterization of acrylamide grafted gellan, application in drug delivery, *Carbohydrate Polymers* **2012**, 90, 496-506.

Viljanmaa, M.; Södergård, A.; Törmälä, P. Lactic acid based polymers as hot melt adhesives for packaging applications, *International Journal of Adhesion & Adhesives* **2002**, 22, 219-226.

Vyazovkin, S.; Sbirrazzuoli, N. Isoconversional kinetic analysis of thermally stimulated processes in polymers, *Macromolecular Rapid Communications* **2006**, 27, 1515-1532.

Wang, H.; Williams, P. A.; Senan, C. Synthesis, characterization and emulsification properties of dodecenyl succinic anhydride derivatives of gum Arabic, *Food Hydrocolloids* **2014**, 37, 143-148.

Wang, J.; Somasundaran, P.; Nagaraj, D. R. Adsorption mechanism of guar gum at solid–liquid interfaces, *Minerals Engineering* **2005**, 18, 77-81.

Wang, Q.; Ellis, P. R., Ross-Murphy, S.B. Dissolution kinetics of water-soluble polymers: The guar gum paradigm, *Carbohydrate Polymers* **2008**, 74, 519-526.

Wan, X.; Li, Y.; Wang, X.; Chen, S.; Gu, X. Synthesis of cationic guar gum-graft-polyacrylamide at low temperature and its flocculating properties, *European Polymer Journal* **2007**, 43, 3655-3661.

Wan, Z.; Xiong, Z.; Ren, H.; Huang, Y.; Liu, H.; Xionga, H.; Wu, Y.; Han, J. Graft copolymerization of methyl methacrylate onto bamboo cellulose under microwave irradiation, *Carbohydrate Polymers* **2011**, 83, 264-269.

Wyasu, G; Okereke, N. Z-J Improving the film forming ability of gum Arabic, *Journal of Natural Product and Plant Resources* **2012**, 2, 314-317.

Yang, K. K.; Wang, X. L.; Wang, Y. Z.; Wu, B.; Jin, Y. D.; Yang, B. Kinetics of thermal degradation and thermal oxidative degradation of poly(p-dioxanone), *European Polymer Journal*. **2003**, 39, 1567-1574.

Yang, M. H.; Lin, Y. H. Measurement and simulation of thermal stability of poly(lactic acid) by thermogravimetric analysis, *Journal of Testing and Evaluation* **2009**, 37, 1-7.

Yan, L.; Chang, P. R.; Zheng, P.; Ma, X. Characterization of magnetic guar gum-grafted carbon nanotubes and the adsorption of the dyes, *Carbohydrate Polymers* **2012**, 87, 1919-1924.

Yoshikawa, M.; Goshi, Y.; Yamada, S.; Koga, N. Multistep kinetic behavior in the thermal degradation of poly(L−lactic acid): a physico-geometrical kinetic interpretation, *The Journal of Physical Chemistry B*. **2014**, 118; 11397-11405.

Zeng, J. B.; Li, Y. D.; Li, S. L.; Wang, Y. Z.; Yang, K. K. Thermal and thermo-oxidative degradation of biodegradable poly(ester urethane) containing poly(l-lactic acid) and poly(butylene succinate) blocks, *Journal of Macromolecular Science, Part B: Physics* **2009**, 48, 635-649.

Zhang, Z. G.; Song, R. H.; Hu, G. L.; Sun, Y. Y. Thermal stability and degradation of poly (lactic acid)/hexamoll® DINCH/montmorillonite composites, *BioResources* **2014**, 9, 4821-4833.

Zhao, Y.; Qiu, J.; Feng, H.; Zhang, M.; Lei, L.; Wu, X. Improvement of tensile and thermal properties of poly(lactic acid) composites with admicellar-treated rice straw fiber, *Chemical Engineering Journal* **2011**, 173, 659-666.

Zohuriaan, M. J.; Shokrolahi, F. Thermal studies on natural and modified gums, *Polymer Testing* **2004**, 23, 575-579.

Zou, H.; Yi, C.; Wang, L.; Liu, H.; Xu, W. Thermal degradation of poly(lactic acid) measured by thermogravimetry coupled to fourier transform infrared spectroscopy, *Journal of Thermal Analysis and Calorimetry* **2009**, 97, 929-935.

Research Output

Patents

1. Indian Patent application filed: Vimal Katiyar, **Neelima Tripathi**, Biobased Adhesive for Structural Applications, Indian Patent application, 980/KOL/2015.
2. Indian Patent application filed: Vimal Katiyar, **Neelima Tripathi**, Akhilesh Kumar Pal, Dispersible biobased additive formulation for biodegradable polymer packaging, Indian Patent application, 981/KOL/2015.

Journals

Neelima Tripathi, Vimal Katiyar. PLA/functionalized-gum arabic based bionanocomposite films for high gas barrier applications, *Journal of Applied Polymer Science*, Volume 133, Issue 21, **2016**.

Neelima Tripathi, Monika, Vimal Katiyar, "Thermal degradation kinetics of poly (lactic acid)/lactic acid-grafted-gum arabic bionanocomposite films". (under review)

Neelima Tripathi, Vimal Katiyar, "Lactic acid oligomer (OLLA) grafted gum arabic based green adhesive for structural applications". (under review)

Book Chapter

Vimal Katiyar, **Neelima Tripathi**, Rahul Patwa and Prakash Kotecha, book chapter titled as 'Environment Friendly Packaging Plastics' in book 'Polymers for Packaging Applications'. (CRC Press, Taylor & Francis Group, ISBN: 9781926895772), 2013.

Papers and posters in conferences/seminars/symposia

1. **Neelima Tripathi,** Vimal Katiyar, 'Lactic Acid-Polysaccharide Gum based Conjugates: A Bio-based Pressure Sensitive Adhesive' in ISBBB 2016, organized by University of Guelph, Ontario, Canada, during May 31-June 03, 2016.
2. **Neelima Tripathi,** Vimal Katiyar, 'Poly Lactic Acid-g-Polysaccharide Gum based Conjugates: A Bio-based Pressure Sensitive Adhesive' in CHEMCON 2015, organized by Indian Institute of Technology Guwahati, Guwahati during December 27-30, 2015.
3. **Neelima Tripathi,** Vimal Katiyar, 'Preparation, Characterization and Non-isothermal Degradation Kinetics of PLA/LA-*g*-GA Bionanocomposite Films' in CHEMCON 2015, organized by Indian Institute of Technology Guwahati, Guwahati during December 27-30, 2015.
4. **Neelima Tripathi,** Vimal Katiyar, 'Lactic Acid-Polysaccharide Gum based Conjugates: A Bio-based Pressure Sensitive Adhesive' in 14th Pacific Polymer, organized by American Chemical Society, Hawaii during December 09 -13, 2015. (abstract accepted)
5. **Neelima Tripathi,** Vimal Katiyar, 'PLA/Lactic Acid Grafted Gum based Bionanocomposites Films for High Gas Barrier Properties' in 14th Pacific Polymer, organized by American Chemical Society, Hawaii during December 09-13, 2015. (abstract accepted)
6. **Neelima Tripathi,** Vimal Katiyar, **'**Novel Bio-based Copolymer for Structural Adhesives and Packaging Applications' in Second Symposium on Advances in Sustainable Polymers (ASP-15), organized by Department of Chemical Engineering, Indian Institute of Technology Guwahati, Guwahati during January 21-22, 2015.

7. **Neelima Tripathi,** Vimal Katiyar, 'Sustainable Bio-based Adhesive for Glass Substrates' in National School on Sustainable Polymers & First Symposium on Advances in Sustainable Polymers (ASP-14), organized by Department of Chemical Engineering, Indian Institute of Technology Guwahati, Guwahati during January 06-11, 2014.
8. **Neelima Tripathi,** Vimal Katiyar, 'Sustainable Bio-based Composites for Packaging Applications' in Polymer Processing Society Asia/Australia, Mumbai during December 04-07, 2013.
9. **Neelima Tripathi,** Vimal Katiyar, 'Stereo-Poly(lactic acid): New Generation Biodegradable Polymer for Engineering Applications' in Advanced Polymers, Fibers and Fabrics, organized by Defence Materials & Stores Research & Development Establishment, Kanpur during December 26-28, 2011.

Awards

1. Won the Gandhian Young Technological Innovation Award/Appreciation 2016 (GYTI 2016) for '**Biobased Adhesive Formulation For Construction Applications**' at Rashtrapati Bhavan, New Delhi on March 13, 2016.
2. **Winner award** in 6th National Award for Technology Innovation entitled as '**Industrial Production of Degradable Packaging Films for Stringent Food Packaging Application**', in the category of Innovation in Polymeric Material organized by Petrochemicals and Downstream Plastic Processing Industry by Government of India at FICCI, New Delhi on January 21, 2016.
3. **Runner-up award** in 6th National Award for Technology Innovation in the category of Innovation in Polymer Waste Management & Recycling Technology and Green Polymeric

Materials & Products organized by Petrochemicals and Downstream Plastic Processing Industry by Government of India at FICCI, New Delhi on January 21, 2016.